Ph.D. DISSERTATION

Resource Allocation for Sum-Throughput Maximization in Wireless Powered Communication Networks

무선 전력 통신 네트워크에서 합통신량 최대화 기반 자원 할당 기법

Dongyeong Song

August 2020

Department of Electrical and Computer Engineering
College of Engineering
Seoul National University

Ph.D. DISSERTATION

Resource Allocation for Sum-Throughput Maximization in Wireless Powered Communication Networks

무선 전력 통신 네트워크에서 합통신량 최대화 기반 자원 할당 기법

Dongyeong Song

August 2020

Department of Electrical and Computer Engineering
College of Engineering
Seoul National University

Resource Allocation for Sum-Throughput Maximization in Wireless Powered Communication Networks

무선 전력 통신 네트워크에서 합통신량 최대화 기반 자원 할당 기법

지도교수 이 정 우

이 논문을 공학박사 학위논문으로 제출함

2020년 05월

서울대학교 대학원

전기·정보 공학부

송 동 영

송동영의 공학박사 학위 논문을 인준함

2020년 06월

위 원 장: _____

부위원장: _____

위 원: _____

위 원: _____

위 원: _____

Resource Allocation for Sum-Throughput Maximization in Wireless Powered Communication Networks

Advisor: Jungwoo Lee

Presented to the Graduate School of Seoul National University
in Partial Fulfillment of the Requirements for

The Degree of Doctor of Philosophy

May 2020

by

Dongyeong Song

Department of Electrical and Computer Engineering
College of Engineering
Seoul National University

This dissertation is approved for

The Degree of Doctor of Philosophy

June 2020

Chair _____
Vice Chair _____
Examiner _____
Examiner _____
Examiner _____

Abstract

With the explosive growth of smart devices equipped with wireless communication, there have been numerous challenges to untangle for supporting user demands in the next generation of communication networks such as Internet of Things networks. One of prime concerns is to overcome the finite lifespan of networks due to the limited battery capacity. Wireless power transfer (WPT) has been considered as a promising solution for providing self-sustainability to energy-constrained networks. WPT enables users to charge their batteries by collecting energy from a radio-frequency signal transmitted by a dedicated energy source. As a framework to the design of wireless networks with WPT, a wireless powered communication network (WPCN) consisting of a hybrid access-point (H-AP) and multiple users has emerged. A H-AP serves users in a WPCN as a base station as well as delivers energy to users as a dedicated energy source. In a WPCN, users charge their batteries by WPT via downlink, and use the energy for uplink transmission. Due to the scarcity of resources, an efficient design is crucial to exploit the system. To support this, I explore system design and resource allocation for WPCNs, especially in the perspective of throughput performance. In addition, I aim to mitigate severe rate disparity which originates from the doubly near-far problem, an inherent characteristic of a WPCN.

To begin with, I discuss a cooperative WPCN, in which a user with good channel condition relays information of a user with bad channel condition to enhance user fairness. The sum-throughput is maximized in the considered network subject to a set of quality of service (QoS) requirements. By analyzing the optimal solution, the conditions under which the WPCN benefits from the cooperation are characterized. Based on the new findings, I propose a novel resource allocation algorithm for sum-throughput maximization, which is helpful to practical use of user coop-

eration. Secondly, I discuss a multi-antenna WPCN where non-orthogonal multiple access (NOMA) transmission is employed in the uplink. To address issues regarding adopting NOMA, user clustering exploiting the multi-antenna system is further applied so that the number of users in a single NOMA transmission is reduced. To deal with the difficulty of jointly optimizing cluster-specific beamforming and time/energy resources for sum-throughput maximization, the beamforming is determined first, and then the resources are optimized for given beamforming. A novel algorithm for cluster-specific beamforming design followed by the sum-throughput maximization algorithm is proposed. Lastly, I consider a WPCN assisted by intelligent reflecting surface (IRS) which has recently received significant attention for its potential of enhancing wireless communication experience. By employing an IRS in a WPCN, users harvest extra energy, and the signal strength of each user can be elevated. For the considered system model, beamforming at the IRS and resources are optimized to maximize sum-throughput. In particular, both NOMA and orthogonal multiple access are considered for uplink transmission, and the performance comparison between the two multiple access schemes are presented.

keywords: Resource allocation, wireless powered communication network (WPCN), wireless communication, energy harvesting, non-orthogonal multiple access (NOMA)

student number: 2014-21613

Contents

Abstract **i**

Contents **iii**

List of Tables **vi**

List of Figures **vii**

1 Introduction **1**

1.1 Related Work 3

1.1.1 Wireless Powered Communication Networks 3

1.1.2 A NOMA-Based WPCN 4

1.2 Contributions and Organization 6

1.3 Notation 8

2 Wireless Powered Communication Networks with User Cooperation **9**

2.1 Introduction 10

2.2 System model 14

2.3 Problem Formulation 18

2.4 Optimal Solution of QoS Constrained Sum-Throughput Maximization 21

2.4.1 Case (I): Positive z_1^*, z_{21}^* and z_{22}^* 25

2.4.2 Case (II): Positive z_1^* and z_{22}^*, and undefinable z_{21}^* 35

2.5 QoS Constrained Sum-Throughput Maximization Algorithm 40
2.5.1 Proposed Algorithm 41
2.5.2 Computational Complexity Comparison 42
2.6 Sum-Throughput Maximization with Processing Cost 46
2.7 Simulation Results 48
2.8 Conclusion 53

3 NOMA-Based Wireless Powered Communication Networks with User Clustering 56

3.1 Introduction 57
3.1.1 Throughput Maximization in WPCN 58
3.1.2 User Clustering in NOMA 59
3.1.3 Motivation and Contribution 60
3.2 System model 62
3.3 Optimal Beamforming And Resource Allocation 66
3.3.1 Beamforming Design 67
3.3.2 Sum-Throughput Maximization 69
3.3.3 TDMA-based WPCN with Cluster-specific Beamforming . 76
3.4 Simulation Results 79
3.5 Conclusion 87

4 IRS-Assisted Wireless Powered Communication Networks: Comparison of NOMA and OMA 89

4.1 Introduction 90
4.2 System Model 91
4.2.1 NOMA-based WPCN 92
4.2.2 OMA-based WPCN 94
4.3 Sum-Throughput Maximization 94

4.3.1 NOMA-based WPCN with throughput constraints 95
4.3.2 OMA-based WPCN with throughput constraints 98
4.4 Simulation Results 99
4.5 Conclusion 102

5 Conclusion **106**
5.1 Summary 106
5.2 Future directions 107

Abstract (In Korean) **117**

감사의 글 **119**

List of Tables

2.1 Classification of the sub-problems in **(P2)**. 25

List of Figures

2.1 Two-user WPCN system model. 15

2.2 Illustration of a two-user WPCN with user cooperation transmission protocol. 18

2.3 Classification of the maximization problem with feasible (θ_1, θ_2) when $\theta_1^{(c1)} + \theta_2^{(c)} > \theta_1^{(c2)}$. 32

2.4 Algorithm concept when $\theta_1^{(c1)} + \theta_2^{(c)} > \theta_1^{(c2)}$, $D_{10} = 10$ m and $D_{20} = D_{12} = 5$ m. 44

2.5 Algorithm concept when $\theta_1^{(c1)} + \theta_2^{(c)} \leq \theta_1^{(c2)}$, $D_{10} = 10$ m, $D_{20} = 9.5$ m, and $D_{12} = 0.5$ m. 44

2.6 Throughput with various QoS constraints when $D_{10} = 10$ m and $D_{20} = D_{12} = 5$ m. 49

2.7 Throughput with various θ_1 and $\theta_2 = 1.5$ bps/Hz when $D_{10} = 10$ m and $D_{20} = D_{12} = 5$ m. 50

2.8 Average sum-throughput with various QoS constraints when $D_{10} = 10$ m and $D_{20} = D_{12} = 5$ m. 51

2.9 Average throughput of U_1 with various QoS constraints when $D_{10} = 10$ m and $D_{20} = D_{12} = 5$ m. 51

2.10 Average throughput of U_2 with various QoS constraints when $D_{10} = 10$ m and $D_{20} = D_{12} = 5$ m. 52

2.11 Achievable rate region with various $P_{c,21}$. 53
2.12 Throughput performance with various $P_{c,21}$ when $\theta_1 = 6$ bps/Hz and $\theta_2 = 0$ bps/Hz. 54
2.13 Energy consumption for transmission during τ_t with various $P_{c,21}$ when $\theta_1 = 6$ bps/Hz and $\theta_2 = 0$ bps/Hz. 54

3.1 An LM-user WPCN system model 63
3.2 An illustration of a received signal decoupled to M independent streams, each of which consists of L messages. 66
3.3 Sum-throughput versus SINR threshold of θ in WPCNs of $(L, M, N, W) = (2, n_M, 5, 3)$ where $n_M \in \{2, ..., 5\}$ for 4, 6, 8, and 10 users. 80
3.4 Sum-throughput versus SINR threshold of θ in WPCNs of $(L, M, N, W) = (2, 6, 4, 3)$, $(L, M, N, W) = (3, 4, 4, 3)$, $(L, M, N, W) = (4, 3, 4, 3)$, and $(L, M, N, W) = (6, 2, 4, 3)$. 81
3.5 Sum-throughput versus SINR threshold of θ with and without the optimization of cluster-specific beamforming in a WPCN of $(L, M, N, W) = (2, 4, 4, 3)$. 82
3.6 Sum-throughput versus SIC error propagation ratio of β comparison between the proposed scheme with various SINR thresholds and the scheme given in [41] in a WPCN of $(L, M, N, W) = (2, 4, 3, 1)$. . . 83
3.7 Sum-throughput and Jain's fairness index with various QoS thresholds of ϕ for NOMA and OMA each with signal alignment in a WPCN of $(L, M, N, W) = (2, 2, 2, 2)$. 85
3.8 Sum-throughput gap between the proposed scheme and the scheme with optimal clustering in WPCNs of $(L, M, N, W) = (2, n_M, 3, 2)$ where $n_M \in \{2, 3, 4\}$ for 4, 6, and 8 users. 86

4.1 An IRS-assisted WPCN with K users 92

4.2 Simulation setup 100
4.3 Sum-throughput versus τ_0 in a NOMA-based WPCN with an IRS for given throughput constraint, ϕ. 101
4.4 Impact of IRS on throughput performance of a NOMA-based WPCN and an OMA-based WPCN along with various throughput constraints, ϕ. 103
4.5 Throughput performance of an IRS-assisted WPCN along with various horizontal distances of IRS, d_H. 104

Chapter 1

Introduction

In the next generation of communication networks such as Internet of Things (IoT) networks, various types of devices will be connected to the wireless network constantly, and a significant amount of energy stored in each device will be consumed [2], [25], [33], [34]. Accordingly, battery limitations of devices are expected to be a major limitation for accommodating emerging services in the next generation of communication systems. For seamless operation of wireless devices, management of energy resource such as wiring to an external power source or replacing batteries is needed. However, due to the ubiquitous nature of the upcoming wireless networks, wired charging or manual battery replacement can be impractical depending on the number of devices or their deployments. Therefore, the need for wireless battery charging arises for devices to achieve sustainable access in energy-constrained wireless networks, and for ease of operation and maintenance of the network [35], [36]. To realize wireless battery charging, especially in the far-field, energy harvesting has been studied which converts a radio-frequency (RF) signal into electrical energy to be stored in a battery [1], [6]. In particular, harvesting energy from RF signals transmitted by a dedicated energy source is called wireless power transfer (WPT). WPT has attracted a significant amount of attention for its controllability compared to ambient

RF energy harvesting [7], [8].

As a new framework on the design of a wireless network with WPT, a wireless powered communication network (WPCN) has been proposed [9]. A WPCN consist of a hybrid access point (H-AP) with external power supply and wireless devices with no energy source, but rechargeable batteries and energy harvesting capability. A H-AP serves multiple devices in a network as a base station (BS) while transferring energy to the devices as a dedicated energy source. In a WPCN, a H-AP transfers energy to energy harvesting devices via downlink (DL), which is called wireless energy transfer (WET), and the devices transmit information to the H-AP using the harvested energy via uplink (UL), which is called wireless information transmission (WIT).

A single transmission in a WPCN consists of DL-WET and UL-WIT so that devices can recharge their batteries and transmit information continually. Accordingly, a harvest-then-transmit protocol was proposed, in which DL-WET occurs before UL-WIT. Due to the restriction on time resources for both DL-WET and UL-WIT, and energy resources harvested for DL-WET, resource allocation has been essential in a WPCN to utilize the system. Various objectives such as sum-throughput maximization for high spectral efficiency, power minimization for energy efficiency, and total transmission time minimization for low latency can be addressed in the resource allocation for a WPCN [9], [18], [19], [42], [44], etc. In addition, several constraints can be taken into account to further increase the system performance [18], [45], [46]. Particularly, since IoT for the next generation of communication networks enables a variety of types of devices to communicate over the air, each device is expected to require a certain level of performance in data transmission depending on its device type, data type, etc [25]. Quality of service (QoS) constraints guarantee to meet such requirements, which can be throughput thresholds on the individual throughput, signal to interference-plus-noise ratio (SINR) thresholds for reliable decoding, etc. In this dissertation, I mainly explore resource allocation for maximizing the sum-throughput

of a WPCN with a set of QoS requirements.

1.1 Related Work

1.1.1 Wireless Powered Communication Networks

Due to the broadcast and superposition nature of wireless medium, multiple access should be employed in UL-WIT for a WPCN with multiple users [31]. Note that the terms, user and device are used interchangeably. One approach is orthogonal multiple access (OMA) such as time division multiple access (TDMA) and frequency division multiple access (FDMA). A resource block in time, frequency, and code domains is allocated to a single user so that it does not experience any inter-user interference. A WPCN where users transmit according to OMA is called an OMA-based WPCN. In particular, TDMA is adopted as OMA in this dissertation. Then, the time for DL-WET and the time allocated for each user to transmit in UL-WIT are jointly optimized.

It has been found that WPCN inherently suffers from the so-called *doubly near-far problem* [9]. Due to the signal power attenuation over distance, a user far from the H-AP harvests much less energy, and needs to spend even more energy to achieve the same rate compared to a user close to the H-AP. Thus, a user close to the H-AP is allocated much more resources than a user far from the H-AP compared to the conventional networks to maximize the sum-throughput. There have been a number of studies on reducing doubly near-far problem for avoiding severe user unfairness [9], [12]- [16], [22], [32]. One of these approaches is to maximize different objective functions such as minimum individual throughput, weighted sum-throughput, proportional fairness, etc [9], [32]. Another approach is to exploit the multi-antenna system [12], [13]. By the design of beamforming using multiple antennas, a user far from the H-AP can increase the amount of harvested energy or transmission rate

more than a user close to the H-AP. Besides, adopting a relay can be considered to increase the rate of a user far from the H-AP, or a user close to the H-AP shares its harvested energy with a user far from the H-AP by transferring a part of it via out-of-band channels [14]- [16], [22]. Nevertheless, the aforementioned techniques may induce sum-throughput loss as they sacrifice the performance of a user that is superior in both energy transfer and spectral efficiency, or may not be cost-effective as they require to employ additional equipment.

Another important solution to the doubly near-far problem is user cooperation [24]. In a WPCN with the user cooperation protocol, a user close to the H-AP acts as a relay, relaying the information of the user far from the H-AP by using a portion of its time and energy resources during UL-WIT. The results showed that user cooperation enhances the throughput of a user far from the H-AP without any deterioration of the throughput that a user close to the H-AP can achieve. Despite the benefits of user cooperation, a user close to the H-AP needs to decode the message of the other user, which may result in additional processing cost and decoding error. Moreover, outage may occur in relay transmission. Thus, there is no need to employ user cooperation when the system does not benefit from it. In Chapter 2, I explore the sum-throughput maximization in a WPCN with user cooperation protocol while ensuring QoS. Particularly, by characterizing the conditions under which user cooperation becomes effective, I propose a novel algorithm that exploits user cooperation efficiently.

1.1.2 A NOMA-Based WPCN

In addition to OMA, non-orthogonal multiple access (NOMA) has been adopted as a multiple access scheme for UL-WIT in a WPCN [23], [41], [44]- [46]. There has been a great interest in NOMA transmission as it is expected to facilitate the features of the next generation communication systems such as higher spectral efficiency, ultra-low

latency, and massive connectivity compared to OMA [37]- [40]. On the contrary to OMA, where a single user is exclusively allocated one resource block, multiple users are given access to the same resource block in NOMA transmission. Particularly, in the uplink NOMA transmission, the BS receives the superposition of signals transmitted by multiple users over the same resource. Thus, the BS performs successive interference cancellation (SIC) to remove inter-user interference and decode the messages. That is, a message of a user is decoded treating interferences as noise, and is subtracted from the received signal at the BS. Thus, a user of its message decoded next experiences less interference than a user of its message decoded before.

Furthermore, NOMA can enhance user fairness by controlling the SIC decoding order in maximizing the sum-throughput. In order to maximize the sum-throughput, a majority of resources are given users with better channel in OMA transmission. On the other hand, decoding order does not affect the sum-throughput in NOMA transmission. Thus, a user with worse channel can achieve higher throughput than in OMA if its message is decoded after SIC. Particularly, NOMA becomes more effective in enhancing user fairness as the difference in channel status between users increases and the number of users served by NOMA decreases because a user with better channel experiences relatively lower level of interference. While NOMA is expected to enhance various system performances from a theoretical perspective, there are several implementation issues related to the NOMA decoding in practice [47]- [49]. The implementation complexity of SIC increases with the growing number of users served by a BS. Furthermore, SIC error propagation may occur due to the incomplete interference cancellation, which results in severe throughput degradation. Therefore, it needs to limit the number of users in a single NOMA transmission, and thus user grouping or clustering has been adopted to NOMA [50], [51].

I focus on that NOMA can be more effective in enhancing user fairness in a WPCN since the effective channels of users differ more in a WPCN due to the

doubly near-far problem than in a conventional network. To this end, I consider a WPCN where NOMA is employed as a multiple access scheme for UL-WIT (i.e., a NOMA-based WPCN) while ensuring QoS. Particularly, in Chapter 3, user clustering is adopted for a NOMA-based WPCN. By grouping users with large channel difference, the drawback of a WPCN is harnessed to enhance user fairness. Furthermore, in Chapter 4, I explore a potential benefit that an intelligent reflecting surface (IRS), which has recently received great attention, can bring to a WPCN [57]. An IRS consists of a number of passive elements that reflect radio-frequency (RF) signals and induce phase shifts on the signals. Since an IRS brings changes in the effective channels of users, the performance of a network assisted by an IRS can be enhanced by designing the beamforming of the passive elements. Thus, I explore the effect of the employment of an IRS on a NOMA-based WPCN and compare it to that of an OMA-based WPCN.

1.2 Contributions and Organization

In this dissertation, I consider various system models for WPCNs where several approaches applied in order to improve the system performance such as spectral efficiency, user fairness, etc. System designs and resource allocation schemes for sum-throughput maximization with QoS constraints in the considered system models are developed.

In Chapter 2, I formulate a sum-throughput maximization problem with QoS constraints for a cooperative WPCN, where a user with better channel condition relays information of a user with worse channel. In particular, QoS constraints are given as individual throughput thresholds. From the derived solution, the conditions under which the WPCN benefits from the cooperation in achieving the maximum sum-throughput are characterized. I propose an efficient resource allocation algorithm

which reduces unnecessary computational cost and processing cost.

In Chapter 3, I consider a NOMA-based WPCN equipped with multiple antennas. Additionally, to address the SIC decoding issues, user clustering by beamforming exploiting the multi-antenna system called signal alignment is applied. Due to the difficulty of jointly optimizing cluster-specific beamforming and resources for sum-throughput maximization, I determine the beamforming relying on signal alignment first, and then the resources are optimized for given beamforming. In particular, a sum-throughput maximization problem with SINR thresholds is formulated to optimize the resources such as time, energy, and DL energy beamforming. Novel algorithms for beamforming design and sum-throughput maximization are proposed. Numerical results show the sum-throughput performance of the proposed scheme and its robustness to SIC error propagation compared to an existing schemes.

In Chapter 4, I consider a NOMA-based WPCN and an OMA-based WPCN, both of which are assisted by an IRS. For both multiple access schemes, sum-throughput maximization problems subject to minimum throughput constraints are formulated. Due to the non-convexity of the problems, they are relaxed into multiple convex problems. The performance of each scheme is evaluated, in particular, in terms of sum-throughput and user fairness, and is compared to each other. Numerical results show that user fairness in NOMA significantly depends on the position of an IRS, but not in OMA, which suggests that it needs to adopt different strategies according to the multiple access scheme to achieve a specific level of user fairness.

In Chapter 5, I summarize my works and indicate the future directions of my works.

1.3 Notation

Boldface lowercase and capital letters indicate vectors and matrices, respectively. For a matrix $\mathbf{A}$, $\mathbf{A}^T$ and $\mathbf{A}^H$ denote a transpose, conjugate complex transpose of $\mathbf{A}$, respectively, and span$(\mathbf{A})$ stands for the space spanned by the column vectors of $\mathbf{A}$. For a vector $\mathbf{a}$, diag$(\mathbf{a})$ represents a diagonal matrix whose diagonal entries are elements of $\mathbf{a}$. $(\cdot)^*$ represents an optimal value of a variable. $\mathbf{I}_n$ is an $n \times n$ identity matrix. $(\mathbf{A})_{ij}$ denotes the (i, j)-th element of the matrix $\mathbf{A}$. A vector $\mathbf{a}$ whose entries follow a complex normal distribution with the mean of μ and the variance of σ^2 is denoted by $\mathbf{a} \sim \mathcal{CN}(\mu, \sigma^2\mathbf{I})$.

Chapter 2

Wireless Powered Communication Networks with User Cooperation

A wireless powered communication network (WPCN) is considered, which has a hybrid access point (H-AP) and two users with energy harvesting capabilities. The H-AP transfers energy to the users during downlink (DL) transmission, and the users transmit information to the H-AP during uplink (UL) transmission by utilizing the harvested energy. To enhance user fairness, a user cooperation protocol is employed in which a user close to the H-AP relays the message of the other user by partially using its allocated time and available energy resources. By jointly optimizing the time allocation for DL energy transfer and UL information transmission, the sum-throughput in the considered network subject to a set of quality of service (QoS) requirements is maximized. The optimization problem is solved through a divide-and-conquer approach along with convex optimization techniques, and thus an analytical solution is derived. In particular, the conditions under which the WPCN benefits from the user cooperation in achieving the maximum sum-throughput are fully characterized. Furthermore, an efficient resource allocation algorithm to find the optimal solution under QoS requirements is presented.

2.1 Introduction

Wireless energy harvesting has recently attracted a significant amount of attention for the next generation communication systems as it is expected to prolong the lifetime of wireless networks delivering self-sustainability without manual battery recharge or replacement [1], [2]. In particular, harvesting energy from far-field radio-frequency (RF) signal radiated from a dedicated energy source has been studied as a promising solution to energy-constrained wireless networks since it is more controllable than other sources such as solar energy, ambient radio power, etc. [3]- [8].

Recently, wireless powered communication networks (WPCNs) have emerged as a new framework to the design of wireless networks, which consist of a hybrid access point (H-AP) with external power supply and wireless devices with no energy source, but rechargeable batteries [9]. In [9], a harvest-then-transmit protocol was proposed in which wireless devices are powered from RF signals radiated from a H-AP via the downlink (DL), called wireless energy transfer (WET), which send information using the harvested energy via the uplink (UL), called wireless information transmission (WIT). In particular, wireless devices send messages to the H-AP in time division multiple access (TDMA). The time allocation for DL-WET and UL-WIT is jointly optimized to maximize the sum-throughput performance.

Subsequently, a number of works on WPCNs have been presented under different network scenarios from various perspectives [10]- [20]. In [10], a WPCN with a full-duplex H-AP was explored. In [11], two types of users in a WPCN were considered: an energy-harvesting type of device and a device powered from an external power source. In [12] and [13], a multi-antenna system is applied to the H-AP to enable DL energy beamforming and UL receive beamforming. In [14]- [16], cooperative communication was applied to WPCNs by deploying a dedicated relay with an energy harvesting circuit. In [17], a device was proposed to harvest more energy by deploying a power beacon with an external power supply, while in [18], idle users scavenge

energy from the interferences, in [19], jamming interference energy is harvested to increase the transmit power, and in [20], an energy-harvesting relay transferring energy was proposed. In [21], a two-user Gaussian interference channel in addition to an extra non-collocated energy harvesting device was studied in which a channel-output feedback link is available from each receiver to the corresponding transmitter.

It has been found that WPCN inherently suffers from the so-called *doubly near-far problem* [9]. Due to the signal power attenuation over distance, a user far from the H-AP harvests much less energy, and needs to spend even more energy to achieve the same rate compared to a user close to the H-AP. This leads to severer user unfairness compared to the conventional wireless communication networks. Many attempts have been made to alleviate the user unfairness in WPCNs [9], [12], [13], [22]- [23], etc. One of these approaches is to maximize the minimum rate among the users by the joint design of DL-WET and UL-WIT, thereby a user far from the H-AP can be allocated with more time to transmit information [9]. Nevertheless, it induces sum-throughput performance loss as it sacrifices the rate of a user close to the H-AP. Another approach exploits the multi-antenna system at the H-AP, making the H-AP deliver more energy to a particular user by energy beamforming during DL-WET [12], [13]. Careful design of the beamforming vector makes it possible for a user with a worse channel to harvest more energy, which reduces the user unfairness. However, it is likely that the uplink spectral efficiency decreases due to the large amount of feedback overhead from the multi-antenna system. In [22], energy cooperation was introduced. Users that harvest more energy transfer part of their energy to those which do not have sufficient energy via out-of-band channels. Hence, the rate disparity between the users becomes smaller at the expense of the rates of users in a better channel state. In [23], non-orthogonal multiple access (NOMA) was applied to a WPCN as a multiple access scheme during UL-WIT. It mitigates user unfairness by controlling the decoding order at the H-AP, but it requires successive interference

cancellation, causing an increment in implementing and processing cost at the H-AP.

Another important solution to the doubly near-far problem is user cooperation [24]. In a WPCN with the user cooperation protocol, a user close to the H-AP acts as a relay, relaying the information of the user far from the H-AP by using a portion of its time and energy resources during UL-WIT. Furthermore, in [24], the weighted sum-throughput (WST) maximization problem was studied, and the corresponding algorithm which returns the optimal time allocation for DL-WET and UL-WIT was proposed. The results showed that user cooperation enhances the throughput of a user far from the H-AP without any deterioration of the throughput of a user close to the H-AP.

Meanwhile, the internet of things (IoT) for the next generation of communication networks enables a variety of types of devices to communicate over the air [25], and each device is expected to require a variety of quality of service (QoS) depending on its purpose of the operation. One of the options to guarantee the QoS is to put a threshold on the signal to noise ratio (SNR) of links as a constraint for reliable decoding. In particular, the constraint on the SNR becomes a linear constraint with respect to the optimization variables in the WPCN with user cooperation since the SNRs of the links depend on the ratio of the energy harvesting time during DL-WET to the transmission time during UL-WIT. However, it is inappropriate to put such constraints because each link easily meets the threshold of SNR by lowering the transmission time. As a matter of fact, this may result in significant degradation of the throughput of a user since the throughput is also proportional to the transmission time for a given SNR. Another option is to put weights on throughputs of users (i.e., to maximize the weighted sum-throughput) as in the prior work [24]. The WST maximization with user cooperation tends to implicitly achieve the desired level of throughput while enhancing user fairness. However, it may fail to guarantee performance when a device requires to achieve specific throughput. In particular, the WST

maximization approach demands exhaustive search over the set of weights to meet the specific throughput requirement, which is challenging. Hence, it needs to regard throughput as a QoS requirement explicitly in WPCNs with user cooperation. In other words, it needs to impose a threshold on the throughput as a constraint to guarantee the QoS. Moreover, the WST maximization has high computational complexity as it searches the optimal point numerically by jointly optimizing the primal and dual problems. In this regard, I formulate a new sum-throughput maximization problem under individual QoS constraints on user throughputs with user cooperation and provide the optimal solution in an analytical form.

The maximization problem is converted into an equivalent convex optimization problem, which can be solved with numerical methods such as the interior-point-method, etc [26]. Nevertheless, such methods are of high complexity in the process of finding the optimal solution, and do not provide any knowledge on how the system works. Therefore, I solve the maximization problem through the divide-and-conquer approach [27] to obtain the optimal solution in an analytical form. The problem is divided into multiple sub-problems which develop into linear systems, and the analytical solutions of sub-problems are derived individually. Subsequently, the solutions to sub-problems are merged into the solution to the original problem. By analyzing the derived solution, I show that the maximization problem is categorized as one of the three cases according to the given QoS constraints: i) the case in which user cooperation becomes beneficial over the conventional WPCNs [9]. ii) the case in which user cooperation does not provide any gain in achieving the maximum sum-throughput. iii) the case in which user cooperation should not be used. The corresponding conditions for the three cases are characterized. Furthermore, I propose a QoS constrained sum-throughput maximization algorithm, of which computational complexity is reduced by avoiding unnecessary computations.

The main contributions of this chapter are threefold. Firstly, I formulate an opti-

mization problem to maximize the sum-throughput in WPCNs with user cooperation under individual QoS constraints. The optimal time allocation for DL-WET and UL-WIT is derived in an analytical form. Secondly, an analytical solution demonstrates under which conditions user cooperation should or should not be exploited. Lastly, I provide an efficient algorithm that returns the optimal time allocation to maximize the sum-throughput for given QoS constraints.

The remainder of this chapter is organized as follows. In section 2.2, the system model of a two-user WPCN with user cooperation is introduced. The sum-throughput maximization problem under QoS constraints is formulated in section 2.3 and the optimal solution is presented in section 2.4. The sum-throughput maximization algorithm under QoS constraints is proposed in section 2.5, and the results are verified with simulations in section 2.7. I conclude the chapter in section 2.8.

2.2 System model

As shown in Fig. 2.1, I consider a network with one H-AP and two users, U_1 and U_2. The H-AP and the users are assumed to be equipped with a single antenna each. It is assumed that the channel undergoes block fading (i.e., the channel coefficient is constant over one transmission time, T) and the channel reciprocity holds. For convenience, I use transceiver indices, i and j where $i, j \in \{0, 1, 2\}$ for the H-AP, U_1 and U_2 respectively. The channel coefficient between the H-AP and U_i where $i \in \{1, 2\}$ is denoted by $\tilde{h}_{i0}$ and that between U_1 and U_2 is denoted by $\tilde{h}_{12}$. The power gain of a channel coefficient, $\tilde{h}_{ij}$ where $ij \in \{10, 20, 12\}$ is denoted by h_{ij} where $h_{ij} = |\tilde{h}_{ij}|^2$. Following the log-distance path loss model [28], h_{ij} is expressed as

$$h_{ij} = 10^{-3} g_{ij} D_{ij}^{-\alpha}, \tag{2.1}$$

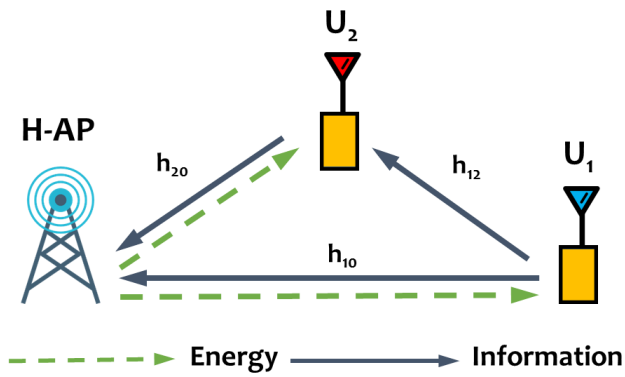

Figure 2.1: Two-user WPCN system model.

where g_{ij} is the power of the short-term fading channel coefficient, α is the path-loss exponent and D_{ij} is the distance between transceiver i and transceiver j.[1] If the channel, for instance, undergoes Rayleigh fading for the short-term fading, $g_{ij} = |\tilde{g}_{ij}|^2$ where $\tilde{g}_{ij} \sim \mathcal{CN}(0, 1)$. The H-AP is assumed to have all the channel state information at the beginning of the transmission block in advance. Without loss of generality, I assume that U_2 has a better channel condition than U_1 (i.e., $h_{20} \geq h_{10}$.) Note that U_2 has higher efficiency in both energy transfer and information transmission by assumption. Hence, U_2 acts as a relay in the considered network to mitigate the doubly near-far problem with the user cooperation protocol [24]. Otherwise, U_1 sacrifices more of its allocated time and energy resources for information transmission of its own message, which results in more severe user unfairness. Therefore, U_2 should forward the message of U_1 after U_1 broadcasting its message. Accordingly, I further assume that the channel between the users is better than the channel between the H-AP and U_1 for more reliable decoding at U_2 in order to utilize user cooperation (i.e., $h_{12} \geq h_{10}$.)

The transmission protocol with user cooperation [24] is as follows. One trans-

[1]The path loss at a reference distance of 1 m is assumed to be 30 dB.

mission block of duration, T, is divided into four different parts, $\tau_0 T$, $\tau_1 T$, $\tau_{21} T$, and $\tau_{22} T$, where they need to satisfy

$$\tau_0 + \tau_1 + \tau_{21} + \tau_{22} \leq 1. \tag{2.2}$$

$\tau_0 T$ is allocated for DL-WET and, $\tau_1 T$, $\tau_{21} T$, and $\tau_{22} T$ are allocated for UL-WIT. In particular, during UL-WIT, $\tau_1 T$ is allocated for U_1 to transmit its information, while $\tau_{21} T$ and $\tau_{22} T$ are allocated for U_2 to relay U_1's message received during $\tau_1 T$ and to transmit its own information, respectively. The relay strategy for user cooperation is assumed to be decode-and-forward (DF) relaying.

For convenience, I assume that the single transmission time, T is normalized to 1. The received signal at transceiver i during τ_t where $t \in \{0, 1, 21, 22\}$ is denoted by $y_i^{(t)}$. During τ_0, the H-AP transmits only an energy signal, $x_0 \sim \mathcal{CN}(0, P_0)$ where P_0 is the transmit power of the H-AP. (i.e., $\mathbb{E}\left[|x_0|^2\right] = P_0$.) The received signal at U_i can be expressed as

$$y_i^{(0)} = \tilde{h}_{i0} x_0 + n_i, i \in \{1, 2\}, \tag{2.3}$$

where n_i is the circularly symmetric complex Gaussian noise and $n_i \sim \mathcal{CN}(0, \sigma_i^2)$. Each user harvests the energy of E_i,

$$E_i = \zeta_i P_0 h_{i0} \tau_0, i \in \{1, 2\}, \tag{2.4}$$

where ζ_i is the energy harvesting efficiency at U_i.[2] During τ_1, U_1 transmits with the transmit power of P_1,

$$P_1 \leq \frac{\eta_1 E_1}{\tau_1} = \eta_1 \zeta_1 P_0 h_{10} \frac{\tau_0}{\tau_1}, \tag{2.5}$$

[2]It is assumed that the noise power is not harvested at each user because the amount of the harvested energy from the noise is significantly small. Furthermore, since the H-AP transmits an energy signal with a fixed power of P_0, E_i is the product of a constant and τ_0 even with the non-linear energy harvesting model.

where η_i, $i \in \{1, 2\}$ denotes a fixed portion of harvested energy to be used for information transmission at each user.[3] The received signals at the H-AP and U_2 become

$$y_i^{(1)} = \tilde{h}_{1i} x_1 + n_i, i \in \{0, 2\}, \tag{2.6}$$

where $x_1 \sim \mathcal{CN}(0, P_1)$. During τ_{21} and τ_{22}, U_2 relays U_1's message received during τ_1 with the transmit power of P_{21} and transmits its own information with the transmit power of P_{22}, respectively. The sum of the energy consumed by U_2 during τ_{21} and τ_{22} is constrained as

$$\tau_{21} P_{21} + \tau_{22} P_{22} \leq \eta_2 E_2 = \eta_2 \zeta_2 P_0 h_{20} \tau_0. \tag{2.7}$$

The received signals at the H-AP during τ_{21} and τ_{22} can be expressed as

$$y_0^{(2l)} = \tilde{h}_{20} x_{2l} + n_0, l \in \{1, 2\}, \tag{2.8}$$

where $x_{2l} \sim \mathcal{CN}(0, P_{2l})$. Fig. 2.2 illustrates the transmission protocol in a time-ordered sequence.

The throughput of U_k's message where $k \in \{1, 2\}$ over a link from a transceiver i to another transceiver j is denoted by $R_k^{(ij)}(\boldsymbol{\tau}, \mathbf{P})$ and $\boldsymbol{\tau} = [\tau_0, \tau_1, \tau_{21}, \tau_{22}]$ and $\mathbf{P} = [P_1, P_{21}, P_{22}]$. The throughputs of the considered links are given by

$$R_1^{(1j)}(\boldsymbol{\tau}, \mathbf{P}) = \tau_1 \log_2 \left(1 + \frac{P_1 h_{1j}}{\sigma_j^2}\right), j \in \{0, 2\}, \tag{2.9}$$

$$R_k^{(20)}(\boldsymbol{\tau}, \mathbf{P}) = \tau_{2k} \log_2 \left(1 + \frac{P_{2k} h_{20}}{\sigma_0^2}\right), k \in \{1, 2\}. \tag{2.10}$$

The throughput of U_1 is denoted by $R_1(\boldsymbol{\tau}, \mathbf{P})$. For the message of U_1 which is Gaussian distributed, the relay channels are orthogonalized in the time domain, (i.e., τ_1 and τ_{21}) and the message is relayed with DF strategy. Hence, according to [29], $R_1(\boldsymbol{\tau}, \mathbf{P})$ is determined as

$$R_1(\boldsymbol{\tau}, \mathbf{P}) = \min \left[R_1^{(10)}(\boldsymbol{\tau}, \mathbf{P}) + R_1^{(20)}(\boldsymbol{\tau}, \mathbf{P}), R_1^{(12)}(\boldsymbol{\tau}, \mathbf{P}) \right]. \tag{2.11}$$

[3] η_i can be adjusted adaptively for each i in order to factor the processing cost in determining the amount of energy to be consumed for information transmission.

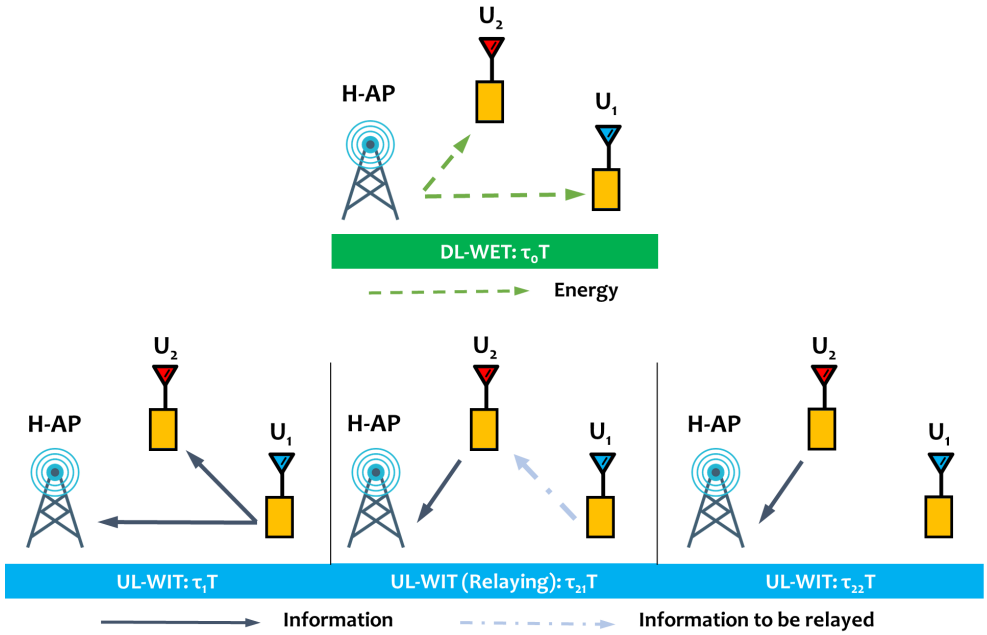

Figure 2.2: Illustration of a two-user WPCN with user cooperation transmission protocol.

On the other hand, since U_2's message is solely delivered over the link from U_2 to the H-AP, the throughput of U_2, which is denoted by $R_2(\boldsymbol{\tau}, \mathbf{P})$, equals $R_2^{(20)}(\boldsymbol{\tau}, \mathbf{P})$.

2.3 Problem Formulation

In this section, I formulate the sum-throughput maximization under QoS constraints for a two-user WPCN with user cooperation. Let the target throughputs of U_1 and U_2 be θ_1 and θ_2, respectively. Following the system model in Section 2.2, I formulate the

maximization problem as

$$\textbf{(P1)}: \max_{\boldsymbol{\tau},\mathbf{P}} \quad R_1(\boldsymbol{\tau},\mathbf{P}) + R_2(\boldsymbol{\tau},\mathbf{P}) \tag{2.12a}$$

$$\text{s.t.} \quad \tau_0 + \tau_1 + \tau_{21} + \tau_{22} \leq 1, \tag{2.12b}$$

$$\tau_1 P_1 \leq \eta_1 E_1, \tag{2.12c}$$

$$\tau_{21} P_{21} + \tau_{22} P_{22} \leq \eta_2 E_2, \tag{2.12d}$$

$$\boldsymbol{\tau} \succeq 0, \mathbf{P} \succeq 0, \tag{2.12e}$$

$$R_1(\boldsymbol{\tau},\mathbf{P}) \geq \theta_1, \tag{2.12f}$$

$$R_2(\boldsymbol{\tau},\mathbf{P}) \geq \theta_2. \tag{2.12g}$$

(2.12b), (2.12c), and (2.12d) are a total transmission time restriction, an energy causality constraint for U_1, and an energy causality constraint for U_2 respectively. (2.12e) derives from the need for the amount of time and power to be non-negative. (2.12f) and (2.12g) are the individual QoS requirements on the throughputs of U_1 and U_2.[4] Note that **(P1)** is not a convex problem, which can be proved by showing the Hessian matrix of the objective function of **(P1)** is neither positive semi-definite nor negative semi-definite.

To make the problem solvable with the convex optimization technique [24], the optimization variable, P_1 is replaced with $\eta_1 \zeta_1 P_0 h_{10} \frac{\tau_0}{\tau_1}$ from (2.12c), which is valid because (2.12c) should hold with its equality at optimum; otherwise, there will be a waste of energy resources in U_1. Furthermore, the new variables, t_{21} and t_{22}, are introduced as

$$t_{21} \triangleq \frac{\tau_{21} P_{21}}{\eta_2 \zeta_2 h_{20} P_0}, \; t_{22} \triangleq \frac{\tau_{22} P_{22}}{\eta_2 \zeta_2 h_{20} P_0}, \tag{2.13}$$

and P_{21} and P_{22} are replaced with $\eta_2 \zeta_2 h_{20} P_0 \frac{t_{21}}{\tau_{21}}$ and $\eta_2 \zeta_2 h_{20} P_0 \frac{t_{22}}{\tau_{22}}$, respectively. It can be easily shown that $t_{21} + t_{22} \leq \tau_0$ from (2.12d) with simple manipulations. t_{21}

[4] **(P1)** is the addition of QoS constraints to the WST maximization problem of [24] where each user's weight is set to one.

and t_{22} can be regarded as the energy harvesting times of U_2 for relaying the message of U_1 and transmitting its own message, respectively. Therefore, the throughputs given in (2.9)-(2.10) become

$$R_1^{(1j)}(\boldsymbol{\tau}, \boldsymbol{t}) = \tau_1 \log_2 \left(1 + \rho_1^{(1j)} \frac{\tau_0}{\tau_1}\right), j \in \{0, 2\}, \tag{2.14}$$

$$R_k^{(20)}(\boldsymbol{\tau}, \boldsymbol{t}) = \tau_{2k} \log_2 \left(1 + \rho_2 \frac{t_{2k}}{\tau_{2k}}\right), k \in \{1, 2\}, \tag{2.15}$$

where $(\boldsymbol{\tau}, \boldsymbol{t}) = [\boldsymbol{\tau}, t_{21}, t_{22}]$,

$$\rho_1^{(1j)} = h_{10} h_{1j} \eta_1 \zeta_1 P_0 / \sigma_j^2, \text{ and } \rho_2 = h_{20}^2 \eta_2 \zeta_2 P_0 / \sigma_0^2. \tag{2.16}$$

The corresponding maximization problem becomes

$$\textbf{(P1}'\textbf{)}: \max_{\boldsymbol{\tau}, \boldsymbol{t}} \quad R_1(\boldsymbol{\tau}, \boldsymbol{t}) + R_2(\boldsymbol{\tau}, \boldsymbol{t}) \tag{2.17a}$$

$$\text{s.t.} \quad \tau_0 + \tau_1 + \tau_{21} + \tau_{22} \leq 1, \tag{2.17b}$$

$$t_{21} + t_{22} \leq \tau_0, \tag{2.17c}$$

$$R_1(\boldsymbol{\tau}, \boldsymbol{t}) \geq \theta_1, \tag{2.17d}$$

$$R_2(\boldsymbol{\tau}, \boldsymbol{t}) \geq \theta_2. \tag{2.17e}$$

Since $R_1(\boldsymbol{\tau}, \boldsymbol{t}) = \min\left[R_1^{(10)}(\boldsymbol{\tau}, \boldsymbol{t}) + R_1^{(20)}(\boldsymbol{\tau}, \boldsymbol{t}), R_1^{(12)}(\boldsymbol{\tau}, \boldsymbol{t})\right]$, a new optimization variable, $\bar{R}$ is adopted to provide the equivalent epigraph representation of **(P1′)**, where $\bar{R} = R_1(\boldsymbol{\tau}, \boldsymbol{t})$. Then, $\bar{R}$ should be at most both terms in the minimum in

$R_1(\boldsymbol{\tau}, \boldsymbol{t})$. Therefore, **(P1′)** is transformed into

$$\textbf{(P2)}: \max_{\bar{R}, \boldsymbol{\tau}, \boldsymbol{t}} \quad \bar{R} + R_2(\boldsymbol{\tau}, \boldsymbol{t}) \tag{2.18a}$$

$$\text{s.t.} \quad \tau_0 + \tau_1 + \tau_{21} + \tau_{22} \leq 1, \tag{2.18b}$$

$$t_{21} + t_{22} \leq \tau_0, \tag{2.18c}$$

$$\bar{R} \leq R_1^{(10)}(\boldsymbol{\tau}, \boldsymbol{t}) + R_1^{(20)}(\boldsymbol{\tau}, \boldsymbol{t}), \tag{2.18d}$$

$$\bar{R} \leq R_1^{(12)}(\boldsymbol{\tau}, \boldsymbol{t}), \tag{2.18e}$$

$$\bar{R} \geq \theta_1, \tag{2.18f}$$

$$R_2(\boldsymbol{\tau}, \boldsymbol{t}) \geq \theta_2. \tag{2.18g}$$

Lemma 1. ***(P2)*** *is a convex problem.*

Proof. For $R_1^{(1j)}(\boldsymbol{\tau}, \boldsymbol{t})$ in (2.14) where $j \in \{0, 2\}$ and $R_k^{(20)}(\boldsymbol{\tau}, \boldsymbol{t})$ in (2.15) where $k \in \{1, 2\}$, they are concave functions with respect to the optimization variables [24, Lemma 3.1]. Hence, the objective function, (2.18a), is a concave function as it is the sum of an affine function and a concave function. Furthermore, the constraints (2.18b)-(2.18g) are either affine or concave with respect to the optimization variables. Therefore, **(P2)** is a convex problem. □

2.4 Optimal Solution of QoS Constrained Sum-Throughput Maximization

In this section, I derive the optimal solution of **(P2)** by solving the Karush-Kuhn-Tucker (KKT) conditions due to the strong duality [26]. In particular, I solve the set of equations from the KKT conditions via a divide-and-conquer approach. That is, I consider all different possible cases according to the signs of the variables, the details of which will be given in the following. The solutions to the considered cases are combined to get the optimal solution to **(P2)** in the following section.

The set of equations of each case can be transformed into a linear system if z_1^*, z_{21}^*, and z_{22}^* are obtained where

$$z_1 = \frac{\tau_0}{\tau_1},\ z_{21} = \frac{t_{21}}{\tau_{21}}, \text{ and } z_{22} = \frac{t_{22}}{\tau_{22}}. \tag{2.19}$$

z_1, z_{21}, and z_{22} can be defined only when their denominator is positive. When τ_1, τ_{21} and τ_{22} are zeros, I call z_1, z_{21} and z_{22} undefinable. Note that z_1^*, z_{21}^*, and z_{22}^* are strictly positive or undefinable, which can be proved by showing that z_1^*, z_{21}^*, and z_{22}^* cannot be zero, respectively. In other words, if there is no energy harvesting time for transmission during τ_1, τ_{21}, and τ_{22}, respectively (i.e., τ_0, t_{21}, and t_{22}, respectively,) there is no need to allocate time for τ_1, τ_{21}, and τ_{22}; otherwise, it will be a waste of time resources.

In order to obtain the KKT conditions for solving the maximization problem, the Lagrangian of **(P2)** is derived as follows:

$$\begin{aligned}\mathcal{L}\left(\bar{R}, \boldsymbol{\tau}, \boldsymbol{t}, \boldsymbol{\lambda}\right) = \bar{R} &+ R_2(\boldsymbol{\tau}, \boldsymbol{t}) \\ &- \lambda_1 \left(\tau_0 + \tau_1 + \tau_{21} + \tau_{22} - 1\right) \\ &- \lambda_2 \left(t_{21} + t_{22} - \tau_0\right) \\ &- \lambda_3 \left(\bar{R} - \left(R_1^{(10)}(\boldsymbol{\tau}, \boldsymbol{t}) + R_1^{(20)}(\boldsymbol{\tau}, \boldsymbol{t})\right)\right) \\ &- \lambda_4 \left(\bar{R} - R_1^{(12)}(\boldsymbol{\tau}, \boldsymbol{t})\right) \\ &- \lambda_5 \left(\theta_1 - \bar{R}\right) - \lambda_6 \left(\theta_2 - R_2(\boldsymbol{\tau}, \boldsymbol{t})\right),\end{aligned} \tag{2.20}$$

where λ_1, ... , λ_6 are the Lagrangian multipliers corresponding to (2.18b)-(2.18g) and should be non-negative. Before proceeding, two functions, $f_\rho(z)$ and $g_\rho(z)$, are defined as

$$f_\rho(z) \triangleq \ln\left(1 + \rho z\right) - \frac{\rho z}{1 + \rho z} \text{ and } g_\rho(z) \triangleq \frac{\rho}{1 + \rho z},$$

where z is a variable which lies in the domain of $\{z | z \geq 0\}$ and ρ is a positive given number. $f_\rho(z)$ is a monotonically increasing function as its first derivative with

respect to z is nonnegative (i.e., $\frac{df_\rho(z)}{dz} = \frac{\rho^2 z}{(1+\rho z)^2} \geq 0$). Moreover, its first derivative with respect to ρz is also non-negative (i.e., $\frac{df_\rho(z)}{d(\rho z)} = \frac{\rho z}{(1+\rho z)^2} \geq 0$). Hence, it can be shown that $f_{\rho_a}(z_a) = f_{\rho_b}(z_b)$ holds only if $\rho_a z_a = \rho_b z_b$. On the other hand, $g_\rho(z)$ is a monotonically decreasing function as its first derivative with respect to z is negative (i.e., $\frac{dg_\rho(z)}{dz} = -\left(\frac{\rho}{1+\rho z}\right)^2 < 0$). Accordingly, $g_\rho(z_a) = g_\rho(z_b)$ holds only if $z_a = z_b$.

Taking derivatives of (2.20) with respect to the optimization variables, $(\bar{R}, \boldsymbol{\tau}, \boldsymbol{t})$, the Lagrangian stationarity conditions become

$$\frac{\partial \mathcal{L}}{\partial \bar{R}} = 0 : 1 + \lambda_5^* = \lambda_3^* + \lambda_4^*, \tag{2.21}$$

$$\frac{\partial \mathcal{L}}{\partial \tau_0} = 0 : (\lambda_1^* - \lambda_2^*) \ln 2 = \lambda_3^* g_{\rho_1^{(10)}}(z_1^*) + \lambda_4^* g_{\rho_1^{(12)}}(z_1^*), \tag{2.22}$$

$$\frac{\partial \mathcal{L}}{\partial \tau_1} = 0 : \lambda_1^* \ln 2 = \lambda_3^* f_{\rho_1^{(10)}}(z_1^*) + \lambda_4^* f_{\rho_1^{(12)}}(z_1^*), \tag{2.23}$$

$$\frac{\partial \mathcal{L}}{\partial \tau_{21}} = 0 : \lambda_1^* \ln 2 = \lambda_3^* f_{\rho_2}(z_{21}^*), \tag{2.24}$$

$$\frac{\partial \mathcal{L}}{\partial \tau_{22}} = 0 : \lambda_1^* \ln 2 = (1 + \lambda_6^*) f_{\rho_2}(z_{22}^*), \tag{2.25}$$

$$\frac{\partial \mathcal{L}}{\partial t_{21}} = 0 : \lambda_2^* \ln 2 = \lambda_3^* g_{\rho_2}(z_{21}^*), \tag{2.26}$$

$$\frac{\partial \mathcal{L}}{\partial t_{22}} = 0 : \lambda_2^* \ln 2 = (1 + \lambda_6^*) g_{\rho_2}(z_{22}^*). \tag{2.27}$$

The equations involved with undefinable z_1^*, z_{21}^*, and z_{22}^* among (2.22)-(2.27) no longer hold. Note that the optimal solution of **(P2)** belongs to either Case (I) or Case (II) where

(I) z_1^*, z_{21}^*, and z_{22}^* are positive.

(II) z_1^* and z_{22}^* are positive and z_{21}^* is undefinable.

The other cases need not be considered since their solutions can be obtained through Cases (I) and (II), or are not optimal. When z_1^* and z_{21}^* are positive and z_{22}^* is undefinable, it coincides with achieving the maximum throughput of U_1 while the throughput of U_2 equals zero, $\theta_1^{(u)}$, and its optimal solution can be obtained in Case (I), which

will be shown in the following. Likewise, when z_1^* and z_{21}^* are undefinable and z_{22}^* is positive, it coincides with achieving the maximum throughput of U_2 while the throughput of U_1 equals zero, $\theta_2^{(u)}$, and its optimal solution can be obtained in Case (II). When z_1^*, z_{21}^*, and z_{22}^* are undefinable, there will be no information transmission in the network. When z_1^* is undefinable, z_{21}^* is positive and z_{22}^* is either positive or undefinable, U_1 does not broadcast its message as τ_1^* is zero. As a result, user cooperation also does not occur, and equivalently z_{21}^* becomes undefinable, which is a contradiction. When z_1^* is definable, and z_{21}^* and z_{22}^* are undefinable, U_1 is the only user which communicates with the H-AP, which means that the network does not exploit user cooperation. Since it has been shown that user cooperation offers gain with respect to U_1's throughput under the system model [24], this occasion is sub-optimal.

For Cases (I) and (II), I have the following lemma.

Lemma 2. *The optimal Lagrangian multipliers, λ_1^*, λ_2^*, and λ_3^* are always positive, and thus,* (2.18b)*,* (2.18c)*, and* (2.18d) *are binding*[5] *at optimum from complementary slackness [26]. That is, $\tau_0^* + \tau_1^* + \tau_{21}^* + \tau_{22}^* = 1$, $t_{21}^* + t_{22}^* = \tau_0^*$ and $\bar{R}^* = R_1^{(10)}(\boldsymbol{\tau}^*, \boldsymbol{t}^*) + R_1^{(20)}(\boldsymbol{\tau}^*, \boldsymbol{t}^*)$.*

Proof. I show the lemma by contradiction. Suppose $\lambda_1^* = 0$ and z_1^* is definable, then, $\lambda_3^* = 0$ and $\lambda_4^* = 0$ from (2.23) since $f_{\rho_1^{(10)}}(z_1^*)$ and $f_{\rho_1^{(12)}}(z_1^*)$ are positive. From (2.21), $1 + \lambda_5^* = 0$, which is a contradiction. Hence, λ_1^* should be positive. It can similarly be shown that λ_2^* and λ_3^* are positive, so I skip the remaining of the proof. Since λ_1^*, λ_2^* and λ_3^* are positive, it is consequential that (2.18b), (2.18c) and (2.18d) hold with equalities from complementary slackness. □

In contrast to the signs of λ_1^*, λ_2^*, and λ_3^*, the signs of λ_4^*, λ_5^*, and λ_6^* can be either zero or positive, respectively. Due to the complementary slackness, (2.18e), (2.18f),

[5] An inequality constraint is called binding when the inequality holds with its equality; otherwise, it will be referred to as non-binding.

Table 2.1: Classification of the sub-problems in **(P2)**.

$(\lambda_4^*, \lambda_5^*, \lambda_6^*)$	(0,0,0)	(0,0,+)	(0,+,0)	(+,0,0)	(0,+,+)	(+,0,+)	(+,+,0)	(+,+,+)
Case (I)	Case (I)-a	invalid	invalid	invalid	Case (I)-b	invalid	Case (I)-c	Case (I)-d
Case (II)	Case (II)-a	Case (II)-b	Case (II)-c	invalid	Case (II)-d	invalid	invalid	invalid

and (2.18g) are binding at optimum when λ_4^*, λ_5^*, and λ_6^* are positive, respectively. By Lemma 2, (2.18e) and (2.18f) at optimum can be equivalently rewritten as

$$R_1^{(10)}(\boldsymbol{\tau}^*, \boldsymbol{t}^*) + R_1^{(20)}(\boldsymbol{\tau}^*, \boldsymbol{t}^*) \leq R_1^{(12)}(\boldsymbol{\tau}^*, \boldsymbol{t}^*), \tag{2.28}$$

$$\theta_1 \leq R_1^{(10)}(\boldsymbol{\tau}^*, \boldsymbol{t}^*) + R_1^{(20)}(\boldsymbol{\tau}^*, \boldsymbol{t}^*). \tag{2.29}$$

I further classify the problem for Cases (I) and (II) according to the signs of λ_4^*, λ_5^*, and λ_6^*. Table 2.1 shows the problem classification and describes the valid/invalid sub-cases of Cases (I) and (II). Each valid sub-case will be explored by finding the optimal values of z_1, z_{21}, and z_{22}, formulating a linear system and solving it to derive the optimal solution while satisfying the inequality conditions. I assume that θ_1 and θ_2 are feasible.

2.4.1 Case (I): Positive z_1^*, z_{21}^* and z_{22}^*

For Case (I), since z_1^*, z_{21}^* and z_{22}^* are positive, the optimal time allocation, $(\boldsymbol{\tau}^*, \boldsymbol{t}^*) \succ 0$, and I have the following Lemma.

Lemma 3. *When* $(\boldsymbol{\tau}^*, \boldsymbol{t}^*) \succ 0$, $\lambda_3^* = 1 + \lambda_6^*$ *and* $z_{21}^* = z_{22}^*$.

Proof. I define a new function, $q_\rho(z)$ as $f_\rho(z)$ divided by $g_\rho(z)$ where z belongs to $\{z | z \geq 0\}$. Rewriting $q_\rho(z)$,

$$q_\rho(z) = \left(\frac{1+\rho z}{\rho}\right) \ln(1+\rho z) - z.$$

This is a monotonically increasing function with respect to z as its first derivative is positive except for $z = 0$ (i.e., $\frac{dq_\rho}{dz} = \ln(1+\rho z) \geq 0$.) Hence, $q_\rho(z_a) = q_\rho(z_b)$, only

if $z_a = z_b$. From (2.24)-(2.27), I have

$$\lambda_3^* f_{\rho_2}(z_{21}^*) = (1 + \lambda_6^*) f_{\rho_2}(z_{22}^*), \tag{2.30}$$

$$\lambda_3^* g_{\rho_2}(z_{21}^*) = (1 + \lambda_6^*) g_{\rho_2}(z_{22}^*). \tag{2.31}$$

Since $(\boldsymbol{\tau}^*, \boldsymbol{t}^*) \succ 0$ in Case (I), it is possible to divide (2.30) by (2.31), which is equivalent to $q_{\rho_2}(z_{21}^*) = q_{\rho_2}(z_{22}^*)$. Therefore, I can conclude that $z_{21}^* = z_{22}^*$ due to the property of $q_\rho(z)$, and consequently, $\lambda_3^* = (1 + \lambda_6^*)$ holds. □

It can be shown that the sub-cases (0,0,+), (0,+,0), (+,0,0), and (+,0,+) in Case (I) are invalid by contradiction. To prove the invalidity of the first case, for example, suppose that $\lambda_4^* = 0$, $\lambda_5^* = 0$, and $\lambda_6^* \neq 0$. Then, λ_3^* becomes one from (2.21). Exploiting Lemma 3, λ_6^* becomes zero which is a contradiction to the assumption. The invalidities of the three other sub-cases can be shown in a similar manner.

For all the following valid sub-cases in Case (I), (2.18b) and (2.18c) from Lemma 2 and the definitions of z_1^*, z_{21}^*, and z_{22}^* from (2.19) become linear equations of $(\boldsymbol{\tau}^*, \boldsymbol{t}^*)$ provided z_1^*, z_{21}^*, and z_{22}^* are obtained. Note that it is sufficient to find z_1^* and z_{21}^* due to the fact that $z_{21}^* = z_{22}^*$ in Case (I) from Lemma 3. Hence, I have the following linear system of $(\boldsymbol{\tau}^*, \boldsymbol{t}^*)$,

$$\underbrace{\begin{bmatrix} 1 & 1 & 1 & 1 & 0 & 0 \\ -1 & 0 & 0 & 0 & 1 & 1 \\ 1 & -z_1^* & 0 & 0 & 0 & 0 \\ 0 & 0 & -z_{21}^* & 0 & 1 & 0 \\ 0 & 0 & 0 & -z_{21}^* & 0 & 1 \end{bmatrix}}_{\mathbf{L}} \begin{bmatrix} \tau_0^* \\ \tau_1^* \\ \tau_{21}^* \\ \tau_{22}^* \\ t_{21}^* \\ t_{22}^* \end{bmatrix} = \underbrace{\begin{bmatrix} 1 \\ 0 \\ 0 \\ 0 \\ 0 \end{bmatrix}}_{\mathbf{Q}}. \tag{2.32}$$

Additional linear equations should be included in (2.32) according to the signs of λ_4^*, λ_5^*, and λ_6^* in each sub-case. From (2.32), τ_0^* and τ_1^* can be written with z_1^* and z_{21}^*,

respectively, as

$$\tau_0^* = \frac{1}{1 + \frac{1}{z_1^*} + \frac{1}{z_{21}^*}}, \tag{2.33}$$

$$\tau_1^* = \frac{\frac{1}{z_1^*}}{1 + \frac{1}{z_1^*} + \frac{1}{z_{21}^*}}. \tag{2.34}$$

Case (I)-a: z_1^* and z_{21}^* can be obtained by solving the Lagrangian stationarity conditions, (2.21)-(2.27) as follows: from $\lambda_4^* = \lambda_5^* = \lambda_6^* = 0$ and $\lambda_3^* = 1$ from Lemma 3 in Case (I)-a, it can be induced that $\rho_1^{(10)} z_1^* = \rho_2 z_{21}^*$ from (2.23) and (2.24) by exploiting the property of $f_\rho(z)$. Furthermore, by eliminating the Lagrangian multipliers from (2.22), (2.24), and (2.26), it can be induced that

$$f_{\rho_2}(z_{21}^*) - g_{\rho_2}(z_{21}^*) = g_{\rho_1^{(10)}}(z_1^*). \tag{2.35}$$

Rewriting (2.35) to an equivalent equation of z_1^* using $\rho_1^{(10)} z_1^* = \rho_2 z_{21}^*$, I have

$$\ln(1 + \rho_1^{(10)} z_1^*) = \frac{\rho_1^{(10)} z_1^* + \rho_1^{(10)} + \rho_2}{1 + \rho_1^{(10)} z_1^*}. \tag{2.36}$$

A non-linear equation of x such as

$$\ln(ax + 1) = \frac{ax + b}{ax + 1}, \tag{2.37}$$

can be rewritten as follows:

$$\left(\frac{ax + 1}{e}\right) \ln\left(\frac{ax + 1}{e}\right) = \frac{b - 1}{e}. \tag{2.38}$$

For a complex number v, the Lambert-W function satisfies $v = W(v)e^{W(v)}$, which becomes (2.38) if I let $W(v)$ be $\ln\left(\frac{ax+1}{e}\right)$ and v be $\frac{b-1}{e}$. Hence, from $W\left(\frac{b-1}{e}\right) = \ln\left(\frac{ax+1}{e}\right)$, the solution of (2.37) is given as

$$x = \frac{e^{W\left(\frac{b-1}{e}\right)+1} - 1}{a}, \tag{2.39}$$

when $a \neq 0$ and $b \neq 1$. For (2.36), a, b and x become $\rho_1^{(10)}$, $\rho_1^{(10)} + \rho_2$, and z_1^*, respectively. Hence, z_1^* and z_{21}^* are given by

$$z_1^* = \frac{e^C - 1}{\rho_1^{(10)}}, \tag{2.40}$$

$$z_{21}^* = \frac{e^C - 1}{\rho_2}, \tag{2.41}$$

where $C = W(\frac{\rho_1^{(10)} + \rho_2 - 1}{e}) + 1$.

From the complementary slackness, $\lambda_4^* = 0$, $\lambda_5^* = 0$, and $\lambda_6^* = 0$ result in (2.18e), (2.18f), and (2.18g) being inequalities. Hence, no further linear equations can be obtained and (2.32) needs to be solved. For given z_1^* and z_{21}^*, (2.32) is an underdetermined linear system since $rank(\mathbf{L}) = 5$. It can be easily shown that the reduced row echelon form of $\mathbf{L}$ has five rows which are not all-zero rows. Hence, multiple solutions exist to yield the same sum-throughput. To provide an optimal time allocation, I can select τ_{21}^* as long as the complementary slackness is satisfied. Accordingly, τ_{21}^* can be selected within the range of

$$\max(0, \psi_A) \leq \tau_{21}^* \leq \min(\psi_B, \psi_C), \tag{2.42}$$

where $\psi_A = \frac{\ln 2}{C}(\theta_1 - \theta_1^{(c1)})$, $\psi_B = \frac{\ln 2}{C}(\theta_1^{(c2)} - \theta_1^{(c1)})$, and $\psi_C = \frac{\ln 2}{C}(\theta_2^{(c)} - \theta_2)$;

$$\theta_1^{(c1)} = \frac{C}{\ln 2} \frac{\rho_1^{(10)}}{\rho_1^{(10)} + \rho_2 + e^C - 1},$$

$$\theta_1^{(c2)} = \log_2 \left(1 + \frac{\rho_1^{(12)}}{\rho_1^{(10)}}(e^C - 1)\right) \frac{\rho_1^{(10)}}{\rho_1^{(10)} + \rho_2 + e^C - 1},$$

$$\theta_2^{(c)} = \frac{C}{\ln 2} \frac{\rho_2}{\rho_1^{(10)} + \rho_2 + e^C - 1}.$$

The derivation of (2.42) is given as follows: since z_1^* and z_{21}^* are given as $\frac{e^C - 1}{\rho_1^{(10)}}$ and $\frac{e^C - 1}{\rho_2}$, respectively, τ_0^* and τ_1^* are determined from (2.33) and (2.34). Using τ_0^* and τ_1^*, the complementary slackness conditions which are the same as (2.28), (2.29), and

(2.18g) can be rewritten as

$$\theta_1^{(c1)} + \tau_{21}^* \frac{C}{\ln 2} \leq \theta_1^{(c2)}, \tag{2.43}$$

$$\theta_1 \leq \theta_1^{(c1)} + \tau_{21}^* \frac{C}{\ln 2}, \tag{2.44}$$

$$\theta_2 \leq \tau_{22}^* \frac{C}{\ln 2}. \tag{2.45}$$

Since $\tau_{22}^* = 1 - \tau_0^* - \tau_1^* - \tau_{21}^*$ from Lemma 2, (2.45) can be rewritten as

$$\theta_2 \leq \theta_2^{(c)} - \tau_{21}^* \frac{C}{\ln 2}. \tag{2.46}$$

Isolating τ_{21}^* from (2.43), (2.44) and (2.46), $\tau_{21}^* \leq \psi_B$, $\tau_{21}^* \geq \psi_A$ and $\tau_{21}^* \leq \psi_C$ are derived. Considering $\tau_{21}^* \geq 0$, the inequalities are merged into (2.42). Furthermore, from (2.42), for τ_{21}^* to be feasible (i.e., $\tau_{21}^* \geq 0$), the following inequalities need to hold.

$$\theta_2 \leq \theta_2^{(c)}, \quad (2.47) \qquad \theta_1 \leq \theta_1^{(c2)}, \quad (2.48) \qquad \theta_1 + \theta_2 \leq \theta_1^{(c1)} + \theta_2^{(c)}. \quad (2.49)$$

(2.47)-(2.49) will be used as criteria for classifying the problem as Case (I)-a for given θ_1 and θ_2. Provided τ_{21}^* exists satisfying (2.42), obtaining the optimal values of the remaining variables is straightforward.

For all the other remaining valid sub-cases in Case (I), the optimal solutions can be derived in a similar manner. The results of the sub-cases are provided first, and the derivation is derivation is presented next.

Case (I)-b: z_1^* and z_{21}^* of Case (I)-b are identical to those of Case (I)-a. That is, $z_1^* = \frac{e^C - 1}{\rho_1^{(10)}}$ and $z_{21}^* = \frac{e^C - 1}{\rho_2}$. For τ_{21}^* and τ_{22}^*, they are given as

$$\tau_{21}^* = \frac{\ln 2}{C}(\theta_1 - \theta_1^{(c1)}), \tag{2.50}$$

$$\tau_{22}^* = \frac{\ln 2}{C}(-\theta_1 + \theta_1^{(c1)} + \theta_2^{(c)}). \tag{2.51}$$

Obtaining the optimal values of the remaining variables is straightforward. For the problem to be classified as Case (I)-b, θ_1 and θ_2 should satisfy the following condi-

tions.

$$\theta_1 + \theta_2 = \theta_1^{(c1)} + \theta_2^{(c)}, \tag{2.52}$$

$$\theta_1^{(c1)} \leq \theta_1 \leq \min(\theta_1^{(c1)} + \theta_2^{(c)}, \theta_1^{(c2)}). \tag{2.53}$$

Derivation of the solution to Case (I)-b: z_1^* and z_{21}^* are $\frac{e^C-1}{\rho_1^{(10)}}$ and $\frac{e^C-1}{\rho_2}$, respectively, which can be derived as in Case (I)-a since $\lambda_4^* = 0$. From the complementary slackness, $\lambda_5^* \neq 0$ and $\lambda_6^* \neq 0$ results in (2.18f), equivalently, (2.29), and (2.18g) being equalities, respectively. Rewriting (2.29) and (2.18g) with the attained z_1^* and z_{21}^*, $\theta_1 = (\tau_1^* + \tau_{21}^*)\frac{C}{\ln 2}$ and $\theta_2 = \tau_{22}^* \frac{C}{\ln 2}$. Hence, a linear system for Case (I)-b can be formulated as

$$\begin{bmatrix} & & \mathbf{L} & & & \\ 0 & \frac{C}{\ln 2} & \frac{C}{\ln 2} & 0 & 0 & 0 \\ 0 & 0 & 0 & \frac{C}{\ln 2} & 0 & 0 \end{bmatrix} \begin{bmatrix} \boldsymbol{\tau}^*, \boldsymbol{t}^* \end{bmatrix}^T = \begin{bmatrix} \mathbf{Q} \\ \theta_1 \\ \theta_2 \end{bmatrix}. \tag{2.54}$$

I form a 7×7 augmented matrix with the coefficient matrix and the constant vector of (2.54). The determinant of the augmented matrix should be zero for a solution to exist. The determinant is given by

$$\frac{C}{\ln 2}\left(z_{21}^*\left(\frac{C}{\ln 2} - \theta_1 - \theta_2\right) + z_1^*\left(\frac{C}{\ln 2} - (z_{21}^* + 1)\,(\theta_1 + \theta_2)\right)\right),$$

and the determinant being zero is equivalent to $\theta_1 + \theta_2 = \theta_1^{(c1)} + \theta_2^{(c)}$, (2.52). Suppose that (2.52) holds, then, by solving the linear system, (2.54), τ_{21}^* and τ_{22}^* are obtained as (2.50) and (2.51). From the complementary slackness, $\lambda_4^* = 0$ results in (2.18e), equivalently, (2.28), being an inequality, which is given as $\theta_1 \leq \theta_1^{(c2)}$. It also needs to satisfy $\tau_{21}^* \geq 0$, equivalently $\theta_1 \geq \theta_1^{(c1)}$ and $\tau_{22}^* \geq 0$, equivalently $\theta_1 \leq \theta_1^{(c1)} + \theta_2^{(c)}$. Rewriting the three relations together, I have $\theta_1^{(c1)} \leq \theta_1 \leq \min(\theta_1^{(c1)} + \theta_2^{(c)}, \theta_1^{(c2)})$, (2.53). Thus, for the problem to be classified as Case (I)-b, (2.52) and (2.53) should be satisfied.

Remark 1. *The maximum sum-throughputs achieved in Case (I)-a and (I)-b are identical as* $\theta_1^{(c1)} + \theta_2^{(c)}$. *It can be shown using* $f_{\rho_1^{(10)}}(z_1^*) = f_{\rho_2}(z_{21}^*)$ *with the property of* $f_\rho(z)$ *and computing the maximum sum-throughputs with Lemma 2.*

Fig. 2.3 conceptually indicates into which sub-problem **(P2)** falls for given (θ_1, θ_2) when $\theta_1^{(c1)} + \theta_2^{(c)} > \theta_1^{(c2)}$. The θ_1-θ_2 curves indicate the maximal θ_1 and θ_2 pair, which does not make the problem infeasible. It is explained concretely in the following section how Fig. 2.3 is made. Note that the axes of Figs. 2.3(a)-2.3(c) differ from each other. Fig. 2.3(a) illustrates Remark 1 that the blue box is the Case (I)-a region and the straight line of slope -1 is the Case (I)-b region, and any pair of (θ_1, θ_2) which belongs to them yields the same maximum sum-throughput as $\theta_1^{(c1)} + \theta_2^{(c)}$.

Case (I)-c: z_1^* and z_{21}^* of Case (I)-c can be obtained by solving the two non-linear equations, (2.55) and (2.56), which should be solved with a non-linear equation solving algorithm such as Newton-Raphson method.

$$\begin{aligned} &\{f_{\rho_2}(z_{21}^*) - f_{\rho_1^{(10)}}(z_1^*)\} g_{\rho_1^{(12)}}(z_1^*) \\ &= \{f_{\rho_2}(z_{21}^*) - g_{\rho_2}(z_{21}^*) - g_{\rho_1^{(10)}}(z_1^*)\} f_{\rho_1^{(12)}}(z_1^*), \end{aligned} \tag{2.55}$$

$$\theta_1 = \frac{\frac{1}{z_1^*}}{1 + \frac{1}{z_1^*} + \frac{1}{z_{21}^*}} \log_2(1 + \rho_1^{(12)} z_1^*). \tag{2.56}$$

Note that (2.55) and (2.56) depend on the channel conditions and θ_1. With the obtained z_1^* and z_{21}^*, let $c_a = \log_2(1 + \rho_1^{(10)} z_1^*)$, $c_b = \log_2(1 + \rho_2 z_{21}^*)$, then, τ_{21}^* and τ_{22}^* are given as

$$\tau_{21}^* = \frac{\theta_1}{c_b} - \frac{c_a}{c_b}\tau_1^*, \tag{2.57}$$

$$\tau_{22}^* = -\frac{\theta_1}{c_b} + \frac{c_a}{c_b}\tau_1^* + \frac{\tau_0^*}{z_{21}^*} \tag{2.58}$$

Obtaining the optimal values of the remaining variables is straightforward. For the problem to be classified as Case (I)-c, θ_2 should satisfy the following condition for

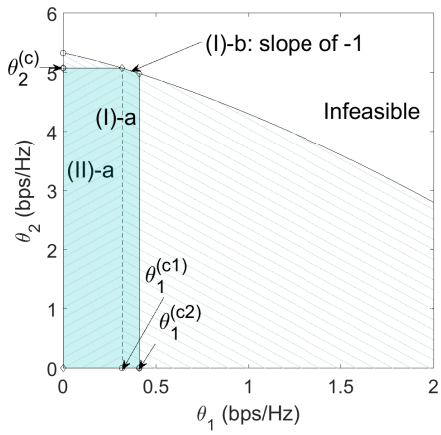

(a) (θ_1, θ_2) classified as Case (I)-a, (I)-b and (II)-a.

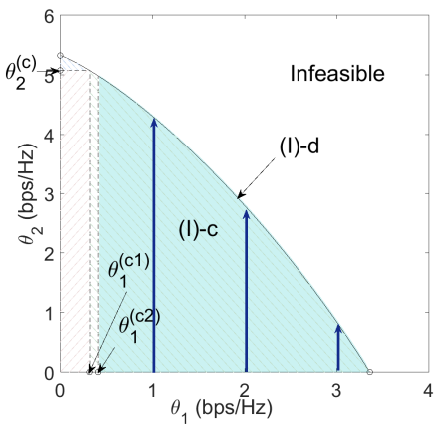

(b) (θ_1, θ_2) classified as Case (I)-c and (I)-d.

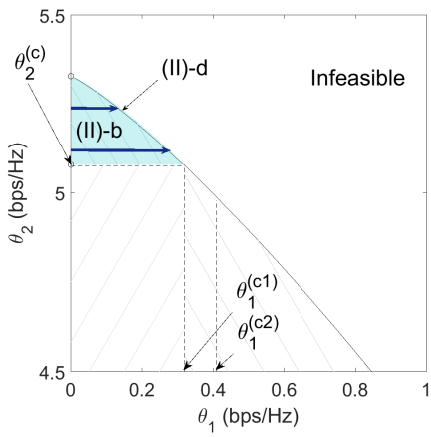

(c) (θ_1, θ_2) classified as Case (II)-b and (II)-d.

Figure 2.3: Classification of the maximization problem with feasible (θ_1, θ_2) when $\theta_1^{(c1)} + \theta_2^{(c)} > \theta_1^{(c2)}$.

the given θ_1,

$$\theta_2 \leq \frac{1}{1+\frac{1}{z_1^*}+\frac{1}{z_{21}^*}}\left(\frac{c_a}{z_1^*}+\frac{c_b}{z_{21}^*}-\frac{\log_2(1+\rho_1^{(12)}z_1^*)}{z_1^*}\right)\left(\triangleq \gamma_{\theta_2}^{\text{(I)-c}}\right). \tag{2.59}$$

Derivation of the solution to Case (I)-c: Using that $\lambda_6^*=0$ and $\lambda_3^*=1$ from Lemma 3, I can induce (2.60) and (2.61) by eliminating the Lagrangian multipliers, λ_1^* and λ_2^* in (2.22)-(2.24) and (2.26).

$$f_{\rho_2}(z_{21}^*)-g_{\rho_2}(z_{21}^*)=g_{\rho_1^{(10)}}(z_1^*)+\lambda_4^* g_{\rho_1^{(12)}}(z_1^*), \tag{2.60}$$

$$f_{\rho_2}(z_{21}^*)=f_{\rho_1^{(10)}}(z_1^*)+\lambda_4^* f_{\rho_1^{(12)}}(z_1^*). \tag{2.61}$$

Removing λ_4^* from (2.60) and (2.61), I have a non-linear equation of z_1^* and z_{21}^*, (2.55). From the complementary slackness, $\lambda_4^*\neq 0$ and $\lambda_5^*\neq 0$ results in (2.18e) and (2.18f), equivalently (2.28) and (2.29) being equalities. In order to obtain another equation of z_1^* and z_{21}^*, (2.28) and (2.29) are manipulated as follows:

$$\begin{aligned}\theta_1 &= \tau_1^*\log_2(1+\rho_1^{(10)}z_1^*)+\tau_{21}^*\log_2(1+\rho_2 z_{21}^*),\\ &= \tau_1^*\log_2(1+\rho_1^{(12)}z_1^*),\\ &= \frac{\frac{1}{z_1^*}}{1+\frac{1}{z_1^*}+\frac{1}{z_{21}^*}}\log_2(1+\rho_1^{(12)}z_1^*),\end{aligned}$$

which is (2.56). Once z_1^* and z_{21}^* are acquired by solving (2.55) and (2.56), (2.28) becomes linear with respect to $(\boldsymbol{\tau}^*,\boldsymbol{t}^*)$ as $\theta_1=\tau_1^* c_a+\tau_{21}^* c_b$ where $c_a=\log_2(1+\rho_1^{(10)}z_1^*)$, $c_b=\log_2(1+\rho_2 z_{21}^*)$. Hence, the linear system for Case (I)-c is given as

$$\begin{bmatrix} & \mathbf{L} & \\ 0 & c_a \quad c_b \quad 0 \quad 0 & 0 \end{bmatrix}\begin{bmatrix} \boldsymbol{\tau}^*,\boldsymbol{t}^* \end{bmatrix}^T=\begin{bmatrix}\mathbf{Q}\\ \theta_1\end{bmatrix}. \tag{2.62}$$

By solving the linear system, (2.62), τ_{21}^* and τ_{22}^* are obtained as (2.57) and (2.58). From the complementary slackness, $\lambda_6^*=0$ results in (2.18g) being an inequality (i.e., $\theta_2\leq R_2^{(20)}(\boldsymbol{\tau}^*,\boldsymbol{t}^*)$). Since $z_{21}^*=z_{22}^*$ from Lemma 3, $c_b=\log_2(1+\rho_2 z_{21}^*)=$

$\log_2(1+\rho_2 z_{22}^*)$ and (2.18g) can be rewritten as $\theta_2 \leq \tau_{22}^* c_b$. It can be further rearranged as follows exploiting (2.56) for θ_1 and (2.58) for τ_{22}^*,

$$\theta_2 \leq -\theta_1 + c_a\tau_1^* + c_b\frac{\tau_0^*}{z_{21}^*}, \tag{2.63}$$

$$(\theta_1+\theta_2) \leq c_a\tau_1^* + c_b\frac{\tau_0}{z_{21}^*}, \tag{2.64}$$

$$\theta_2 \leq \frac{1}{1+\frac{1}{z_1^*}+\frac{1}{z_{21}^*}}\left(\frac{c_a}{z_1^*}+\frac{c_b}{z_{21}^*}-\frac{\log_2(1+\rho_1^{(12)}z_1^*)}{z_1^*}\right), \tag{2.65}$$

which is (2.59).

Case (I)-d: z_1^*, z_{21}^* and $(\boldsymbol{\tau}^*, \boldsymbol{t}^*)$ are identical to those of Case (I)-c. In particular, for the problem to be classified as Case (I)-d, θ_2 should satisfy (2.59) at its equality for the given θ_1 (i.e., $\theta_2 = \gamma_{\theta_2}^{\text{(I)-c}}$.)

Derivation of the solution to Case (I)-d: The two non-linear equations of z_1^* and z_{21}^*, (2.55) and (2.56) can be obtained in a similar manner in Case (I)-c, hence I skip the detailed derivation. Besides, from the complementary slackness, $\lambda_6^* \neq 0$ results in (2.18g) being an equality (i.e., $\theta_2 = \tau_{22}^* c_b$.) Hence, a linear system for Case (I)-d can be obtained as

$$\begin{bmatrix} & \mathbf{L} & & & & \\ 0 & c_a & c_b & 0 & 0 & 0 \\ 0 & 0 & 0 & c_b & 0 & 0 \end{bmatrix} \begin{bmatrix} \boldsymbol{\tau}^*, \boldsymbol{t}^* \end{bmatrix}^T = \begin{bmatrix} \mathbf{Q} \\ \theta_1 \\ \theta_2 \end{bmatrix}. \tag{2.66}$$

(2.66) is an overdetermined system, hence, for it to have a solution, the determinant of an augmented matrix composed of the coefficient matrix and the constant vector of (2.66) should be zero. The determinant is given as

$$-c_b(z_{21}^*(-c_a+\theta_1+\theta_2)+z_1^*((\theta_1+\theta_2)(z_{21}^*+1)-c_b)),$$

and the determinant being zero is equivalent to (2.59) of when its equality holds. Therefore, on the condition that the given θ_1 and θ_2 satisfy (2.59) with its equality, the optimal solution of Case (I)-c is still the optimal solution of Case (I)-d.

Remark 2. *The maximum sum-throughputs achieved in Case (I)-c and (I)-d under the same θ_1 are identical. For both sub-cases, z_1^* and z_{21}^* depend on the values of ρ's and θ_1 from* (2.55) *and* (2.56)*. Hence, for the same θ_1 under the same channel condition, the optimal solutions of Case (I)-c and (I)-d are the same and consequently achieve the same maximum sum-throughputs.*

Fig. 2.3(b) illustrates Remark 2 that the interior of the blue box is the Case (I)-c region and the curved boundary is the Case (I)-d region, and any pair of (θ_1, θ_2) lying on any vertical arrow in the blue box yields the same maximum sum-throughput. It can be seen that since the gain of allocating resources to U_2 is greater, the throughput of U_1 is adjusted to the QoS requirement, and U_2 is allocated with the remaining time resources for transmission of its own information. Furthermore, as z_{21}^* is positive, U_1 benefits from user cooperation in enhancing its throughput.

2.4.2 Case (II): Positive z_1^* and z_{22}^*, and undefinable z_{21}^*

Since z_{21}^* is undefinable, $\tau_{21}^* = 0$, which makes $t_{21}^* = 0$ from the definition of t_{21}, (2.13), and $t_{22}^* = \tau_0^*$ from (2.18c). Sub-cases (+,0,0), (+,0,+), (+,+,0), and (+,+,+) in Case (II) are invalid since the sub-cases with non-zero λ_4^* result in (2.18c), equivalently, (2.28) being an equality from the complementary slackness. Then, τ_{21}^* should be positive; otherwise, (2.28) becomes a strict inequality, since $R_1^{(10)}(\boldsymbol{\tau}^*, \boldsymbol{t}^*) < R_1^{(12)}(\boldsymbol{\tau}^*, \boldsymbol{t}^*)$ because $\rho_1^{(10)} < \rho_1^{(12)}$. Hence, this contradicts the assumption that t_{21}^* is zero from the assumption that z_{21}^* is undefinable.

For Case (II), I form the following linear system of $(\tau_0^*, \tau_1^*, \tau_{22}^*)$ as

$$\begin{bmatrix} 1 & 1 & 1 \\ 1 & -z_1^* & 0 \\ 1 & 0 & -z_{22}^* \end{bmatrix} \begin{bmatrix} \tau_0^* \\ \tau_1^* \\ \tau_{22}^* \end{bmatrix} = \begin{bmatrix} 1 \\ 0 \\ 0 \end{bmatrix}. \tag{2.67}$$

From (2.67), the optimal solution of Case (II) can be written with z_1^* and z_{22}^* as

$$(\boldsymbol{\tau}^*, \boldsymbol{t}^*) = \frac{1}{1 + \frac{1}{z_1^*} + \frac{1}{z_{22}^*}} \times [1, \frac{1}{z_1^*}, 0, \frac{1}{z_{22}^*}, 0, 1]. \tag{2.68}$$

Hence, I will focus on finding the values of z_1^* and z_{22}^* and solving the inequality conditions for each valid sub-case.

Case (II)-a: z_1^* and z_{22}^* of Case (II)-a are identical to z_1^* and z_{21}^* of Case (I)-a. That is, $z_1^* = \frac{e^C - 1}{\rho_1^{(10)}}$ and $z_{22}^* = \frac{e^C - 1}{\rho_2}$, of which derivation is analogous to that of z_1^* and z_{21}^* in Case (I)-a. From the complementary slackness corresponding to λ_4^*, λ_5^*, and λ_6^*, (2.18e), (2.18f) (equivalently, (2.28) and (2.29)), and (2.18g) are non-binding. By exploiting $\tau_{21}^* = 0$ and $\rho_1^{(10)} < \rho_1^{(12)}$, it can be easily shown that (2.28) holds trivially. (2.29) and (2.18g) can be rewritten with the optimal solution as

$$\theta_1 \leq \theta_1^{(c1)}, \tag{2.69}$$

$$\theta_2 \leq \theta_2^{(c)}. \tag{2.70}$$

Note that (2.69) and (2.70) are included in the classification criteria of Case (I)-a, (2.47)-(2.49). Hence, multiple solutions exist when $\theta_1 \leq \theta_1^{(c1)}$ and $\theta_2 \leq \theta_2^{(c)}$ owing to that **(P2)** is not strictly convex.

Remark 3. *The maximum sum-throughput achieved in Case (II)-a is equal to that of Case (I)-a and (I)-b as $\theta_1^{(c1)} + \theta_2^{(c)}$ from Remark 1. It can be easily shown by computing the maximum sum-throughput using the optimal solution of Case (II)-a. It is worth noting that there is no user cooperation gain over $\theta_1 \leq \theta_1^{(c1)}$ and $\theta_2 \leq \theta_2^{(c)}$ as the identical maximum sum-throughput can be obtained either with or without user cooperation.*

Fig. 2.3(a) illustrates Remark 3 that the left interior of the dashed line in the blue box is the Case (II)-a region, and any pair of (θ_1, θ_2) which belongs to it yields the same maximum sum-throughput of $\theta_1^{(c1)} + \theta_2^{(c)}$ as in Case (I)-a and (I)-b. It can be seen

that since the slope of the straight line corresponding to Case (I)-b is -1, the sum of θ_1 and θ_2 on this line is the system maximum sum-throughput (i.e., $\theta_1^{(c1)} + \theta_2^{(c)}$.) Moreover, the QoS requirements in Case (I)-a and (II)-a are low that they can be easily fulfilled while achieving the system maximum sum-throughput. Note that the system maximum sum-throughput itself does not benefit from user cooperation, since it can be achieved in the Case (II)-a region which does not exploit user cooperation. Nevertheless, in the region of Case (I)-a and (I)-b except Case (II)-a, the system maximum sum-throughput can be achieved only when exploiting user cooperation.

For all the other remaining valid sub-cases in Case (II), the optimal solutions can be derived in a similar manner. The results of the sub-cases are provided first, and the derivation is derivation is presented next.

Case (II)-b: z_1^* and z_{22}^* of Case (II)-b can be obtained by solving the following two non-linear equations, (2.71), (2.72), which should be solved with a non-linear equation solving algorithm such as Newton-Raphson method.

$$f_{\rho_1^{(10)}}(z_1^*)(f_{\rho_2}(z_{22}^*) - g_{\rho_2}(z_{22}^*)) = f_{\rho_2}(z_{22}^*) g_{\rho_1^{(10)}}(z_1^*), \tag{2.71}$$

$$\theta_2 = \frac{\frac{1}{z_{22}^*}}{1 + \frac{1}{z_1^*} + \frac{1}{z_{22}^*}} \log_2(1 + \rho_2 z_{22}^*). \tag{2.72}$$

Note that (2.71) and (2.72) depend on the channel conditions and θ_2. For the problem to be classified as Case (II)-b, θ_1 should satisfy the following condition for the given θ_2,

$$\theta_1 \leq \frac{\frac{1}{z_1^*}}{1 + \frac{1}{z_1^*} + \frac{1}{z_{22}^*}} \log_2(1 + \rho_1^{(10)} z_1^*) (\triangleq \gamma_{\theta_1}^{\text{(II)-b}}). \tag{2.73}$$

Derivation of the solution to Case (II)-b: Using that $\lambda_4^* = \lambda_5^* = 0$ and $\lambda_3^* = 1$ from (2.21), I can induce a non-linear equation of z_1^* and z_{22}^*, (2.71) by eliminating the Lagrangian multipliers as in Case (I)-c. From the complementary slackness, $\lambda_6^* \neq 0$ results in (2.18g) being an equality, which is equivalent to (2.72). Meanwhile, $\lambda_4^* = 0$

and $\lambda_5^* = 0$ results in (2.28) and (2.29) being inequalities. (2.28) holds trivially as in Case (II)-a. (2.29) can be rewritten as (2.73).

Case (II)-d: z_1^*, z_{22}^* and $(\boldsymbol{\tau}^*, \boldsymbol{t}^*)$ are identical to those of Case (II)-b. In particular, for the problem to be classified as Case (II)-d, θ_1 should satisfy (2.73) at its equality for the given θ_2 (i.e., $\theta_1 = \gamma_{\theta_1}^{\text{(II)-b}}$.)

Derivation of the solution to Case (II)-d: The values of z_1^* and z_{22}^* are identical to those of Case (II)-d, of which derivation is skipped as it is similar to that of Case (II)-b. Furthermore, from the complementary slackness corresponding to $\lambda_5^* \neq 0$, (2.29) should be binding, which is equivalent to that (2.73) being replaced with equality.

Remark 4. *The maximum sum-throughputs achieved in Case (II)-b and (II)-d under the same θ_2 are identical. For both sub-cases, z_1^* and z_{22}^* depend on the values of ρ's and θ_2 from* (2.71) *and* (2.72)*. Hence, for the same θ_2 under the same channel condition, the optimal solutions of Case (II)-b and (II)-d are the same, and consequently achieve the same maximal sum-throughputs.*

Fig. 2.3(c) illustrates Remark 4 that the interior of the blue box is the Case (II)-b region and the curved boundary is the Case (II)-d, and any pair of (θ_1, θ_2) lying on any horizontal arrow in the blue box yields the same maximum sum-throughput. On the contrary to Remark 2, it can be seen that since the gain of allocating resources to U_1 is greater, the throughput of U_2 is adjusted to the QoS requirement, and U_1 is allocated with the remaining time resources for broadcasting. Furthermore, as z_{21}^* is undefinable, user cooperation should not be exploited.

Remark 5. *The optimal solutions achieving the maximum feasible QoS constraints for U_1 and U_2, $\theta_1^{(u)}$ and $\theta_2^{(u)}$ can be obtained in Case (I) and (II), respectively. In particular, if $\theta_1^{(c1)} + \theta_2^{(c)} \leq \theta_1^{(c2)}$, U_1 can achieve $\theta_1^{(u)}$ in Case (I)-b. If not, $\theta_1^{(u)}$ can be achieved in Case (I)-d. U_2 can achieve $\theta_2^{(u)}$ in Case (II)-d.*

Proof. When z_1^* and z_{21}^* are positive and z_{22}^* is undefinable, $\theta_1^{(u)}$ can be achieved.

Considering τ_{22}^* and t_{22}^* are zeros, the optimal solution for yielding $\theta_1^{(u)}$ can be derived with the Lagrangian stationarity conditions and complementary slackness, as in Cases (I) and (II), the derivation of which is skipped due to the space limit. In particular, if $\theta_1^{(c1)} + \theta_2^{(c)} \leq \theta_1^{(c2)}$, z_1^* and z_{21}^* for achieving $\theta_1^{(u)}$ are identical to those of Case (I)-b. Otherwise, they can be achieved with the non-linear equations of z_1^* and z_{21}^* of Case (I)-d. Furthermore, it can be seen that the optimal solution coincides with that of Case (I)-b or (I)-d when $\theta_1 = \theta_1^{(u)}$ and $\theta_2 = 0$ while not violating the inequality conditions for Case (I)-b or (I)-d. Likewise, the similar argument can be applied to achieving $\theta_2^{(u)}$, and it can be shown that the optimal solution coincides with that of Case (II)-b. □

Lemma 4. *On the maximum feasible pair of θ_1 and θ_2, θ_2 is a decreasing concave function of θ_1. Equivalently, the throughput of U_2 is a decreasing concave function with respect to the throughput of U_1.*

Proof. Suppose I have feasible $\boldsymbol{\theta_A} = (\theta_{1A}, \theta_{2A})$ and $\boldsymbol{\theta_B} = (\theta_{1B}, \theta_{2B})$, and their corresponding optimal solutions $(\boldsymbol{\tau}_A^*, \boldsymbol{t}_A^*)$ and $(\boldsymbol{\tau}_B^*, \boldsymbol{t}_B^*)$. Consider a convex combination of $\boldsymbol{\theta_A}$ and $\boldsymbol{\theta_B}$ denoted by $\boldsymbol{\theta_{AB}} = (\theta_{1AB}, \theta_{2AB})$, and another convex combination of $(\boldsymbol{\tau}_A^*, \boldsymbol{t}_A^*)$ and $(\boldsymbol{\tau}_B^*, \boldsymbol{t}_B^*)$ denoted by $(\boldsymbol{\tau}_{AB}, \boldsymbol{t}_{AB})$. Then, **(P2)** with $\boldsymbol{\theta_{AB}}$ is a feasible problem, the reason for which is as follows: $(\boldsymbol{\tau}_{AB}, \boldsymbol{t}_{AB})$ satisfies (2.18b) and (2.18c) from the convex combination. (2.18d), (2.18e), and (2.18f) are equivalent to $R_1^{(10)}(\boldsymbol{\tau}, \boldsymbol{t}) + R_1^{(20)}(\boldsymbol{\tau}, \boldsymbol{t}) \geq \theta_1$, and $R_1^{(12)}(\boldsymbol{\tau}, \boldsymbol{t}) \geq \theta_1$, respectively. Due to the concavity of $R_u^{(ij)}(\boldsymbol{\tau}, \boldsymbol{t})$, $R_1^{(10)}(\boldsymbol{\tau}_{AB}, \boldsymbol{t}_{AB}) + R_1^{(20)}(\boldsymbol{\tau}_{AB}, \boldsymbol{t}_{AB}) \geq \theta_{1AB}$ and $R_1^{(12)}(\boldsymbol{\tau}_{AB}, \boldsymbol{t}_{AB}) \geq \theta_{1AB}$ hold. In a similar manner, (2.18g) is satisfied as $R_2^{(20)}(\boldsymbol{\tau}, \boldsymbol{t}) \geq \theta_{2AB}$ holds. Hence, the feasible region of (θ_1, θ_2) is a convex set on $\mathbb{R}_+^2$. Furthermore, since the boundary of a convex set is a convex curve and $(\theta_1^{(u)}, 0)$ and $(0, \theta_2^{(u)})$ lie in the boundary, θ_2 is a decreasing concave function of θ_1 on the boundary of the convex set. □

Case (II)-c: z_1^* and z_{22}^* of Case (II)-c can be obtained by solving (2.71) and (2.73) with its equality. Furthermore, θ_2 should be less than or equal to the R.H.S. of (2.72). The derivation of the equations is analogous to that of Case (II)-b. Nevertheless, Case (II)-c is not a valid case except when (2.72) holds with equality (i.e., when Case (II)-c is equivalent to Case (II)-d), since it does not yield the maximum sum-throughput for the given θ_1 and θ_2. When $\theta_1 \leq \theta_1^{(c1)}$ and $\theta_2 \geq \theta_2^{(c)}$, the problem can be classified as Case (II)-b, (II)-c or (II)-d, which will be described concretely in the following section. Then, Case (II)-b intends to increase U_1's throughput from θ_1 while U_2's throughput is satisfied at θ_2. On the other hand, Case (II)-c intends to increase U_2's throughput from θ_2 while U_1's throughput being satisfied at θ_1. The amount of increased throughput in Case (II)-b is larger than that in Case (II)-c, the reason of which is as follows. From (2.52) in Case (I)-b and Lemma 4, $(\theta_1^{(c1)}, \theta_2^{(c)})$ is shown to be on the boundary of the feasible (θ_1, θ_2). As $\frac{d\theta_2}{d\theta_1}|_{\theta_1=\theta_1^{(c1)}} = -1$ from Case (I)-b and $-1 \leq \frac{d\theta_2}{d\theta_1} \leq 0$ when $0 \leq \theta_1 \leq \theta_1^{(c1)}$ due to the concavity of θ_2 with respect to θ_1 on the boundary from Lemma 4, it achieves higher sum-throughput to increase U_1's throughput, as for Case (II)-b compared to Case (II)-c. Therefore, I conclude that Case (II)-c is invalid, except when it coincides with Case (II)-d. Refer to Figs. 2.4 and 2.5 in the following section for an illustrative description. Each plot in the figures shows the boundaries of the feasible (θ_1, θ_2).

2.5 QoS Constrained Sum-Throughput Maximization Algorithm

I propose a sum-throughput maximization algorithm with individual QoS constraints to find the optimal time allocation, $(\boldsymbol{\tau}^*, \boldsymbol{t}^*)$. For given θ_1 and θ_2, the algorithm classifies **(P2)** as one of the sub-cases. According to the divide-and-conquer approach, once the optimal solution for specific θ_1 and θ_2 is obtained, the algorithm no longer

considers the problem of the θ_1 and θ_2, even though multiple solutions might exist. In the following, I compare the computational complexity of two algorithms in solving **(P2)**, the proposed algorithm and the interior-point method [26] which is one of the common algorithms for an inequality constrained convex optimization problem. In addition, I compare the computational complexity of the WST maximization algorithm [24] with the proposed algorithm in fulfilling the QoS requirements.

2.5.1 Proposed Algorithm

I first consider the problems with $\theta_1 \leq \theta_1^{(c1)}$ and $\theta_2 \leq \theta_2^{(c)}$, which can be classified as Case (I)-a or (II)-a. Since either case yields the identical maximum sum-throughput as stated in Remark 3, I let the problem be classified as Case (II)-a. Excluding the intervals of Case (II)-a from those of Case (I)-a, the problems with $\theta_1^{(c1)} \leq \theta_1 \leq \theta_1^{(c2)}$ and $\theta_1 + \theta_2 < \theta_1^{(c1)} + \theta_2^{(c)}$ are classified as Case (I)-a. For Case (I)-a, τ_{21}^* can be randomly chosen within (2.42) without affecting the maximum sum-throughput as stated in Remark 1. For simplicity, τ_{21}^* is allocated with the minimum of the available values (i.e., $\tau_{21}^* = \max(0, \psi_A)$.) Moreover, the problems with $\theta_1^{(c1)} \leq \theta_1 \leq \min(\theta_1^{(c1)} + \theta_2^{(c)}, \theta_1^{(c2)})$ and $\theta_1 + \theta_2 = \theta_1^{(c1)} + \theta_2^{(c)}$ are classified as Case (I)-b.

I subsequently consider the problems with the remaining intervals of θ_1 and θ_2, which are $\theta_1 \geq \min(\theta_1^{(c1)} + \theta_2^{(c)}, \theta_1^{(c2)})$ and $\theta_2 \geq \theta_2^{(c)}$, and I match them to remaining sub-cases, Case (I)-c, (I)-d, (II)-b and (II)-d. It can be inferred that $\theta_1 \geq \min(\theta_1^{(c1)} + \theta_2^{(c)}, \theta_1^{(c2)})$ can be matched to Case (I)-c or (I)-d using Lemma 4 and Remark 2. From Lemma 4, on the maximum feasible pair of θ_1 and θ_2, $\frac{d\theta_2}{d\theta_1} \leq -1$ holds for $\theta_1 \geq \min(\theta_1^{(c1)} + \theta_2^{(c)}, \theta_1^{(c2)})$. Thus, in order to achieve the maximum sum-throughput, the throughput of U_2 needs to increase, while the throughput of U_1 is fixed at θ_1, which is consistent with Remark 2. Nevertheless, if $\min(\theta_1^{(c1)} + \theta_2^{(c)}, \theta_1^{(c2)}) = \theta_1^{(c1)} + \theta_2^{(c)}$, then $\theta_1^{(u)} = \theta_1^{(c1)} + \theta_2^{(c)}$, which can be obtained in Case (I)-b as stated in Remark 5. There-

fore, only when $\min(\theta_1^{(c1)}+\theta_2^{(c)}, \theta_1^{(c2)}) = \theta_1^{(c2)}$, the problem can be classified as Case (I)-c or (I)-d unless it is infeasible. The feasibility can be checked with $\theta_2 \leq \gamma_{\theta_2}^{\text{(I)-c}}$ from (2.59) of Case (I)-c. Furthermore, Case (I)-c and (I)-d have the identical optimal solution and sum-throughput as stated in Remark 2; hence, further classification is no longer needed.

Likewise, $\theta_2 \geq \theta_2^{(c)}$ is matched to Case (II)-b or (II)-d, and the problem can be classified as either one of the two cases unless it is infeasible. The feasibility can be checked with $\theta_1 \leq \gamma_{\theta_1}^{\text{(II)-b}}$ from (2.73) of Case (II)-b. Furthermore, Case (II)-b and (II)-d have the identical optimal solution and sum-throughput as stated in Remark 4; hence, further classification is no longer needed either. The proposed algorithm is summarized in Algorithm 1.

Figs. 2.4 and 2.5 illustrate the concept of the algorithm when $\theta_1^{(c1)} + \theta_2^{(c)} > \theta_1^{(c2)}$ and not, respectively. Each figure shows the sub-case to which the problem belongs for given θ_1 and θ_2. The θ_1-θ_2 curves indicate the maximal θ_1 and θ_2 pair, which does not make the problem infeasible. They are plotted numerically following the simulation setup without short-term fading, the details of which are given in the following section.

2.5.2 Computational Complexity Comparison

For the computational complexity of the proposed algorithm, it suffices to find the computational complexity of the sub-problem with the highest computational complexity, which is Case (I)-c since the proposed algorithm sequentially classifies the problem into one of the sub-problems. The classification preliminarily needs to compute C for having $\theta_1^{(c1)}$, $\theta_1^{(c2)}$, and $\theta_2^{(c)}$. The Lambert W function value can be evaluated using the Newton method, of which complexity is given by $\mathcal{O}((\log_2 \log_2 \epsilon^{-1})d^{2.5})$ for this case where ϵ is the target estimation error, and d refers to the number of digits of precision. Subsequently, it needs to compute $\theta_1^{(u)}$ for checking the feasibility of

Algorithm 1 Sum-Throughput Maximization with QoS Constraint for Cooperative WPCN

if $\theta_1 \leq \theta_1^{(c1)}$ and $\theta_2 \leq \theta_2^{(c)}$ **then**
    $(\boldsymbol{\tau}^*, \boldsymbol{t}^*) \leftarrow$ Case (II)-a
else
    if $\theta_1^{(c1)} < \theta_1 \leq \theta_1^{(c2)}$ and $\theta_1 + \theta_2 < \theta_1^{(c1)} + \theta_2^{(c)}$ **then**
        $(\boldsymbol{\tau}^*, \boldsymbol{t}^*) \leftarrow$ Case (I)-a
    else
        if $\theta_1^{(c1)} \leq \theta_1 \leq \min(\theta_1^{(c1)} + \theta_2^{(c)}, \theta_1^{(c2)})$ and $\theta_1 + \theta_2 = \theta_1^{(c1)} + \theta_2^{(c)}$ **then**
            $(\boldsymbol{\tau}^*, \boldsymbol{t}^*) \leftarrow$ Case (I)-b
if $\theta_1^{(c1)} + \theta_2^{(c)} > \theta_1^{(c2)}$ **then**
    if $\theta_1 > \theta_1^{(c2)}$ **then**
        $(z_1^*, z_{21}^*) \leftarrow$ (2.55), (2.56) of Case (I)-c
        $\gamma_{\theta_2}^{\text{(I)-c}} \leftarrow$ (2.59) of Case (I)-c
        if $\theta_2 \leq \gamma_{\theta_2}^{\text{(I)-c}}$ **then**
            $(\boldsymbol{\tau}^*, \boldsymbol{t}^*) \leftarrow$ Case (I)-c
if $\theta_2 > \theta_2^{(c)}$ **then**
    $(z_1^*, z_{22}^*) \leftarrow$ (2.71), (2.72) of Case (II)-b
    $\gamma_{\theta_1}^{\text{(II)-b}} \leftarrow$ (2.73) of Case (II)-b
    if $\theta_1 \leq \gamma_{\theta_1}^{\text{(II)-b}}$ **then**
        $(\boldsymbol{\tau}^*, \boldsymbol{t}^*) \leftarrow$ Case (II)-b

▷ If given θ_1 and θ_2 do not satisfy any of the conditional statements, the problem is infeasible.

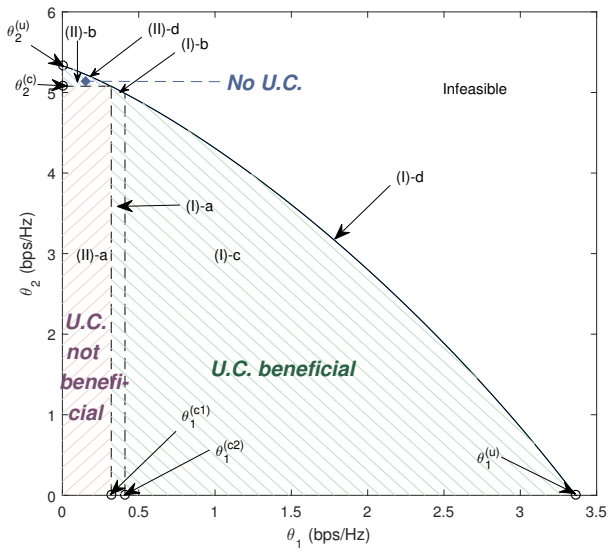

Figure 2.4: Algorithm concept when $\theta_1^{(c1)} + \theta_2^{(c)} > \theta_1^{(c2)}$, $D_{10} = 10$ m and $D_{20} = D_{12} = 5$ m.

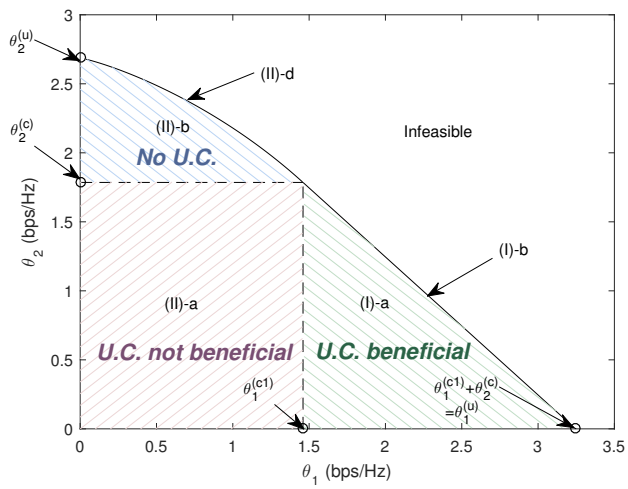

Figure 2.5: Algorithm concept when $\theta_1^{(c1)} + \theta_2^{(c)} \leq \theta_1^{(c2)}$, $D_{10} = 10$ m, $D_{20} = 9.5$ m, and $D_{12} = 0.5$ m.

the problem, and to solve (2.55) and (2.56) for obtaining the optimal solution. Both of them can then be done using the Newton-Raphson method for a pair of equations of two variables, the computational complexity of which is $\mathcal{O}((\log_2 \log_2 \epsilon^{-1})2^3 d^{2.5})$. As a result, dropping the constants in calculating the big $\mathcal{O}$ complexity, the computational complexity of the proposed algorithm is not higher than $\mathcal{O}((\log_2 \log_2 \epsilon^{-1})d^{2.5})$.

On the other hand, the interior-point method [26], in particular, the barrier method approximates an inequality constrained optimization problem as an equality constrained smooth problem using the barrier function which is an approximation of an indicator function. For solving **(P2)**, the barrier method requires $\mathcal{O}\left(\sqrt{6}\log_2\left(\frac{6/l^{(0)}}{\delta}\right)\right)$ iterations of updating l for achieving the suboptimality gap of $\frac{6}{l}$ smaller than δ. The approximated problem for given l is solved via the multivariate Newton-Raphson method, which has the computational complexity of $\mathcal{O}\left((\log_2 \log_2 \epsilon^{-1})7^3 d^{2.5}\right)$ achieving the estimation error below ϵ. Therefore, dropping the constants in calculating the big $\mathcal{O}$ complexity, the interior-point method has the computational complexity of $\mathcal{O}\left(\left(\log_2 \delta^{-1}\right)(\log_2 \log_2 \epsilon^{-1})d^{2.5}\right)$.

To further compare the computational complexity of the proposed algorithm with the WST maximization algorithm [24], I assume that the accurate weights to fulfill the QoS requirements are found for the WST maximization algorithm. The WST maximization algorithm has the inner loop for finding its dual function with the given Lagrangian multipliers and the outer loop for updating the Lagrangian multipliers. The inner loop exploits the bisection method with the computational complexity of $\mathcal{O}(\log_2(\frac{\epsilon_0}{\epsilon})d^2)$, and the outer loop exploits the ellipsoid method with the computational complexity of $\mathcal{O}(2 \times 4^2 \times \log_2 \frac{RG}{\delta} 4^2 d^{2.5})$ where R and G are the radius of the initial ellipsoid and the constant from the characteristic of its objective. Dropping the constants in calculating the big $\mathcal{O}$ complexity, the computational complexity of the WST maximization algorithm is given by $\mathcal{O}\left((\log_2 \epsilon^{-1})(\log_2 \delta^{-1})d^{4.5}\right)$, which is expected to be higher than the computational complexity of the proposed algorithm.

2.6 Sum-Throughput Maximization with Processing Cost

In this section, I consider processing cost at each user in maximizing the sum-throughput for the considered network. In particular, processing cost is the power consumed at each user in addition to transmit power during its allocated time. Thus, U_1 consumes the processing cost for broadcasting its message during τ_1, which is denoted by $P_{c,1}$. U_2 consumes the processing cost for relaying the message of U_1 during τ_{21}, which is denoted by $P_{c,21}$, and the processing cost for transmitting its own message during τ_{22}, which is denoted by $P_{c,22}$. Since the processing cost is taken account into explicitly, I let η_i of (2.4) be 1. The QoS-constrained problem, **(P1)** is then modified as

$$\begin{aligned}
\textbf{(P3)}: \max_{\boldsymbol{\tau},\mathbf{P}} \quad & R_1(\boldsymbol{\tau},\mathbf{P}) + R_2(\boldsymbol{\tau},\mathbf{P}) && \text{(2.74a)}\\
\text{s.t.} \quad & \tau_0 + \tau_1 + \tau_{21} + \tau_{22} \leq 1, && \text{(2.74b)}\\
& (P_1 + P_{c,1})\tau_1 \leq E_1, && \text{(2.74c)}\\
& (P_{21} + P_{c,21})\tau_{21} + (P_{22} + P_{c,22})\tau_{22} \leq E_2, && \text{(2.74d)}\\
& \boldsymbol{\tau} \succeq 0, \mathbf{P} \succeq 0, && \text{(2.74e)}\\
& R_1(\boldsymbol{\tau},\mathbf{P}) \geq \theta_1, && \text{(2.74f)}\\
& R_2(\boldsymbol{\tau},\mathbf{P}) \geq \theta_2. && \text{(2.74g)}
\end{aligned}$$

Due to the non-convexity of **(P3)**, **(P3)** is transformed into a convex problem by following the similar approach in Section 2.3 as follows:

$$P_1 + P_{c,1} = \zeta_1 P_0 h_{10} \frac{\tau_0}{\tau_1}, t_{21} = \frac{(P_{21} + P_{c,21})\tau_{21}}{\zeta_2 h_{20} P_0}, \text{ and } t_{22} = \frac{(P_{22} + P_{c,22})\tau_{22}}{\zeta_2 h_{20} P_0}.$$

Then, **(P3)** can be rewritten as

$$\textbf{(P4)}: \max_{\bar{R},\boldsymbol{\tau},\boldsymbol{t}} \quad \bar{R} + R_2(\boldsymbol{\tau},\boldsymbol{t}) \tag{2.75a}$$

$$\text{s.t.} \quad \tau_0 + \tau_1 + \tau_{21} + \tau_{22} \leq 1, \tag{2.75b}$$

$$t_{21} + t_{22} \leq \tau_0, \tag{2.75c}$$

$$\zeta_1 P_0 h_{10} \tau_0 \geq P_{c,1}\tau_1, \tag{2.75d}$$

$$\zeta_2 P_0 h_{20} t_{21} \geq P_{c,21}\tau_{21}, \tag{2.75e}$$

$$\zeta_2 P_0 h_{20} t_{22} \geq P_{c,22}\tau_{22}, \tag{2.75f}$$

$$\boldsymbol{\tau} \succeq 0, \tag{2.75g}$$

$$\bar{R} \leq R_1^{(10)}(\boldsymbol{\tau},\boldsymbol{t}) + R_1^{(20)}(\boldsymbol{\tau},\boldsymbol{t}), \tag{2.75h}$$

$$\bar{R} \leq R_1^{(12)}(\boldsymbol{\tau},\boldsymbol{t}), \tag{2.75i}$$

$$\bar{R} \geq \theta_1, \tag{2.75j}$$

$$R_2^{(20)}(\boldsymbol{\tau},\boldsymbol{t}) \geq \theta_2, \tag{2.75k}$$

where

$$R_1^{(10)}(\boldsymbol{\tau},\boldsymbol{t}) = \tau_1 \log_2\left(1 + \frac{h_{10}}{\sigma^2}\left(\zeta_1 P_0 h_{10}\frac{\tau_0}{\tau_1} - P_{c,1}\right)\right),$$

$$R_1^{(12)}(\boldsymbol{\tau},\boldsymbol{t}) = \tau_1 \log_2\left(1 + \frac{h_{12}}{\sigma^2}\left(\zeta_1 P_0 h_{10}\frac{\tau_0}{\tau_1} - P_{c,1}\right)\right),$$

$$R_1^{(20)}(\boldsymbol{\tau},\boldsymbol{t}) = \tau_{21} \log_2\left(1 + \frac{h_{20}}{\sigma^2}\left(\zeta_2 P_0 h_{20}\frac{t_{21}}{\tau_{21}} - P_{c,21}\right)\right),$$

$$R_2^{(20)}(\boldsymbol{\tau},\boldsymbol{t}) = \tau_{22} \log_2\left(1 + \frac{h_{20}}{\sigma^2}\left(\zeta_2 P_0 h_{20}\frac{t_{22}}{\tau_{22}} - P_{c,22}\right)\right).$$

Note that **(P4)** is a convex problem, and (2.75d)-(2.75f) indicate that the amount of harvested energy for each transmit time should be larger than the amount of energy for processing.

2.7 Simulation Results

Numerical results are provided in this section. In the following, I simulate the sum-throughput maximization for WPCN with user cooperation under various QoS constraints and compare it with the sum-throughput maximization for WPCN *without user cooperation* under the same QoS constraints. For the evaluation of sum-throughput maximization without user cooperation, I use a convex optimization tool, CVX [30]. The maximization problem without user cooperation is formulated with **(P2)** by setting τ_{21} and t_{21} equal to zero; thus, it still keeps the convexity of **(P2)**. For simulation, the H-AP, U_1, and U_2 are assumed to be on a straight line (i.e., 1-D model) and U_2 is located between the H-AP and U_1. The transmit power of the H-AP, P_0, the bandwidth, and the noise power spectral density are assumed to be 0.1W, 1MHz, and -160dBm/Hz, respectively. Furthermore, the energy harvesting efficiency and the ratio of harvested energy to be used for transmission at each user, ζ_i and η_i are assumed to be 0.5 for all i.

First, I consider the case where the short-term fading is assumed to be neglected (i.e., $g_{ij} = 1$ for all $ij \in \{10, 20, 12\}$) in order to observe instantaneous and theoretical performance of each user's throughput and their sum over various QoS constraints. Fig. 2.6 shows the throughputs of U_1, U_2 and their sum along with given (θ_1, θ_2) when $D_{10} = 10$ m, $D_{20} = 5$ m, and $D_{12} = 5$ m. It is observed that in the surface of the sum-throughput, the sum-throughput remains still along with various θ_2 and θ_1 being fixed. It can be seen that as the value of θ_1 being fixed increases, the range of θ_2 which does not make the problem infeasible decreases. Equivalently, the sum-throughput becomes smaller along with increasing θ_1 with θ_2 being fixed.

Fig. 2.7 shows Fig. 2.6 from θ_1-axis perspective while the QoS constraint of U_2, θ_2 is fixed at 1.5 bps/Hz, and the throughput obtained by the sum-throughput maximization scheme *without user cooperation* under the same setting. In Fig. 2.7, ST, U_1, and U_2 stand for the sum-throughput, the throughput of U_1, and the throughput

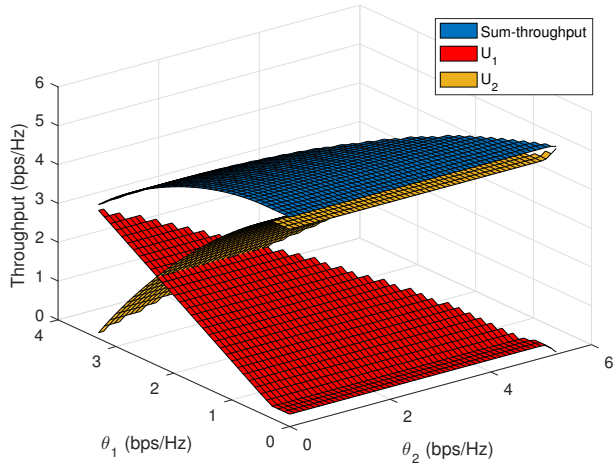

Figure 2.6: Throughput with various QoS constraints when $D_{10} = 10$ m and $D_{20} = D_{12} = 5$ m.

of U_2, respectively while (w/ cooperation) and (w/o cooperation) refer to the sum-throughput maximizations with user cooperation and without user cooperation. It is observed that for all the θ_1, the sum-throughput maximization with user cooperation achieves higher or identical sum-throughputs compared to without user cooperation. Note that the U_2 plots of both schemes cannot extend below 1.5 bps/Hz which is given by θ_2; hence, the ST and U_1 plots end when U_2 achieves θ_2. For relatively low θ_1 (around below 0.5 bps/Hz), the sum-throughputs remain still for both schemes at the same level, which indicates that for some QoS constraints, user cooperation does not offer gain in terms of sum-throughput.

I secondly consider the case where the short-term fading coefficient, g_{ij} is assumed to be $g_{ij} = |\tilde{g}_{ij}|^2$ where $\tilde{g}_{ij} \sim \mathcal{CN}(0, 1)$ for all $ij \in \{10, 20, 12\}$ in order to observe the overall impact of the user cooperation on each user's throughput and their sum under the fading channel assumptions. Figs. 2.8-2.10 show the average sum-throughputs, U_1's throughputs, and U_2's throughputs over a range of QoS con-

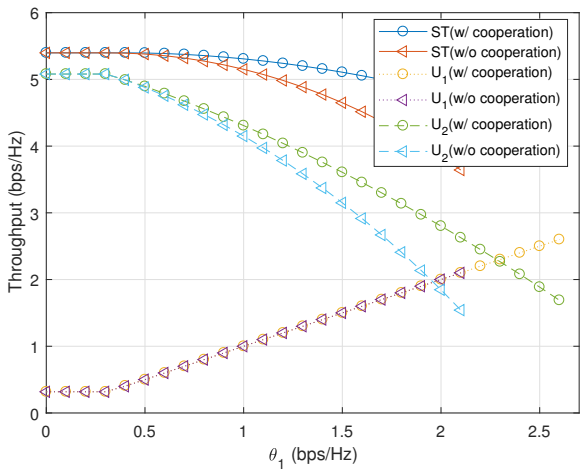

Figure 2.7: Throughput with various θ_1 and $\theta_2 = 1.5$ bps/Hz when $D_{10} = 10$ m and $D_{20} = D_{12} = 5$ m.

straints according to user cooperation mode, where $D_{10} = 10$ m, $D_{20} = 5$ m, and $D_{12} = 5$ m. It can be seen that the average throughputs in Figs. 2.8-2.10 decrease as the values of QoS constraints get higher since the probability of the maximization problem being infeasible increases. In Fig. 2.8, the average sum-throughputs with user cooperation are higher than those without user cooperation. In particular, the user cooperation gain is distinct in general when given θ_1 is relatively high, while it is degraded when given θ_2 is high, which indicates that the user with worse channel condition benefits from user cooperation. In Fig. 2.9, the difference of the average throughputs of U_1 between the two schemes is relatively distinct, unlike that of U_2 in Fig. 2.10, which indicates that the user unfairness is alleviated.

In addition, I simulate the throughput performance of when processing cost is considered. For the evaluation of sum-throughput maximization with processing cost constraints, I use a convex optimization tool, CVX [30] as well. The simulation parameters are the same as those of simulations without processing cost constraints

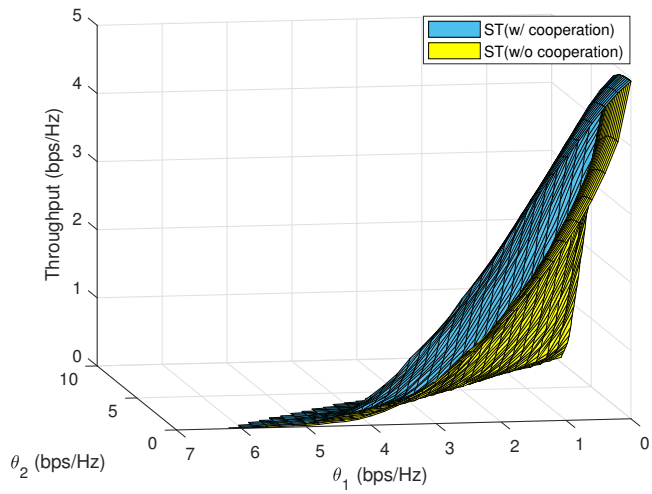

Figure 2.8: Average sum-throughput with various QoS constraints when $D_{10} = 10$ m and $D_{20} = D_{12} = 5$ m.

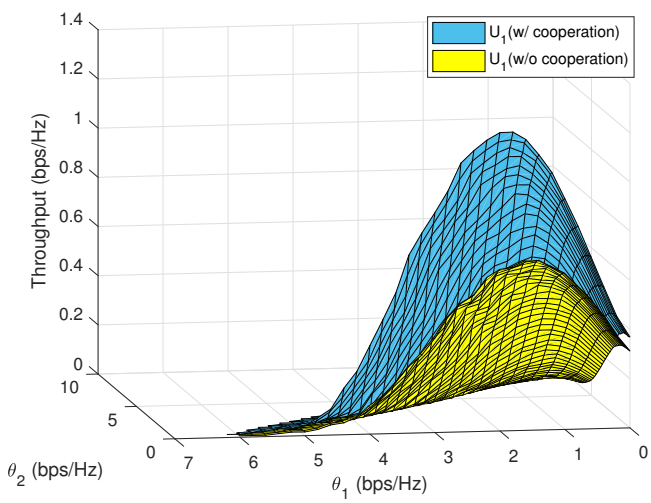

Figure 2.9: Average throughput of U_1 with various QoS constraints when $D_{10} = 10$ m and $D_{20} = D_{12} = 5$ m.

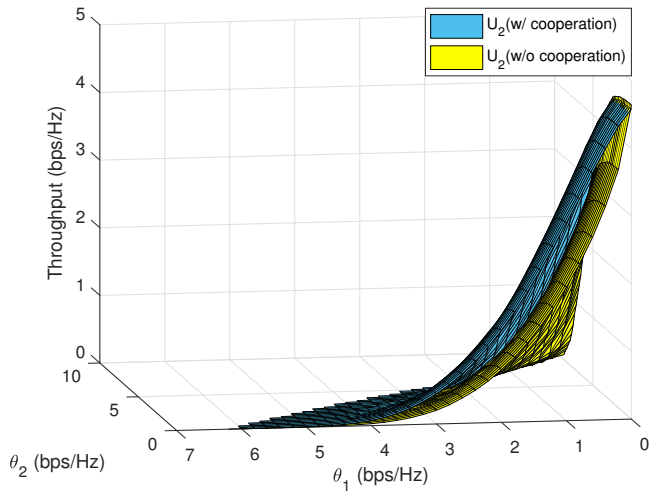

Figure 2.10: Average throughput of U_2 with various QoS constraints when $D_{10} = 10$ m and $D_{20} = D_{12} = 5$ m.

except that the noise power spectral density, the energy harvesting efficiency, and the ratio of harvested energy to be used for transmission at each user are assumed to be -174dBm/Hz, 0.7, and 1, respectively. Furthermore, the small-scale fading is assumed to be neglected, and $P_{c,1}$ and $P_{c,22}$ are assumed to be 0 for simplicity.

Fig. 2.11 shows the achievable rate region with various $P_{c,21}$. As seen in the figure, the achievable rate of U_2 is not affected by $P_{c,21}$ since $P_{c,21}$ is the processing cost for relaying the message of U_1. On the other hand, the achievable rate of U_1 decreases with growing $P_{c,21}$. In other words, the throughput gain by cooperation is reduced so that R_1 converges at the achievable rate of when there is no user cooperation.

Fig. 2.12 shows the sum-throughput and the throughput achieved by U_2 with various $P_{c,21}$ when θ_1 is set to 6 bps/Hz and θ_2 is set to 0 bps/Hz. As seen in the figure, R_{sum} and R_2 decrease and converge at the throughput of the case without user cooperation with growing $P_{c,21}$. Note that U_1 achieves θ_1 for any given $P_{c,21}$. Fig. 2.13 shows the amount of energy consumed for transmission during τ_1, τ_{21}, and τ_{22}

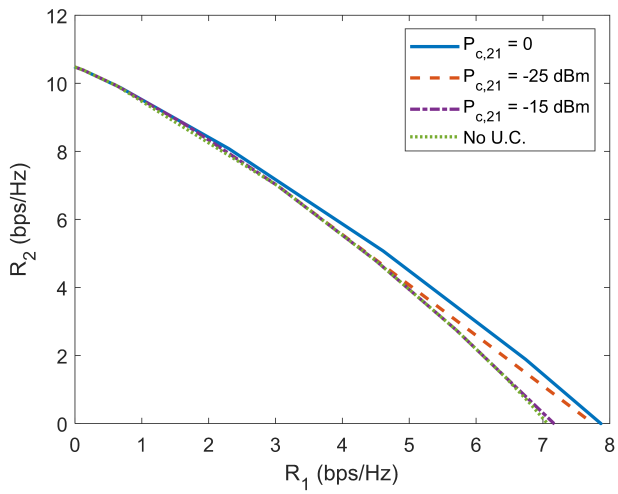

Figure 2.11: Achievable rate region with various $P_{c,21}$.

with various $P_{c,21}$. The dashed line indicates the amount of energy consumed for processing of cooperation. It can be seen that the energy used for relay transmission (i.e., the line of τ_{21}) decreases with growing $P_{c,21}$. In other words, since the gain from user cooperation decreases as the processing cost increases, the resources allocated for user cooperation are also reduced. Furthermore, since the time for cooperation decreases, the energy consumed for processing of cooperation decreases beyond $P_{c,21}$ of -25 dBm.

2.8 Conclusion

In this chapter, I have considered a sum-throughput maximization problem under individual QoS constraints for WPCN with user cooperation, and have derived an optimal solution using convex optimization technique. In particular, the maximization problem is divided into multiple sub-problems and each sub-problem is solved separately by converting it into a linear system. From the analysis of the sub-problems,

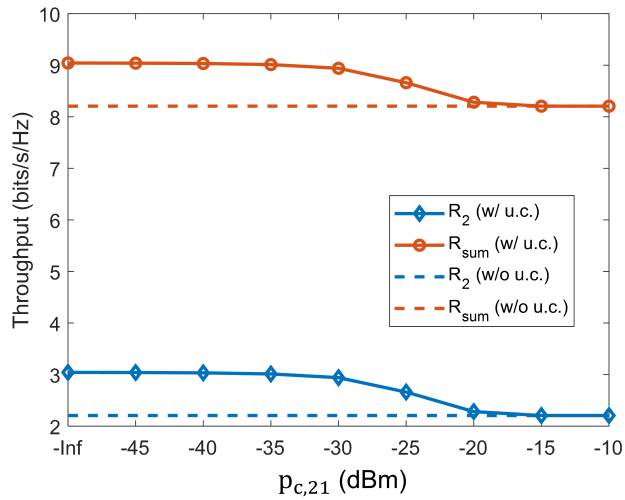

Figure 2.12: Throughput performance with various $P_{c,21}$ when $\theta_1 = 6$ bps/Hz and $\theta_2 = 0$ bps/Hz.

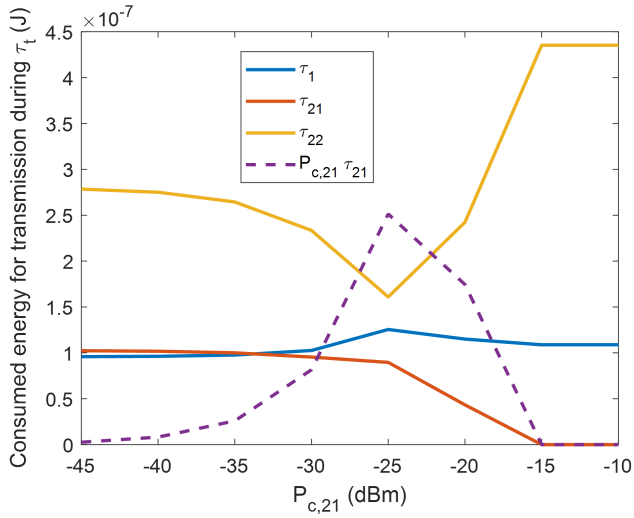

Figure 2.13: Energy consumption for transmission during τ_t with various $P_{c,21}$ when $\theta_1 = 6$ bps/Hz and $\theta_2 = 0$ bps/Hz.

conditions under which user cooperation becomes beneficial have been identified. I have then proposed a maximization algorithm that classifies the problem into one of the sub-problems depending on the given QoS values and returns the optimal time allocation of the corresponding sub-problem. In simulations, the throughputs under various QoS constraints have been presented, and the gain of user cooperation over the scheme without user cooperation has been demonstrated.

Chapter 3

NOMA-Based Wireless Powered Communication Networks with User Clustering

In this chapter, I consider WPCNs consisting of a power beacon (PB), a base station, and energy harvesting users, all equipped with multiple antennas. A PB transfers energy to the users using energy beamforming in the downlink, and the users transmit information using the harvested energy in the uplink, where non-orthogonal multiple access (NOMA) transmission is employed. For the uplink NOMA transmission, users are grouped into multiple clusters by cluster-specific beamforming. In particular, signal alignment is exploited for the beamforming so that the channels of users in a cluster are aligned in the same direction. By signal alignment, the number of users of messages decoded by successive interference cancellation (SIC) is reduced, which can be effective at lowering the decoding complexity and SIC error propagation. Due to the difficulty of jointly optimizing cluster-specific beamforming and time/energy resources for sum-throughput maximization, I determine the beamforming relying on signal alignment first, and then the resources are optimized for given beamforming. To be more specific, I propose a novel iterative algorithm for cluster-specific beamforming design followed by the sum-throughput maximization algorithm. Numerical

results show the sum-throughput performance of the proposed scheme and its robustness towards SIC error propagation compared to existing schemes.

3.1 Introduction

As applications of the Internet-of-Things (IoT) continue to grow, battery limitations of IoT devices are expected to be a major limitation for accommodating emerging services in the next generation of communication systems [33], [34]. Thus, for the seamless operation of IoT devices, consistent power supply or monitoring and maintenance of power is needed. However, wired charging or manual battery replacement can be impractical depending on the number of IoT devices or their deployments. In addition, machine type communication devices, one of the major components that comprise IoT networks, are presumed to be maintained without manual manipulation [35]. Therefore, the need for wireless battery charging arises for devices to achieve sustainable access in energy-constrained wireless networks such as IoT networks, and for ease of operation and maintenance of the network [36].

To realize wireless battery charging, especially in the far-field, energy harvesting has been studied which converts a radio-frequency (RF) signal into electrical energy to be stored in a battery [1], [6]. In particular, harvesting energy from RF signals transmitted by a dedicated energy source is called wireless power transfer (WPT) [7]. WPT has attracted a significant amount of attention for its controllability compared to ambient RF energy harvesting [8]. In this regard, a new framework called wireless powered communication networks (WPCNs) has been proposed [9]. A WPCN consists of multiple users with energy harvesting capability, a base station (BS), and an energy source called a power beacon (PB). Specifically, when a BS also delivers an energy signal as a PB, it is called a hybrid access point (H-AP). In [9], a harvest-then-transmit protocol was proposed, in which a PB transfers energy to the

users, called wireless energy transfer (WET) in the downlink (DL) before users send their messages to a BS, called wireless information transmission (WIT) in the uplink (UL). Hence, allocating time and energy resources for DL-WET and UL-WIT has been essential in a WPCN to increase the throughput.

Meanwhile, an IoT network needs to employ a multiple access scheme to serve multiple IoT devices. In particular, it is required to provide higher spectral efficiency, ultra-low latency, and higher connectivity in the next generation communication system [37]. Non-orthogonal multiple access (NOMA) has emerged as a key enabling technology due to its potential of facilitating the features of the next generation communication systems compared to orthogonal multiple access (OMA) [38]- [39]. Particularly, in the uplink NOMA transmission, the BS serves multiple users which transmit their data over the same resource (i.e., time, frequency, code, etc), thereby generating inter-user interferences due to the broadcast and superposition nature of the wireless medium [40]. The BS, then, is able to decode the messages of users by successive interference cancellation (SIC). That is, a message of a user is decoded treating interferences as noise, and is subtracted from the received signal at the BS. Thus, a user of its message decoded next experiences less interference than a user of its message decoded before. In what follows, related works on WPCN and NOMA are reviewed.

3.1.1 Throughput Maximization in WPCN

Various scenarios on WPCNs have been considered [12]- [46], etc. In [12]- [41], a multi-antenna system has been adapted to a WPCN. A multi-antenna PB is capable of DL energy beamforming which makes the H-AP deliver more energy to a particular user. A BS and users with multiple antennas can exploit multiple-input multiple-output (MIMO) technologies. In [12] and [13], the minimum individual throughput has been maximized and the average throughput performance has been analyzed in a

WPCN with a multi-antenna H-AP. In [41], the sum-throughput has been maximized in a WPCN with a multi-antenna H-AP and users with multiple antennas.

Furthermore, NOMA has been adopted as a multiple access scheme for UL-WIT in [23]- [46], etc. Particularly, a WPCN consisting of a H-AP with a single antenna and multiple users each with a single antenna has been considered in [23]- [45]. In [23], sum-throughput and equal individual data rate have been maximized. When serving users with NOMA, a user of its message decoded early by SIC experiences a lot of interference, so user fairness cannot be guaranteed. To improve user fairness, time-sharing SIC decoding was proposed. That is, the SIC decoding order is varied by time, and users experience interference evenly. In [44], a synchronous and an asynchronous NOMA transmission schemes have been considered. Energy efficiency (EE) which takes processing cost into account has been maximized. It has been shown that with growing transmit power at the H-AP, EE increases in the synchronous case, whereas EE increases and decreases in the asynchronous case. In [45], the throughput performance of TDMA and NOMA has been compared considering energy efficiency and circuit energy consumption. By thorough analysis, it has been shown that TDMA is more effective than NOMA in terms of spectral efficiency as well as energy consumption. In [46] a multi-antenna system has been adopted to the H-AP in a NOMA-based WPCN. For the considered system, the sum-throughput has been maximized subject to minimum throughput constraint.

3.1.2 User Clustering in NOMA

While NOMA is expected to enhance various system performance measures from a theoretical perspective, there are several implementation issues related to the NOMA decoding in practice [47]- [49]. For NOMA, it has been a concern that the decoding complexity and the implementation complexity of SIC increase with the growing number of users [47]. Furthermore, the error propagation has been an issue in SIC

decoding [48], [49], etc. That is, a signal that has not been completely removed affects the decoding of the subsequent messages, which results in severe throughput degradation. Hence, as the number of users served by a BS grows, the probability that error propagation occurs increases. Therefore, it is necessary to limit the number of interference cancellations. User pairing/clustering has been studied as one of the solutions to the aforementioned problems by dividing users into groups of smaller users and lowering the number of messages decoded by SIC [50], [51].

In [52]- [54], etc, multiple antennas are utilized for *cluster-specific beamforming* in MIMO-NOMA networks with various system models such as uplink/downlink transmission, multi-cell networks, etc. Beamforming matrices are designed for grouping users into clusters and suppressing the inter-cluster interferences. As a result, each cluster becomes equivalent to a network where fewer number of users are served by a BS. Particularly, in [52], $2M$ users are divided into M clusters of 2 users. The channels of users in each cluster are aligned in the same direction by beamforming, called *signal alignment*. The effective channel of the received signal after suppressing inter-cluster interferences can be seen as M parallel channels. Thus, the number of users of messages decoded by SIC is reduced to two.

3.1.3 Motivation and Contribution

A WPCN has a so-called doubly near-far problem inherently, which causes severe user unfairness [9]. A user with bad channel harvests less energy than a user with good channel during DL-WET, and needs more energy to transmit at desired rate during UL-WIT. Due to the doubly near-far problem, the difference in channel conditions of users in a WPCN can be considered to be larger than that in a conventional network. NOMA is known to be effective in enhancing user fairness from SIC decoding as the number of users is small and the difference in channel conditions is large [50]. In MIMO-NOMA, the number of users in a NOMA transmission can

be reduced through user clustering which exploits the beamforming of transceivers. Particularly, in a WPCN, users with large channel difference which comes from the doubly near-far problem can be clustered to further improve user fairness. Moreover, exploiting beamforming can reduce the complexity of SIC decoding as well as the throughput loss from SIC error propagation in a NOMA-based WPCN with many users. As a result, it is expected that the system performance of a WPCN can be improved by adopting cluster-specific beamforming in NOMA transmission.

To this end, I consider a WPCN system based on NOMA transmission with cluster-specific beamforming, and aim to maximize the sum-throughput of the network. Due to the difficulty of jointly optimizing cluster-specific beamforming and resources for sum-throughput maximization, I design the beamforming first, and then the resources such as DL energy beamforming, time, and energy are optimized for given beamforming. Particularly, in the design of cluster-specific beamforming, the transmit beamforming at the users are designed to consist of inner and outer precoding. The concept of signal alignment is adopted at the outer precoding, where the number of users in each cluster is extended from two to an arbitrary number. By outer precoding, the channels of users in a cluster are aligned in the same direction. Inner precoding is designed to increase the sum-throughput of the system by maximizing the signal to noise ratio (SNR) of the signals aligned by the outer precoding. The receive beamforming at the BS suppresses the inter-cluster interference, and the messages of users in each cluster are decoded with SIC. For given cluster-specific beamforming, a sum-throughput maximization problem is formulated with the signal to interference-plus-noise ratio (SINR) thresholds for reliable decoding. The maximization problem is transformed into an equivalent convex problem, [26], and a novel algorithm is proposed to obtain the optimal solution to the problem. The contributions of this chapter are summarized as follows:

- I consider a WPCN consisting of a PB, a BS, and multiple users, all of which

have multiple antennas. A cluster-specific beamforming with signal alignment is employed. A sum-throughput maximization problem for the considered network is formulated subject to SINR thresholds.

- The number of beamformed users in each cluster is generalized. To increase the sum-throughput performance, the beamforming consisting of inner and outer precoding is further optimized.

- Novel algorithms for beamforming design and sum-throughput maximization are proposed. Numerical results show that the proposed scheme is robust to SIC error propagation, and the sum-throughput is enhanced by the beamforming design. Moreover, compared to OMA with the same beamforming, the proposed scheme is shown to alleviate user unfairness as well as to achieve higher sum-throughput.

3.2 System model

I consider a network which consists of a PB with W antennas, a BS with M antennas, and LM users each with N antennas as in Fig. 3.1. A user is assumed to have a rechargeable battery and no external power source so that it operates only using the energy harvested from the signal transmitted by the PB. LM users are divided into L groups, each of which consists of M users. Each group is denoted by Group l where $l = 1, ..., L$. For convenience, U_{ml} denotes the m-th user in Group l where $m = 1, ..., M$ and $l = 1, ..., L$. The channel between the PB and U_{ml} is denoted by $\mathbf{G}_{ml} \in \mathbb{C}^{N \times W}$. The channel between U_{ml} and the BS is denoted by $\mathbf{H}_{ml} \in \mathbb{C}^{M \times N}$. The entries of $\mathbf{G}_{ml}$ and $\mathbf{H}_{ml}$ are assumed to be independent and identically distributed (i.i.d.) continuous random variables. For the sake of simplicity, I assume that a PB and a BS are at the same location, and the number of antennas at the PB and the BS can be different. It is also assumed that the users in a lower indexed group

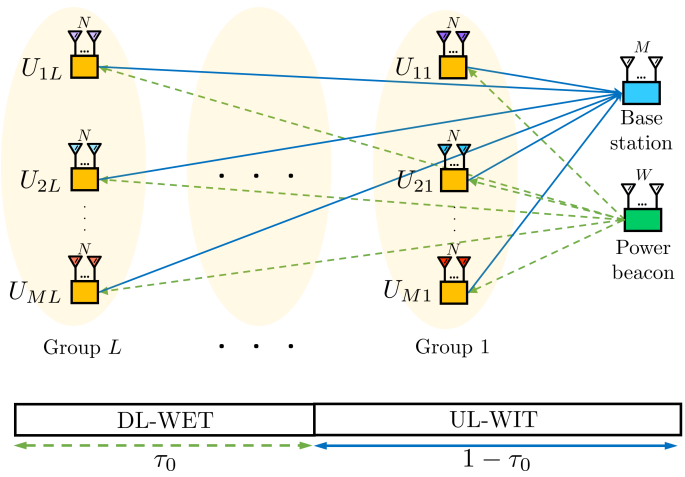

Figure 3.1: An LM-user WPCN system model

have better channel conditions than users in a higher indexed group. (i.e., U_{ml} has better channel condition than U_{nk} for any m and n where $l < k$.) In particular, a better channel has a higher Frobenius norm of a channel coefficient matrix than a worse channel. For the signal alignment to be feasible [52], $N > \frac{L-1}{L}M$ should be satisfied, the reason for which is given in the following section.

Following the *harvest-then-transmit* protocol [9], the total transmission time, T is divided into $\tau_0 T$ for DL-WET, and $(1-\tau_0)T$ for UL-WIT where $0 \leq \tau_0 \leq 1$. For simplicity, I consider a unit transmission time (i.e., $T = 1$). During τ_0, the PB transmits an energy signal, $\mathbf{u} \in \mathbb{C}^{W\times 1}$ of zero-mean with the power of P_E where $\mathbb{E}[\mathbf{u}\mathbf{u}^H] = \mathbf{S}$ and $\mathbf{S} \succeq 0$. The received signal at U_{ml}, $\mathbf{y}_{ml} \in \mathbb{C}^{N\times 1}$ becomes

$$\mathbf{y}_{ml} = \mathbf{G}_{ml}\mathbf{u} + \mathbf{n}_{ml}, \forall m, l, \tag{3.1}$$

where $\mathbf{n}_{ml} \sim \mathcal{CN}(0, \sigma^2\mathbf{I}_N)$ is a noise vector. Furthermore, due to the maximum transmit power constraint at the PB, $\text{Tr}(\mathbf{S}) \leq P_E$ should be satisfied. Assuming that the amount of the harvested energy from noise is significantly small that it is

negligible, each user harvests energy, the amount of which is

$$E_{ml} = \eta_{ml}\tau_0 \text{Tr}(\mathbf{G}_{ml}\mathbf{S}\mathbf{G}_{ml}^H), \forall m, l, \tag{3.2}$$

where η_{ml} is the energy harvesting efficiency at U_{ml}.

During $(1-\tau_0)$, each user transmits information of $s_{ml} \sim \mathcal{CN}(0,1)$ using its harvested energy. The channels of U_{m1}, U_{m2}, ..., U_{mL} with respect to BS are aligned into the same direction by beamforming vectors $\mathbf{v}_{m1}$, $\mathbf{v}_{m2}$, ..., $\mathbf{v}_{mL}$ for all m where $\mathbf{v}_{ml} \in \mathbb{C}^{N\times 1}$. The received signal at the BS, $\mathbf{y}_{\text{BS}} \in \mathbb{C}^{M\times 1}$ is written as

$$\mathbf{y}_{\text{BS}} = \sum_{m=1}^{M}\sum_{l=1}^{L} \mathbf{H}_{ml}\mathbf{v}_{ml}\alpha_{ml}s_{ml} + \mathbf{n}_{\text{BS}}, \tag{3.3}$$

where $\mathbf{n}_{\text{BS}} \sim \mathcal{CN}(0, \sigma^2\mathbf{I}_M)$ is a noise vector and α_{ml} is a power coefficient. Since the energy consumed at U_{ml} during $(1-\tau_0)$ cannot exceed the energy harvested during τ_0, α_{ml} should satisfy

$$\alpha_{ml}^2 \text{Tr}(\mathbf{v}_{ml}\mathbf{v}_{ml}^H) \leq \frac{E_{ml}}{(1-\tau_0)}, \forall m, l. \tag{3.4}$$

From [52], the condition for signal alignment is given by

$$\text{span}(\mathbf{H}_{m1}\mathbf{v}_{m1}) = \text{span}(\mathbf{H}_{m2}\mathbf{v}_{m2}) = ... = \text{span}(\mathbf{H}_{mL}\mathbf{v}_{mL}), \forall m. \tag{3.5}$$

That is, the subspace spanned by $\mathbf{H}_{ml}\mathbf{v}_{ml}$ for each l should be identical to each other. For simplicity, assume that $\mathbf{v}_{ml}$ is designed from $\mathbf{H}_{m1}\mathbf{v}_{m1} = \mathbf{H}_{m2}\mathbf{v}_{m2} = ... = \mathbf{H}_{mL}\mathbf{v}_{mL}$.[1] Then, due to the alignment, the received signal, (3.3) is rewritten as

$$\begin{aligned}\mathbf{y}_{\text{BS}} &= \sum_{m=1}^{M}\sum_{l=1}^{L} (\mathbf{H}_{ml}\mathbf{v}_{ml}\alpha_{ml}s_{ml}) + \mathbf{n}_{\text{BS}} \\ &= \begin{bmatrix} \mathbf{H}_{11}\mathbf{v}_{11} & ... & \mathbf{H}_{M1}\mathbf{v}_{M1} \end{bmatrix} \left\{ \sum_{l=1}^{L} \begin{bmatrix} \alpha_{1l}s_{1l} \\ \vdots \\ \alpha_{Ml}s_{Ml} \end{bmatrix} \right\} + \mathbf{n}_{\text{BS}}. \end{aligned} \tag{3.6}$$

[1] Due to the constraint on the transmit power of a user given in (3.4), the magnitudes (channel gains) of the aligned channels are not identical to each other.

A zero-forcing (ZF) matrix, $\mathbf{P}^H = \begin{bmatrix} \mathbf{p}_1 & \cdots & \mathbf{p}_M \end{bmatrix}^H$ where $\mathbf{p}_m \in \mathbb{C}^{M\times 1}$ is applied to the BS to decouple the received signal into M independent streams. Thus, $\mathbf{p}_m$ needs to satisfy

$$\mathbf{p}_m^H \mathbf{H}_{\bar{m}1} \mathbf{v}_{\bar{m}1} = 0, \forall m, \tag{3.7}$$

where $\bar{m} \in \{1, ..., M\}\backslash\{m\}$. The received signal after applying the ZF matrix is further rewritten as

$$\mathbf{P}^H \mathbf{y}_{\text{BS}} =$$

$$\begin{bmatrix} \mathbf{p}_1^H \mathbf{H}_{11} \mathbf{v}_{11} & 0 & \dots & 0 \\ 0 & \mathbf{p}_2^H \mathbf{H}_{21} \mathbf{v}_{21} & \dots & 0 \\ \vdots & \vdots & \ddots & \vdots \\ 0 & 0 & \dots & \mathbf{p}_M^H \mathbf{H}_{M1} \mathbf{v}_{M1} \end{bmatrix} \left\{ \sum_{l=1}^{L} \begin{bmatrix} \alpha_{1l} s_{1l} \\ \vdots \\ \alpha_{Ml} s_{Ml} \end{bmatrix} \right\} + \mathbf{P}^H \mathbf{n}_{\text{BS}}. \tag{3.8}$$

As seen in (3.8), the effective channel can be regarded as parallel channels of M NOMA clusters (i.e., there is no inter-cluster interference.) In particular, each cluster can be seen as consisting of L users each with a single antenna. Fig. 3.2 illustrates the effective channel of (3.8). The channels of U_{ml}'s with the same m are aligned into the same direction and the L users form Cluster m. The m-th stream of the received signal decoupled by the ZF matrix, $\mathbf{P}^H$ is given by

$$\mathbf{p}_m^H \mathbf{y}_{\text{BS}} = \mathbf{p}_m^H \mathbf{H}_{m1} \mathbf{v}_{m1} (\sum_{l=1}^{L} \alpha_{ml} s_{ml}) + \mathbf{p}_m^H \mathbf{n}_{\text{BS}}, \forall m. \tag{3.9}$$

For (3.9), the messages of U_{m1}, U_{m2}, ..., U_{mL} are decoded with SIC for L users for all $m \in \{1, ..., M\}$. Note that U_{m1}, U_{m2}, ..., U_{mL} are the L users in Cluster m in Fig. 3.2. The decoding order is in the descending order with respect to the channel status for user fairness (i.e., the message of U_{mi} is decoded ahead of that

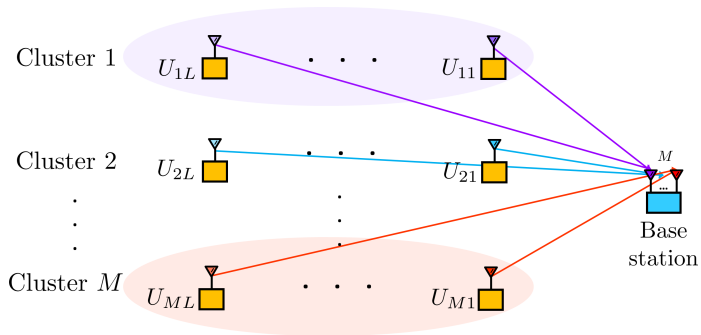

Figure 3.2: An illustration of a received signal decoupled to M independent streams, each of which consists of L messages.

of U_{mj} where $i < j$.); otherwise, the user with poor channel condition may achieve significantly small throughput. Assuming that the ZF matrix, $\mathbf{P}^H$ is normalized, the SINR of U_{ml} is given by

$$\text{SINR}_{ml} = \begin{cases} \dfrac{|h_m|^2 \alpha_{ml}^2}{\sum_{j=l+1}^{L} |h_m|^2 \alpha_{mj}^2 + \sigma^2}, & l = 1, ..., L-1, \quad (3.10a) \\ \dfrac{|h_m|^2 \alpha_{mL}^2}{\sigma^2}, & l = L, \quad (3.10b) \end{cases}$$

where $h_m = \mathbf{p}_m^H \mathbf{H}_{m1} \mathbf{v}_{m1}, \forall m$. The throughput of U_{ml} is given as

$$R_{ml} = (1 - \tau_0) \log \left(1 + \text{SINR}_{ml}\right), \forall m, l, \quad (3.11)$$

and the sum-throughput is given as

$$R_{\text{sum}} = (1 - \tau_0) \sum_{m=1}^{M} \log \left(1 + \frac{|h_m|^2 \sum_{l=1}^{L} \alpha_{ml}^2}{\sigma^2}\right). \quad (3.12)$$

3.3 Optimal Beamforming And Resource Allocation

In this section, I design the beamforming vector of UL-WIT, $\mathbf{v}_{ml}$ for signal alignment, and optimize it to maximize the SNR of the aligned signals. Subsequently, a

sum-throughput maximization problem is formulated for given designed beamforming vectors. In addition, SINR thresholds are added as constraints to the maximization problem for reliable decoding.

3.3.1 Beamforming Design

The beamforming vector, $\mathbf{v}_{ml}$ consists of an outer precoding matrix, $\mathbf{V}_{ml}$ and an inner precoding vector, $\mathbf{w}_{ml}$ as

$$\mathbf{v}_{ml} = \mathbf{V}_{ml}\mathbf{w}_{ml}. \tag{3.13}$$

The outer precoding, $\mathbf{V}_{ml}$ aligns the channels of users in a cluster in the same direction. The SNRs of the aligned signals are maximized by the joint design of the inner precoding, $\mathbf{w}_{ml}$ and the ZF matrix, $\mathbf{P}^H$. The sizes of $\mathbf{V}_{ml}$ and $\mathbf{w}_{ml}$ are given by $N \times N_{\mathbf{V}}$ and $N_{\mathbf{V}} \times 1$ where $N_{\mathbf{V}} \leq LN-(L-1)M$, the reason of which is as follows: For simplicity, $\mathbf{V}_{ml}$ is designed from $\mathbf{H}_{m1}\mathbf{V}_{m1} = \mathbf{H}_{m2}\mathbf{V}_{m2} = ... = \mathbf{H}_{mL}\mathbf{V}_{mL}$, which can be rewritten as

$$\underbrace{\begin{bmatrix} \mathbf{H}_{m1} & -\mathbf{H}_{m2} & \mathbf{0}_{M\times N} & \cdots & \mathbf{0}_{M\times N} \\ \mathbf{H}_{m1} & \mathbf{0}_{M\times N} & -\mathbf{H}_{m3} & \ddots & \vdots \\ \vdots & \vdots & \ddots & \ddots & \mathbf{0}_{M\times N} \\ \mathbf{H}_{m1} & \mathbf{0}_{M\times N} & \cdots & \mathbf{0}_{M\times N} & -\mathbf{H}_{mL} \end{bmatrix}}_{\mathbf{A}_m} \begin{bmatrix} \mathbf{V}_{m1} \\ \mathbf{V}_{m2} \\ \vdots \\ \mathbf{V}_{mL} \end{bmatrix} = \mathbf{0}_{(L-1)M\times N_{\mathbf{V}}}. \tag{3.14}$$

As seen in (3.14), the size of $\mathbf{A}_m$ is $(L-1)M \times LN$, and $[\mathbf{V}_{m1}^T, \mathbf{V}_{m2}^T, ..., \mathbf{V}_{mL}^T]^T$ is generated from the null space of $\mathbf{A}_m$. Note that for signal alignment to be feasible, $(L-1)M < LN$ should be satisfied, which is equivalent to $N > \frac{L-1}{L}M$. Moreover, $\mathbf{A}_m$ has a full-rank of $(L-1)M$ almost surely since all the elements of $\mathbf{H}_{ml}$ are i.i.d. continuous random variables from the assumption. Therefore, $[\mathbf{V}_{m1}^T, \mathbf{V}_{m2}^T, ..., \mathbf{V}_{mL}^T]^T$ can be chosen as the $LN \times N_{\mathbf{V}}$ matrix which consists of the $N_{\mathbf{V}}$ columns out of

$LN-(L-1)M$ right singular vectors of $\mathbf{A}_m$ corresponding to the zero singular values. In other words, it suffices to align $\mathbf{H}_{m1}$, $\mathbf{H}_{m2}$, ..., $\mathbf{H}_{mL}$ in the same direction which occupies the dimension of $LN-(L-1)M$ or less for $[\mathbf{V}_{m1}^T, \mathbf{V}_{m2}^T, ..., \mathbf{V}_{mL}^T]^T$ to exist. Therefore, $N_{\mathbf{V}} \leq LN-(L-1)M$ should be satisfied. Note that it is assumed that $\mathbf{H}_{m1}\mathbf{v}_{m1} = \mathbf{H}_{m2}\mathbf{v}_{m2} = ... = \mathbf{H}_{mL}\mathbf{v}_{mL}$ in Section 3.2. From (3.13) and (3.14), it can be rewritten as

$$\mathbf{H}_{m1}\mathbf{V}_{m1}\mathbf{w}_{m1} = \mathbf{H}_{ml}\mathbf{V}_{ml}\mathbf{w}_{ml} = \mathbf{H}_{m1}\mathbf{V}_{m1}\mathbf{w}_{ml}, \forall l. \tag{3.15}$$

Thus, $\mathbf{w}_{ml}$ for all l becomes identical to each other (i.e., $\mathbf{w}_{m1} = \mathbf{w}_{m2} = ... = \mathbf{w}_{mL}$.) Let $\mathbf{w}_m$ denote $\mathbf{w}_{ml}$ for all l, and $\mathbf{v}_{ml}$ then becomes $\mathbf{V}_{ml}\mathbf{w}_m$. To maximize the SNR of the aligned signals by exploiting $\mathbf{w}_m$, the channels need to be aligned in the same direction of the highest available dimension. In other words, $N_{\mathbf{V}}$ needs to be equal to $LN-(L-1)M$. Therefore, I assume that $N_{\mathbf{V}} = LN-(L-1)M$ in the following.

Since I let $\mathbf{H}_{m1}\mathbf{v}_{m1} = \mathbf{H}_{m2}\mathbf{v}_{m2} = ... = \mathbf{H}_{mL}\mathbf{v}_{mL}$ where $\mathbf{v}_{ml} = \mathbf{V}_{ml}\mathbf{w}_m$, (3.7) can be rewritten as

$$\mathbf{p}_m^H\mathbf{H}_{\bar{m}1}\mathbf{V}_{\bar{m}1}\mathbf{w}_{\bar{m}} = 0, \forall m. \tag{3.16}$$

From (3.16), $\mathbf{p}_m^H$ should lie in the left null space of an $M \times (M-1)$ matrix which consists of all $\mathbf{H}_{\bar{m}1}\mathbf{V}_{\bar{m}1}\mathbf{w}_{\bar{m}}$. For example, when $m=1$, $\mathbf{p}_1^H$ lies in the left null space of the $M \times (M-1)$ matrix, $\left[\begin{array}{ccccc} \mathbf{H}_{21}\mathbf{V}_{21}\mathbf{w}_2 & \mathbf{H}_{31}\mathbf{V}_{31}\mathbf{w}_3 & \cdots & \mathbf{H}_{M1}\mathbf{V}_{M1}\mathbf{w}_M \end{array}\right]$. To normalize the decoding matrix (i.e., $|\mathbf{p}_m|^2 = 1$), $\mathbf{p}_m$ is given by the left singular vector of the $M \times (M-1)$ matrix corresponding to the zero singular value. Note that the noise variance is still given by $\sigma^2\mathbf{I}_M$ since $\mathbf{P}$ is normalized.

From (3.9), the SNR for $\sum_{l=1}^{L}\alpha_{ml}s_{ml}$ is given by $\frac{|\mathbf{p}_m^H\mathbf{H}_{m1}\mathbf{V}_{m1}\mathbf{w}_m|^2}{\sigma^2}$, which can be maximized by an iterative approach for designing $\mathbf{w}_m$ as follows: I initialize $\mathbf{w}_m$ with a random vector, and $\mathbf{P}$ follows from the given $\mathbf{w}_m$ by (3.16). Then, for given $\mathbf{P}$, $|\mathbf{p}_m^H\mathbf{H}_{m1}\mathbf{V}_{m1}\mathbf{w}_m|^2$ can be rewritten as $\mathbf{w}_m^H\mathbf{\Psi}_m\mathbf{w}_m$ where $\mathbf{\Psi}_m$ is given by $\mathbf{\Psi}_m = \mathbf{V}_{m1}^H\mathbf{H}_{m1}^H\mathbf{p}_m\mathbf{p}_m^H\mathbf{H}_{m1}\mathbf{V}_{m1}$. Since $\mathbf{\Psi}_m$ is a rank-1 Hermitian matrix, there exists a

Algorithm 2 Design of Cluster-Specific Beamforming

1: Set $\mathbf{V}_{ml} \leftarrow$ (3.14).

2: Initialize $\mathbf{w}_m$ with random vectors.

3: Compute $\mathbf{P} \leftarrow$ (3.16)

4: **repeat**

5: $\mathbf{w}_m \leftarrow$ the eigenvector of $\mathbf{\Psi}_m$ corresponding to the unique non-zero eigenvalue.

6: Compute $\mathbf{P} \leftarrow$ (3.16)

7: **until** $\mathbf{w}_m$ converges satisfying a pre-determined accuracy.

▷ Transmit/receive beamforming, $\mathbf{v}_{ml}(= \mathbf{V}_{ml}\mathbf{w}_m)$ and $\mathbf{P}$ are determined.

unique non-zero eigenvalue of $\mathbf{\Psi}_m$. Hence, $\mathbf{w}_m^H \mathbf{\Psi}_m \mathbf{w}_m$ is maximized by setting $\mathbf{w}_m$ to the eigenvector of $\mathbf{\Psi}_m$ corresponding to the unique non-zero eigenvalue. $\mathbf{P}$ can be determined from (3.16) for given $\mathbf{w}_m$ again as $\mathbf{P} = \left[\begin{array}{ccc} \mathbf{p}_1 & \cdots & \mathbf{p}_M \end{array} \right]$. Updating $\mathbf{w}_m$ and $\mathbf{P}$ alternately is repeated until they converge.[2] The proposed algorithm for the design of transmit/receive beamforming is summarized in Algorithm 2.

3.3.2 Sum-Throughput Maximization

I formulate a sum-throughput maximization problem in the considered network, where the beamforming matrices are determined from 3.3.1. The sum-throughput is maximized by jointly optimizing the time allocation for DL-WET and UL-WIT (i.e., τ_0), the transmit power of the users during UL-WIT (i.e., α_{ml}.), and the transmit covariance matrix $\mathbf{S}$ during DL-WET. Furthermore, I impose a threshold, θ_{ml} on the SINR$_{ml}$ for reliable decoding (i.e., SINR$_{ml} \geq \theta_{ml}$). The maximization problem is

[2]Through numerical simulations, I confirm that the proposed algorithm has converged (0 failure out of 10^6 trials) satisfying $\sum_{m=1}^{M} ||\mathbf{w}_m[k+1] - \mathbf{w}_m[k]||_1 \leq 10^{-6}$ where $||\cdot||_1$ is the $l1$-norm and k is the number of iteration.

given as

$$\textbf{(P1)}: \max_{\tau_0, \{\alpha_{ml}\}, \mathbf{S}} \quad R_{\text{sum}} \tag{3.17a}$$

$$\text{subject to} \quad 0 \leq \tau_0 \leq 1, \tag{3.17b}$$

$$\alpha_{ml} \geq 0, \forall m, l, \tag{3.17c}$$

$$\alpha_{ml}^2 \text{Tr}(\mathbf{v}_{ml}\mathbf{v}_{ml}^H) \leq \frac{E_{ml}}{(1-\tau_0)}, \forall m, l, \tag{3.17d}$$

$$\text{Tr}(\mathbf{S}) \leq P_E, \tag{3.17e}$$

$$\text{SINR}_{ml} \geq \theta_{ml}, \forall m, l. \tag{3.17f}$$

(3.17a) is the sum-throughput, (3.17b) is the time restriction on DL-WET and UL-WIT, (3.17c) comes from the non-negativity of the power, (3.17d) comes from that the consumed energy during UL-WIT cannot exceed the harvested energy during DL-WET. (3.17e) is that the maximum transmit power at the PB during DL-WET is given by P_E. (3.17f) is the SINR threshold constraint. Note that **(P1)** is not a convex optimization problem. It can be proved by showing that the Hessian matrix of the objective function is neither positive semi-definite nor negative semi-definite.

In order to transform **(P1)** into a convex problem, α_{ml} is replaced using $\gamma_{ml} = \alpha_{ml}^2 (1 - \tau_0), \forall m, l$, and $\mathbf{S}$ is replaced using $\mathbf{W} = \tau_0 \mathbf{S}$ [9]. Let **(P1′)** denote the

transformed problem, which is given by

$$\textbf{(P1}'\textbf{)}: \max_{\tau_0,\{\gamma_{ml}\}\geq 0,\mathbf{W}} \quad (1-\tau_0)\sum_{m=1}^{M}\log\left(1+\frac{\sum_{l=1}^{L}|h_m|^2\gamma_{ml}}{\sigma^2(1-\tau_0)}\right) \tag{3.18a}$$

$$\text{subject to} \quad 0\leq\tau_0\leq 1, \tag{3.18b}$$

$$\gamma_{ml}\leq q_{ml}\text{Tr}(\mathbf{G}_{ml}\mathbf{W}\mathbf{G}_{ml}^H), \forall m,l, \tag{3.18c}$$

$$\text{Tr}(\mathbf{W})\leq\tau_0 P_E, \tag{3.18d}$$

$$\theta_{ml}(\sum_{j=l+1}^{L}|h_m|^2\gamma_{mj}+\sigma^2(1-\tau_0))-|h_m|^2\gamma_{ml}\leq 0,$$

$$\forall m,l=1,...,L-1 \tag{3.18e}$$

$$\theta_{mL}(\sigma^2(1-\tau_0))-|h_m|^2\gamma_{mL}\leq 0,\forall m, \tag{3.18f}$$

$$\mathbf{W}\succeq 0, \tag{3.18g}$$

where $q_{ml}=\frac{\eta_{ml}}{\text{Tr}(\mathbf{v}_{ml}\mathbf{v}_{ml}^H)}$. If I assume that the summation in (3.18e) becomes zero when $j>L$, (3.18f) can be represented with (3.18e). Hence, let (3.18e) include (3.18f) in the following for simplicity. **(P1′)** is a convex optimization problem [26]. The objective, (3.18a) is concave as it is a perspective of a concave function. The constraints, (3.18b)-(3.18g) are affine in the optimization variables.

To solve **(P1′)** efficiently, I solve a sum-throughput maximization problem for given τ_0, which is denoted by $f(\tau_0)$. τ_0 is optimized via a 1-D search method such as the golden section method. I have

$$f(\tau_0): \max_{\{\gamma_{ml}\}\geq 0,\mathbf{W}} \quad (1-\tau_0)\sum_{m=1}^{M}\log\left(1+\frac{\sum_{l=1}^{L}|h_m|^2\gamma_{ml}}{\sigma^2(1-\tau_0)}\right)$$

$$\text{subject to} \quad \text{(3.18c), (3.18d), (3.18e), and (3.18g).}$$

The Lagrangian of $f(\tau_0)$ is given by

$$\mathcal{L}(\{\gamma_{ml}\}, \mathbf{W}, \{\lambda\}, \mathbf{Z}) = (1-\tau_0) \sum_{m=1}^{M} \log\left(1 + \frac{\sum_{l=1}^{L} |h_m|^2 \gamma_{ml}}{\sigma^2(1-\tau_0)}\right) + \sum_{m=1}^{M}\sum_{l=1}^{L} c_{ml}\gamma_{ml} + \mathrm{Tr}((\mathbf{F}+\mathbf{Z})\mathbf{W}) + \lambda_2\tau_0 P_E - \sum_{m=1}^{M}\sum_{l=1}^{L} \lambda_{3,ml}\theta_{ml}\sigma^2(1-\tau_0), \tag{3.20}$$

where

$$c_{ml} = -\lambda_{1,ml} + \lambda_{3,ml}|h_m|^2 - \sum_{j=1}^{l-1} \lambda_{3,mj}\theta_{mj}|h_m|^2, \tag{3.21}$$

$$\mathbf{F} = \sum_{m=1}^{M}\sum_{l=1}^{L} \lambda_{1,ml} q_{ml} \mathbf{G}_{ml}^H \mathbf{G}_{ml} - \lambda_2 \mathbf{I}_W, \tag{3.22}$$

and $\{\lambda_{1,ml}\}$, λ_2, $\{\lambda_{3,ml}\}$, and $\mathbf{Z}$ are the Lagrangian multipliers of (3.18c), (3.18d), (3.18e), and (3.18g), respectively. Note that $\mathbf{W}^* \succ \mathbf{0}$; otherwise, there will be no energy harvesting, which results in zero throughput. Therefore, $\mathbf{Z}^*$ should be a zero matrix from the complementary slackness. Furthermore, $\lambda_2^* > 0$ holds from the complementary slackness as well. In case $\lambda_2^* = 0$, $\mathrm{Tr}(\mathbf{W}^*) < \tau_0 P_E$, which is not optimal. It means that the PB does not transmit an energy signal with its maximum power, lowering the amount of energy harvested at every user.

The dual function of $f(\tau_0)$ is given by

$$\mathcal{G}(\{\lambda\}, \mathbf{Z}) = \max_{\{\gamma_{ml}\}\geq 0, \mathbf{W}} \mathcal{L}(\{\gamma_{ml}\}, \mathbf{W}, \{\lambda\}, \mathbf{Z}). \tag{3.23}$$

To avoid an unbounded dual function, $c_{ml} < 0, \forall m, l$, and $\mathbf{F} \preceq 0$ need to be satisfied. The dual problem is given by $\min_{\{\lambda\}\geq 0, \mathbf{Z}\succeq 0} \mathcal{G}(\{\lambda\}, \mathbf{Z})$ subject to the conditions of avoiding unbounded dual function. For given $\{\lambda\}$, I find $\mathbf{W}^\star$ that maximizes $\mathcal{L}(\{\gamma_{ml}\}, \mathbf{W}, \{\lambda\}, \mathbf{Z})$ [41].

Theorem 1. *$\mathbf{W}^\star$ is given by $\tau_0 P_E \mathbf{\Gamma}_Q \mathbf{\Gamma}_Q^H$ where $\mathbf{\Gamma}_Q$ is the eigenvector corresponding to the maximum eigenvalue of $\mathbf{Q}$ $(= \sum_{m=1}^{M}\sum_{l=1}^{L} \lambda_{1,ml} q_{ml} \mathbf{G}_{ml}^H \mathbf{G}_{ml})$.*

Proof. $\mathbf{F}$ is rewritten as $\mathbf{F} = \mathbf{Q} - \lambda_2 \mathbf{I}_W$, where $\mathbf{Q} = \sum_{m=1}^{M} \sum_{l=1}^{L} \lambda_{1,ml} q_{ml} \mathbf{G}_{ml}^H \mathbf{G}_{ml}$. The eigen-decomposition of $\mathbf{F}$ is given by

$$\mathbf{F} = \mathbf{U}_Q (\mathbf{\Delta}_Q - \lambda_2 \mathbf{I}_W) \mathbf{U}_Q^H, \tag{3.24}$$

where $\mathbf{\Delta}_Q = \text{diag}(\delta_1, ..., \delta_W)$, and $\delta_1 \leq \delta_2 \leq ... \leq \delta_W$ are the eigenvalues of $\mathbf{Q}$. Hence, for $\mathbf{F} \preceq 0$ to be satisfied, $\lambda_2 \geq \delta_i, \forall i$. Tr$(\mathbf{FW})$ can be rewritten as

$$\begin{aligned} \text{Tr}(\mathbf{FW}) &= \text{Tr}(\mathbf{U}_Q (\mathbf{\Delta}_Q - \lambda_2 \mathbf{I}_W) \mathbf{U}_Q^H \mathbf{W}) \\ &= \text{Tr}((\mathbf{\Delta}_Q - \lambda_2 \mathbf{I}_W) \mathbf{U}_W \mathbf{W} \mathbf{U}_W^H) \\ &= \text{Tr}((\mathbf{\Delta}_Q - \lambda_2 \mathbf{I}_W) \mathbf{\Delta}_W) \\ &= \sum_{w=1}^{W} (\delta_w - \lambda_2) \rho_w, \end{aligned} \tag{3.25}$$

where $\mathbf{U}_W$ is an unitary matrix, $\mathbf{\Delta}_W = \text{diag}(\rho_1, ..., \rho_W)$ and $\rho_1, ..., \rho_W$ are the eigenvalues of $\mathbf{W}$. As $\mathbf{W} \succeq 0$, $\rho_w \geq 0$. Consequently, to maximize Tr$(\mathbf{FW})$, ρ_1, ..., $\rho_{(w-1)}$ becomes zero, and ρ_w becomes positive in case $\delta_w = \lambda_2$. Thus, Tr$(\mathbf{FW})$ is maximized by setting $\mathbf{W}$ to $\beta \mathbf{\Gamma}_Q \mathbf{\Gamma}_Q^H$ where $\mathbf{\Gamma}_Q$ is a matrix which consists of vectors of $\mathbf{U}_Q$ corresponding to $\delta_w = \lambda_2, \forall w \in \{1, ..., W\}$. Due to that Tr$(\mathbf{W}) = \tau_0 P_E$ from the complementary slackness corresponding to λ_2, β becomes $\tau_0 P_E$. Note that $\mathbf{\Gamma}_Q$ lies in the null space of $\mathbf{F}$ as it consists of vectors of $\mathbf{U}_Q$ corresponding to zero eigenvalues. □

For given $\{\lambda\}$ and $\mathbf{W}^\star$, I find $\{\gamma_{ml}^\star\}$ that maximizes $\mathcal{L}(\{\gamma_{ml}\}, \mathbf{W}, \{\lambda\}, \mathbf{Z})$ by solving the KKT conditions [26]. The Lagrangian stationarity condition with respect to γ_{pq} where $p \in \{1, ..., M\}, q \in \{1, ..., L\}$ is given by

$$\frac{\partial \mathcal{L}}{\partial \gamma_{pq}} = 0 : \frac{|h_p|^2 / \sigma^2}{1 + \frac{\sum_{l=1}^{L} |h_p|^2 \gamma_{pl}}{\sigma^2 (1 - \tau_0)}} + c_{pq} = 0, \forall p, q. \tag{3.26}$$

Rewriting (3.26), I have

$$\sum_{l=1}^{L} \gamma_{pl} = \frac{1 - \tau_0}{-c_{pq}} - \frac{\sigma^2 (1 - \tau_0)}{|h_p|^2}, \forall p, q. \tag{3.27}$$

As seen in (3.27), $\gamma_{pq}^{\star}$ cannot be obtained explicitly for given $\{\lambda\}$. For given $\{\lambda\}$ which is not optimal, $\{\gamma_{ml}^{\star}\}$ is given by the following lemma.

Lemma 5. *$\{\gamma_{ml}^{\star}\}$ that maximizes $\mathcal{L}(\{\gamma_{ml}\}, \mathbf{W}, \{\lambda\}, \mathbf{Z})$ for non-optimal $\{\lambda\}$ is given by*

$$\gamma_{m\hat{l}}^{\star} = \frac{1-\tau_0}{-c_{m\hat{l}}} - \frac{\sigma^2(1-\tau_0)}{|h_m|^2}, \tag{3.28}$$

$$\gamma_{mk}^{\star} = 0, k \in \{1, ..., L\}\backslash\{\hat{l}\}, \tag{3.29}$$

where $\hat{l} = \arg\max_l c_{ml}$.

Proof. Factoring out the constants of (3.20), the maximization of the Lagrangian in (3.20) is equivalent to maximizing

$$f_{m,\mathcal{L}} = (1-\tau_0)\log\left(1 + \frac{|h_m|^2 \sum_{l=1}^{L} \gamma_{ml}}{\sigma^2(1-\tau_0)}\right) + \sum_{l=1}^{L} c_{ml}\gamma_{ml}, \tag{3.30}$$

for all m. Then, $\sum_{l=1} \gamma_{ml}$ should be set to the largest among the right-hand side (R.H.S.) terms of (3.27) for $p = m$ and $q = 1, ..., L$. The q corresponding to the maximum R.H.S. term is denoted by $\hat{l}$, which is equivalent to the l corresponding to the maximum c_{ml} (i.e., $\hat{l} = \arg\max_l c_{ml}$.) Furthermore, since $\gamma_{ml} \geq 0$ and $c_{ml} < 0$, $\sum_{l=1}^{L} c_{ml}\gamma_{ml}$ of (3.30) is maximized by setting $\gamma_{m\hat{l}}$ equal to the R.H.S. of (3.27) with $p = m$ and $q = \hat{l}$, while γ_{mk} where $k \in \{1, ..., L\}\backslash\{\hat{l}\}$ needs to be zero. □

On the other hand, when given $\{\lambda\}$ is optimal, the R.H.S. term of (3.27) should be identical for all q. Then, the Lagrangian of (3.20) is no longer a function of $\{\gamma_{ml}\}$. Therefore, $\{\gamma_{ml}^{*}\}$ will be determined from the KKT conditions along with the Lagrangian stationarity condition. In particular, the complementary slackness is given by

$$\lambda_{1,ml}^{*}(\gamma_{ml}^{*} - q_{ml}\mathrm{Tr}(\mathbf{G}_{ml}\mathbf{W}^{*}\mathbf{G}_{ml}^{H})) = 0, \tag{3.31}$$

$$\lambda_{3,ml}^{*}(\theta_{ml}(\sum_{j=l+1}^{L} |h_m|^2\gamma_{mj}^{*} + \sigma^2(1-\tau_0)) - |h_m|^2\gamma_{ml}^{*}) = 0, \tag{3.32}$$

for all m and l. Note that since $\mathbf{W}^\star$ depends on $\{\lambda_{1,ml}\}$ from Theorem 1, $\mathbf{W}^\star$ is equal to $\mathbf{W}^*$ as in (3.31) when given $\{\lambda\}$ is optimal.

With the obtained dual function, the Lagrangian multipliers are updated by a subgradient method to solve the dual problem. Note that $\mathbf{Z}^* = 0$ so that it does not need to be updated. In addition, λ_2 follows from $\{\lambda_{1,ml}\}$ as given in the proof of Theorem 1 so that it does not need to be updated either. Thus, $\lambda_{1,ml}$ and $\lambda_{3,ml}$ are the Lagrangian multipliers to be updated, and their subgradients, $\nu_{n,ml}$ $\left(= \frac{\partial \mathcal{L}}{\partial \lambda_{n,ml}}\right)$ where $n \in \{1, 3\}$ are given as

$$\nu_{1,ml} = q_{ml}\mathrm{Tr}(\mathbf{G}_{ml}\mathbf{W}^\star\mathbf{G}_{ml}^H) - \gamma_{ml}^\star, \tag{3.33}$$

$$\nu_{3,ml} = |h_m|^2\gamma_{ml}^\star - \theta_{ml}(\sum_{j=l+1}^{L} |h_m|^2\gamma_{mj}^\star + \sigma^2(1-\tau_0)). \tag{3.34}$$

Applying the subgradient method, $\lambda_{n,ml}$ can be updated as

$$\lambda_{n,ml}^{(k+1)} = \left[\lambda_{n,ml}^{(k)} - s \cdot \nu_{n,ml}\right]^+, \tag{3.35}$$

where k is the number of iteration, s is a positive step size, and $[\cdot]^+ = \max(0, \cdot)$. With the updated Lagrangian multipliers, the dual function is obtained by Theorem 1 and Lemma 5. The update is repeated until the duality gap is smaller than the predetermined accuracy. That is,

$$0 \leq \sum_{m=1}^{M}\sum_{l=1}^{L} c_{ml}\gamma_{ml}^\star + \lambda_2\tau_0 P_E - \sum_{m=1}^{M}\sum_{l=1}^{L} \lambda_{3,ml}\theta_{ml}\sigma^2(1-\tau_0) \leq \epsilon_d$$

Subsequently, $\mathbf{W}^*$ is set to $\mathbf{W}^\star$, and $\{\gamma_{ml}^*\}$ are obtained by (3.26), (3.31), and (3.32).

Since **(P1′)** is jointly concave with respect to τ_0, $\{\gamma_{ml}\}$, and $\mathbf{W}$, $f(\tau_0)$ is concave with respect to τ_0. Therefore, the optimal τ_0 can be found using a 1-D search method such as the golden section method. The proposed sum-throughput maximization algorithm is summarized in Algorithm 3 where in particular, the algorithm for solving $f(\tau_0)$ is given in Algorithm 4.

Algorithm 3 Sum-Throughput Maximization for NOMA-based WPCN with Cluster-Specific Beamforming

Set $\tau_A = 0$, $\tau_B = 1$, $\rho = \frac{\sqrt{5}-1}{2}$, $\tau_{01} = \tau_A + (1-\rho)(\tau_B - \tau_A)$, and $\tau_{02} = \tau_A + \rho(\tau_B - \tau_A)$.
Compute $f(\tau_{01})$ and $f(\tau_{02})$.
repeat
    if $f(\tau_{01}) \leq f(\tau_{02})$ **then**
        $\tau_B \leftarrow \tau_{02}$, $\tau_{02} \leftarrow \tau_{01}$, $\tau_{01} \leftarrow \tau_A + (1-\rho)(\tau_B - \tau_A)$
    else
        $\tau_A \leftarrow \tau_{01}$, $\tau_{01} \leftarrow \tau_{02}$, $\tau_{02} \leftarrow \tau_A + \rho(\tau_B - \tau_A)$
    Compute $f(\tau_{01})$ and $f(\tau_{02})$
until $\tau_B - \tau_A$ is lower than pre-determined accuracy.
▷ τ_0 is optimized via the golden section method.

3.3.3 TDMA-based WPCN with Cluster-specific Beamforming

In addition, I consider using TDMA transmission while adopting the proposed beamforming for signal alignment [52]. The time for UL-WIT, $(1-\tau_0)$ is divided into L parts, $\tau_1, ..., \tau_L$. During τ_l, the M users in Group l transmit their information via M parallel channels. In other words, one user in each cluster is able to transmit during τ_l. Therefore, modifying (3.9), the received signal which is decoupled by ZF for the m-th stream during τ_l can be written as

$$\mathbf{p}_m^H \mathbf{y}_{\text{BS}}[\tau_l] = \mathbf{p}_m^H \mathbf{H}_{m1} \mathbf{v}_{m1} (\alpha_{ml} s_{ml}) + \mathbf{p}_m^H \mathbf{n}_{\text{BS}}, \forall m, l. \tag{3.36}$$

Algorithm 4 $f(\tau_0)$ Solver

1: Initialize $\{\lambda_{n,ml}\}$ with nonnegative random numbers subject to $c_{ml} < 0$, for $n = 1, 3$ and $\forall m, l$.

2: **repeat**

3: Compute $\mathbf{\Gamma}_Q$ via the eigen-decomposition of $\mathbf{Q} = \sum_{m=1}^{M}\sum_{l=1}^{L} \lambda_{1,ml} q_{ml} \mathbf{G}_{ml}^H \mathbf{G}_{ml}$.

4: Compute $\{\gamma_{ml}^\star\} \leftarrow$ (3.28), (3.29)

5: Compute $\{\nu_{n,ml}\} \leftarrow$ (3.33), (3.34)

6: Update $\{\lambda_{n,ml}\}$ with (3.35)

7: **until** duality gap is smaller than accuracy, ϵ_d.

8: Compute $\mathbf{W}^* \leftarrow \mathbf{W}^\star$ from Th. 1

9: Compute $\{\gamma_{ml}^*\} \leftarrow$ (3.26), (3.31), and (3.32)

▷ The transmit power during UL-WIT, $\{\gamma_{ml}\}$ is optimized for given τ_0.

The SNR of the message of U_{ml} is given by $\text{SNR}_{ml} = \frac{|h_m|^2 \alpha_{ml}^2}{\sigma^2}$. The individual throughput and the sum-throughput are given by

$$R_{ml}^{(\text{T})} = \tau_l \log\left(1 + \text{SNR}_{ml}\right), \forall m, l, \tag{3.37}$$

$$R_{\text{sum}}^{(\text{T})} = \sum_{l=1}^{L}\sum_{m=1}^{M} \tau_l \log\left(1 + \text{SNR}_{ml}\right), \tag{3.38}$$

where (T) stands for TDMA. As for the proposed scheme, I formulate a sum-throughput maximization problem, **(P2)** as below. In particular, to guarantee the quality of service (QoS), I put a throughput threshold on the individual throughput as $R_{ml}^{(\text{t})} \geq$

$\phi_{ml}, \forall m, l$. I then have

$$\textbf{(P2)}: \max_{\{\tau\},\{\alpha_{ml}\},\mathbf{S}} \quad R_{\text{sum}}^{(\text{T})} \tag{3.39a}$$

$$\text{subject to} \quad 0 \leq \tau_l \leq 1, l = 0, 1, ..., L, \tag{3.39b}$$

$$\sum_{l=0}^{L} \tau_l \leq 1, \tag{3.39c}$$

$$\alpha_{ml} \geq 0, \forall m, l, \tag{3.39d}$$

$$\alpha_{ml}^2 \text{Tr}(\mathbf{v}_{ml}\mathbf{v}_{ml}^H)\tau_l \leq E_{ml}, \forall m, l, \tag{3.39e}$$

$$\text{Tr}(\mathbf{S}) \leq P_E, \tag{3.39f}$$

$$R_{ml}^{(\text{T})} \geq \phi_{ml}, \forall m, l. \tag{3.39g}$$

Due to the couplings of optimization variables, **(P2)** is not a convex problem. In order to transform **(P2)** into a convex problem, **(P2′)**, the optimization variables are similarly replaced with $\mathbf{W} = \tau_0\mathbf{S}$ and $\gamma_{ml} = \tau_l\alpha_{ml}^2$. I have

$$\textbf{(P2}'\textbf{)}: \max_{\{\tau\},\{\gamma_{ml}\}\geq 0,\mathbf{W}} \quad \sum_{l=1}^{L}\sum_{m=1}^{M} \tau_l \log\left(1 + \frac{|h_m|^2\gamma_{ml}}{\sigma^2\tau_l}\right) \tag{3.40a}$$

$$\text{subject to} \quad 0 \leq \tau_l \leq 1, l = 0, 1, ..., L, \tag{3.40b}$$

$$\sum_{l=0}^{L} \tau_l \leq 1, \tag{3.40c}$$

$$\gamma_{ml} \leq q_{ml}\text{Tr}(\mathbf{G}_{ml}\mathbf{W}\mathbf{G}_{ml}^H), \forall m, l, \tag{3.40d}$$

$$\text{Tr}(\mathbf{W}) \leq \tau_0 P_E, \tag{3.40e}$$

$$\tau_l \log\left(1 + \frac{|h_m|^2\gamma_{ml}}{\sigma^2\tau_l}\right) \geq \phi_{ml}, \forall m, l. \tag{3.40f}$$

Note that (3.40a) and the left-hand side (L.H.S.) term of (3.40f) are the perspectives of concave functions. The other constraints are affine in the optimization variables, so that **(P2′)** is a convex optimization problem.

3.4 Simulation Results

Numerical results are provided in this section. A WPCN of (L, M, N, W) consists of L groups each with M users with N antennas, a BS with M antennas, and a PB with W antennas. Let d_{ml} denote the distance between U_{ml} and the BS while d_{ml}^{PB} denotes the distance between U_{ml} and the PB. As the PB and the BS are assumed to be at the same location, d_{ml}^{PB} equals d_{ml} in the following. The channel coefficients, $\mathbf{G}_{ml}$ and $\mathbf{H}_{ml}$ follow a log-distance path loss model for large-scale fading, and Rayleigh fading for small-scale fading [28]. That is, $\mathbf{G}_{ml} = \frac{\tilde{\mathbf{G}}_{ml}}{\sqrt{1+(d_{ml}^{\text{PB}})^{\alpha}}}$ and $\mathbf{H}_{ml} = \frac{\tilde{\mathbf{H}}_{ml}}{\sqrt{1+(d_{ml})^{\alpha}}}$ where $\left(\tilde{\mathbf{G}}_{ml}\right)_{ij} \sim \mathcal{CN}(0,1)$, and $\left(\tilde{\mathbf{H}}_{ml}\right)_{ki} \sim \mathcal{CN}(0,1)$ for $i \in \{1, ..., N\}$, $j \in \{1, ..., W\}$, and $k \in \{1, ..., M\}$. α denotes the path loss exponent. The transmit power of the PB, P_E, the noise variance, σ^2, and the energy harvesting efficiency of U_{ml}, η_{ml} are assumed to be 10 dBm, -70 dBm, and 0.7 for all U_{ml}, respectively unless stated otherwise. Furthermore, for simplicity, I assume that $\theta_{ml} = \theta, \forall m, l$.

Fig. 3.3 shows the sum-throughput versus θ with the varying number of users. I consider a network of $(L, M, N, W) = (2, n_M, 5, 3)$ where $n_M \in \{2, ..., 5\}$ (i.e., there are 4, 6, 8, 10 users in the network.) For any n_M, the distances of users are given by d_{ml} for all $m \in \{1, ..., n_M\}$ and $l \in \{1, 2\}$, where $[d_{11}, d_{21}, d_{31}, d_{41}, d_{51}] = [3, 4, 5, 6, 7]$ m, $[d_{12}, d_{22}, d_{32}, d_{42}, d_{52}] = [10, 11, 12, 13, 14]$ m. It can be seen that the sum-throughput starts to decrease beyond a certain level of θ for any case, the reason for which is as follows. Due to the high θ, most of the time resources are allocated for the energy harvesting to meet the SINR constraints, which means that τ_0 for DL-WET becomes near 1. In other words, the transmission time, $1 - \tau_0$ for UL-WIT becomes near 0, which results in low sum-throughput. Moreover, as n_M increases by 1, two users are added to the network, and the dimension of the received signal increases by 1. The channels of the added users are aligned in the same direction and occupy a 1 dimension of the received signal as a parallel channel. Thus, the sum-throughput

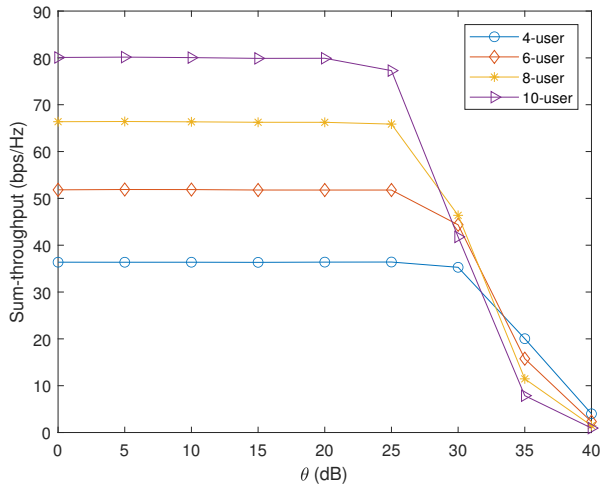

Figure 3.3: Sum-throughput versus SINR threshold of θ in WPCNs of $(L, M, N, W) = (2, n_M, 5, 3)$ where $n_M \in \{2, ..., 5\}$ for 4, 6, 8, and 10 users.

increases by a similar amount as n_M increases by 1 when θ is lower than 20 dB in the figure. Nevertheless, at $\theta = 35$ dB, the sum-throughput decreases with the growing number of users. This is because the users added to the network have bad channel conditions, so that τ_0 for DL-WET becomes high to satisfy a high SINR threshold, whereas $1 - \tau_0$ for UL-WIT decreases.

In Fig. 3.4, I consider 4 WPCNs with 12 users which have different user groupings. In particular, I compare the sum-throughput of WPCNs of $(L, M, N, W) = (2, 6, 4, 3)$, $(L, M, N, W) = (3, 4, 4, 3)$, $(L, M, N, W) = (4, 3, 4, 3)$, $(L, M, N, W) = (6, 2, 4, 3)$ along with various θ's. The distances between the users and the BS are given by $2, 3, ..., 13$ m. As in the system model, the users in the group of a lower index have better channel condition than the users in the group of a higher index. Fig. 3.4 shows the sum-throughput versus θ with the considered user configurations. It can be seen that higher sum-throughput is achieved with lower L and higher M for the same θ, which is obvious since higher number of antennas at PB provide sum-

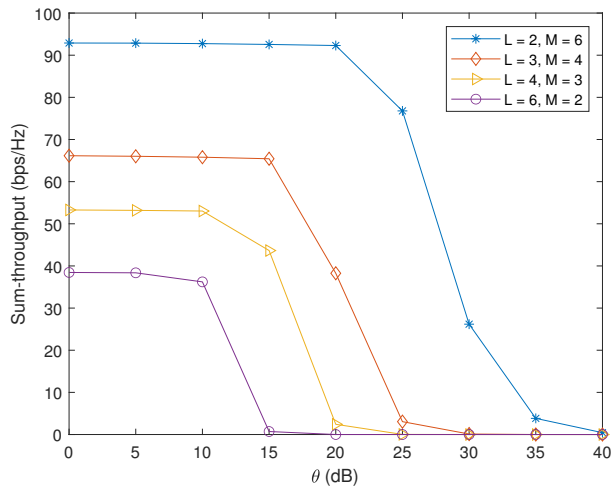

Figure 3.4: Sum-throughput versus SINR threshold of θ in WPCNs of $(L, M, N, W) = (2, 6, 4, 3)$, $(L, M, N, W) = (3, 4, 4, 3)$, $(L, M, N, W) = (4, 3, 4, 3)$, and $(L, M, N, W) = (6, 2, 4, 3)$.

throughput gain. Note that the number of users of messages decoded by a single SIC is given by L. Accordingly, when L is high, the user of its message decoded earlier experiences more interferences compared to when L is low, and more resources are needed to meet the SINR thresholds. As a result, the drastic degradation of the sum-throughput along with increasing θ begins to start earlier for higher L.

In Fig. 3.5, a WPCN of $(L, M, N, W) = (2, 4, 4, 3)$ is considered where the distances of the users are given as $[d_{11}, d_{21}, d_{31}, d_{41}] = [3, 4, 5, 6]$ m, $[d_{12}, d_{22}, d_{32}, d_{42}] = [10, 11, 12, 13]$ m. Particularly, the sum-throughput versus θ is compared when clustering-specific beamforming, $\mathbf{v}_{ml}$ is further optimized and when it is not. Each plot is labeled 'SA with Opt.' and 'SA without Opt.' The impact of the optimization of $\mathbf{v}_{ml}$ is observed in the sum-throughput gap of the two plots, which is the gain from the optimization. To be more specific, the beamforming for 'SA with Opt.' is optimized as proposed in Algorithm 2. On the other hand, the beamforming for 'SA without Opt.'

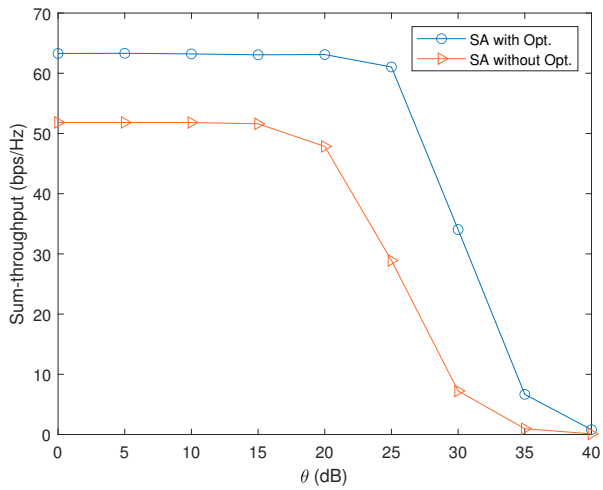

Figure 3.5: Sum-throughput versus SINR threshold of θ with and without the optimization of cluster-specific beamforming in a WPCN of $(L, M, N, W) = (2, 4, 4, 3)$.

is simply for signal alignment. Thus, the outer precoding of $\mathbf{v}_{ml}$, $\mathbf{V}_{ml}$ can be selected as one of the right singular vectors of $\mathbf{A}_m$ of (3.14) corresponding to the zero singular values. The inner precoding of $\mathbf{v}_{ml}$, $\mathbf{w}_m$ becomes a scalar in this case and the ZF matrix, $\mathbf{P}^H$ is determined from (3.16). The gain from the optimization can be seen for all θ in the figure. Furthermore, the drastic degradation of the sum-throughput starts at higher θ in 'SA with Opt.' than in 'SA without Opt.'

I compare the sum-throughputs with SIC error propagation between the scheme proposed in [41] and the proposed one. The error propagation model is adapted from [55] as follows. Since the signals which should be cancelled are not completely removed, they are treated as noise with the remaining interferences. The ratio of the signal left after cancellation is indicated by β. Note that when $\beta = 0$, the SIC is performed perfectly, whereas when $\beta = 1$, the SIC is completely failed. For the scheme proposed in [41], users are denoted by U_i where $i \in \{1, ..., LM\}$, and the lower the index is, the better the channel condition a user has. The SIC is performed in the de-

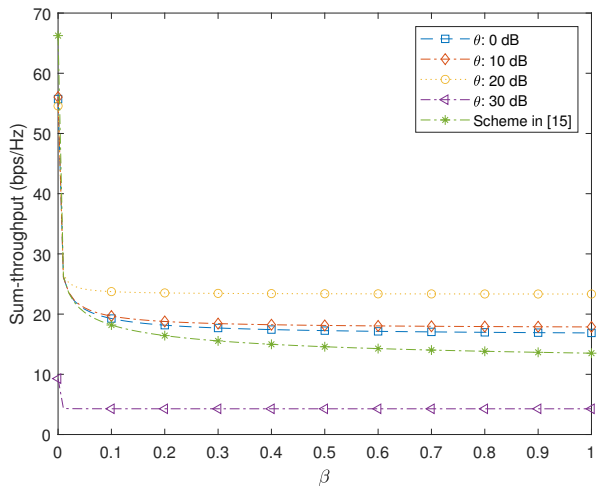

Figure 3.6: Sum-throughput versus SIC error propagation ratio of β comparison between the proposed scheme with various SINR thresholds and the scheme given in [41] in a WPCN of $(L, M, N, W) = (2, 4, 3, 1)$.

scending order with respect to the channel status (i.e., The message of U_i is decoded ahead of the message of U_j where $j > i$). Then, the throughput of U_i with error propagation is given by

$$R_i = (1-\tau_0)\log\det\Big(\mathbf{I}_M + \mathbf{H}_i\mathbf{V}_i\mathbf{H}_i^H\Big((1-\tau_0)\sigma^2\mathbf{I}_M + \sum_{j=i+1}^{LM}\mathbf{H}_j\mathbf{V}_j\mathbf{H}_j^H + \beta\sum_{k=1}^{i-1}\mathbf{H}_k\mathbf{V}_k\mathbf{H}_k^H\Big)^{-1}\Big), \tag{3.41}$$

where $\mathbf{V}_i$ is the information transmit covariance matrix multiplied by the transmit time, which is optimized under the assumption of the perfect SIC as given in [41]. On the other hand, for the proposed scheme, U_{ml} with $l \geq 2$ is the user which is affected by the error propagation. Hence, the throughput of U_{m1} remains the same,

and the throughput of U_{ml} for $l = 2, ..., L$ is given by

$$R_{ml} = (1-\tau_0)\log\Big(1+\frac{|h_m|^2\gamma_{ml}}{|h_m|^2(\beta\sum_{j=1}^{l-1}\gamma_{mj}+\sum_{j=l+1}^{L}\gamma_{mj})+\sigma^2(1-\tau_0)}\Big). \tag{3.42}$$

Fig. 3.6 is the simulation result with various θ's for a network of $(L, M, N, W) = (2, 4, 3, 1)$ where $[d_{11}, d_{21}, d_{31}, d_{41}] = [3, 4, 5, 6]$ m, $[d_{12}, d_{22}, d_{32}, d_{42}] = [10, 11, 12, 13]$ m. It can be seen that as β increases, the sum-throughput decreases due to the imperfect SIC for both schemes. However, the sum-throughput drops faster as β increases when using the scheme proposed in [41] than the proposed scheme. Particularly, the proposed scheme achieves higher sum-throughput when θ is set to 0, 10, and 20 dB beyond a certain level of β. On the other hand, when $\theta = 30$ dB, the system achieves notably low sum-throughput for all β. It is because that τ_0 for DL-WET becomes higher to meet the SINR thresholds, which in turn $(1-\tau_0)$ for UL-WIT decreases significantly compared to the cases of lower θ as aforementioned. Therefore, the proposed scheme can be more robust and effective to SIC error propagation by putting an appropriate SINR threshold.

In Fig. 3.7, I compare the sum-throughput performance of the proposed scheme and the one with TDMA transmission, **(P2)** of (3.39) for a WPCN of $(L, M, N, W) = (2, 2, 2, 2)$ where $[d_{11}, d_{21}, d_{31}, d_{41}] = [3, 4, 5, 6]$ m, $[d_{12}, d_{22}, d_{32}, d_{42}] = [10, 11, 12, 13]$ m. Each scheme is denoted by 'NOMA-SA' and 'OMA-SA' where SA stands for signal alignment. For OMA-SA, I let $\phi_{ml} = \phi, \forall m, l$. As **(P1′)** has an SINR threshold as a constraint, in order to compare both schemes fairly, θ will be set to $\theta = e^{\frac{\phi}{1-\tau_0}} - 1$. Note that when θ is set as such, the convexity of **(P1′)** (i.e., NOMA-SA) is not guaranteed due to the coupling of τ_0 and $\{\gamma_{ml}\}$. Hence, τ_0 will be given, which makes **(P1′)** become equivalent to $f(\tau_0)$, and τ_0 that maximizes $f(\tau_0)$ will be searched via the golden section method in spite of no guarantee of convexity. As seen in the upper plots of Fig. 3.7, NOMA-SA achieves almost the same sum-throughput as OMA-SA

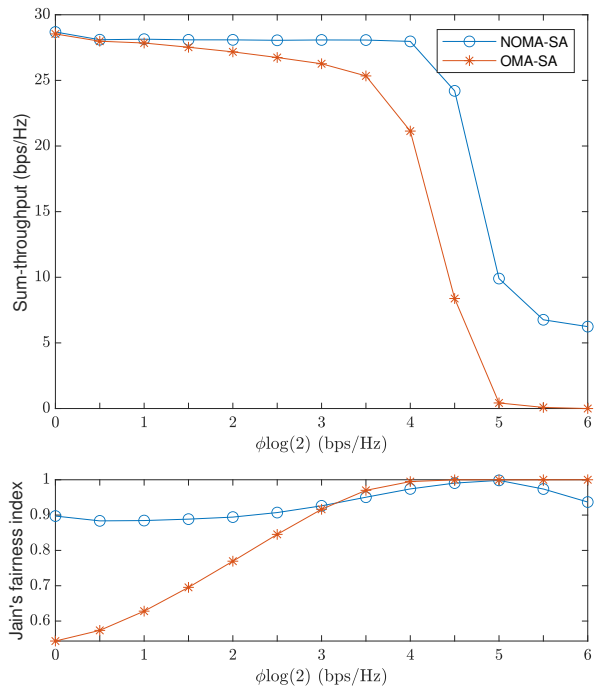

Figure 3.7: Sum-throughput and Jain's fairness index with various QoS thresholds of ϕ for NOMA and OMA each with signal alignment in a WPCN of $(L, M, N, W) = (2, 2, 2, 2)$.

when $\phi = 0$. Moreover, in contrast to the results of [45] which takes energy consumption into account, NOMA transmission achieves higher sum-throughput than TDMA transmission when $\phi > 0$. In particular, the sum-throughput of NOMA-SA remains constant up to a certain level of ϕ and starts to drop drastically with growing ϕ, as in the plots of other results. On the other hand, the sum-throughput of OMA-SA decreases gradually. The lower plots of Fig. 3.7 show *Jain's fairness index*, $\mathcal{J}$ which is defined as [56]

$$\mathcal{J}(x_1, x_2, ..., x_n) \triangleq \frac{(\sum_{i=1}^{n} x_i)^2}{n \cdot \sum_{i=1}^{n} x_i^2}, \tag{3.43}$$

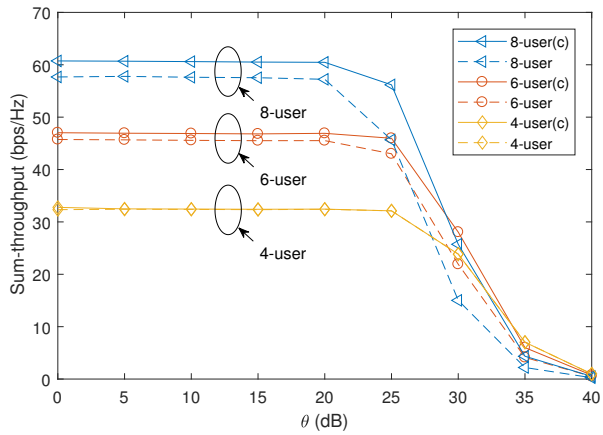

Figure 3.8: Sum-throughput gap between the proposed scheme and the scheme with optimal clustering in WPCNs of $(L, M, N, W) = (2, n_M, 3, 2)$ where $n_M \in \{2, 3, 4\}$ for 4, 6, and 8 users.

where x_i and n would be the individual throughput and the number of users, respectively. When $\mathcal{J}$ approaches one, the rate disparity becomes zero, while when it approaches zero, user unfairness is very severe. It can be seen that NOMA-SA generally achieves higher user fairness. The reason why the index of the TDMA-SA approaches one in higher ϕ is that the throughputs of all users decrease simultaneously, which is not desirable.

In Fig. 3.8, a WPCN of $(L, M, N, W) = (2, n_M, 3, 2)$ is considered where $n_M \in \{2, 3, 4\}$ (i.e., there are 4, 6, and 8 users in the network.) For any n_M, the distances of users are given by d_{ml} for all $m \in \{1, ..., n_M\}$ and $l \in \{1, 2\}$, where $[d_{11}, d_{21}, d_{31}, d_{41}] = [3, 4, 5, 6]$ m, $[d_{12}, d_{22}, d_{32}, d_{42}] = [10, 11, 12, 13]$ m. The sum-throughputs of two clusterings are compared for all n_M with various θ's. In the plots labeled '$2n_M$-user', the users, U_{ml}'s with the same m for all l are clustered as proposed. On the other hand, in the plots labeled '$2n_M$-user(c)', users are clustered optimally. That is, $n_M!$ clusterings are considered, and the one that yields the maximum

sum-throughput among them is chosen via a full-search. As seen in the figure, the sum-throughput gap becomes higher as the number of users increases. Note that there is almost no gain in 4-user case. Due to the randomness of the channel coefficients, random clustering or clustering U_{ml}'s with different m for all l does not provide clustering gain. Thus, 4-user(c) is practically equivalent to a random clustering case as the number of ways of clustering is just two. For the same reason, as the number of ways of clustering gets higher (i.e., as the number of users increases), the clustering gain also becomes higher. The clustering gain can depend on the differences of the MIMO channels to be aligned in the same direction, the orthogonality of the aligned channels, and the amount of energy harvested at each user, etc. Therefore, by clustering the users optimally, the sum-throughput performance of the proposed scheme can be improved. Due to the coupled factors of clustering gain, finding optimal clustering is beyond the scope of the chapter.

3.5 Conclusion

In this chapter, I have formulated a sum-throughput maximization problem for NOMA-based WPCN with cluster-specific beamforming. The cluster-specific beamforming groups LM users into M clusters, each with L users. The channels of users in a cluster are aligned in the same direction by the signal alignment. The inter-cluster interferences are suppressed by the ZF beamforming at the BS. The SNR of the aligned signals in each cluster is maximized by further optimizing the beamforming matrices. A novel algorithm for maximizing the sum-throughput in the considered networks has been proposed. Numerical results have demonstrated that NOMA transmission with the proposed beamforming for a WPCN can be effective for throughput degradation from the SIC error propagation. Moreover, the proposed scheme has shown to alleviate user unfairness as well as to achieve higher sum-throughput compared to the

TDMA where the same beamforming is employed.

Chapter 4

IRS-Assisted Wireless Powered Communication Networks: Comparison of NOMA and OMA

In this chapter, I consider wireless powered communication networks (WPCNs) consisting of a hybrid access-point (H-AP) with a single antenna, an intelligent reflecting surface (IRS), and multiple users each with a single antenna. During downlink, users harvest energy from both an energy signal transmitted from a H-AP and the reflected signal at the IRS. During uplink, users transmit information using harvested energy following non-orthogonal multiple access (NOMA) or OMA. Particularly, signals from users and reflected signals at the IRS are superposed, and are received at the H-AP. A sum-throughput maximization subject to the minimum throughput constraints is formulated, and is relaxed into multiple convex problems. Numerical results show that the IRS enhances throughput performance, while it is more effective in OMA than in NOMA to set throughput constraints for enhancing user fairness. In addition, user fairness is significantly dependent on the location of the IRS in a NOMA-based WPCN, while it is not in an OMA-based WPCN.

4.1 Introduction

Recently, an intelligent reflecting surface (IRS) has emerged as a promising solution to improve the performance of wireless networks [57], [58]. An IRS consists of a number of passive elements that reflect radio-frequency (RF) signals and induce phase shifts on the signals. With recent advances in metamaterials, it is envisioned that an IRS can be applied to the wireless networks by reconfiguring the passive elements to have desired adjustment of phase shifts and amplitudes of the reflected signals [59]. Thus, by designing the beamforming of the passive elements at the IRS, an IRS-assisted network can enhance throughput, energy efficiency, coverage, etc.

In addition to an IRS, wireless power transfer (WPT) has been studied for prolonging the lifetime of energy-constrained wireless networks [6]. WPT enables wireless devices to harvest energy from a signal transmitted from a dedicated energy source, thereby overcoming outages caused by battery shortage. As a new framework on the design of a wireless network with WPT, simultaneous wireless information and power transfer (SWIPT) and a wireless powered communication network (WPCN) have been proposed [4], [9]. In SWIPT, a hybrid access point (H-AP) transfers energy to energy receivers (ERs) and transmits information to information receivers (IRs) via downlink. In a WPCN, a H-AP transfers energy to energy harvesting users via downlink, and the users transmit information to the H-AP using the harvested energy via uplink.

IRS-assisted wireless networks with WPT have been considered in several work [60]- [63]. In [60]- [62], an IRS-assisted SWIPT system consisting of a H-AP with multiple antennas, and multiple ERs and IRs each with a single antenna has been considered. The beamforming at the H-AP and the passive elements of the IRS have been optimized for weighted sum-throughput maximization [60], transmit power minimization under quality of service constraints [61], and minimum receiver power maximization subject to signal to interference-plus-noise ratio (SINR) constraints [62].

In [63], an IRS-assisted WPCN consisting of a H-AP and two users has been considered, where a user with better channel helps the other user by relaying the message of the other user. For the considered network, the minimum throughput has been maximized.

As a multiple access scheme for uplink in a WPCN, non-orthogonal multiple access (NOMA) has been considered in [23] for its higher spectral efficiency, user fairness, and low latency compared to orthogonal multiple access (OMA) [37]. Since the IRS brings changes in the effective channels of users, it can heavily affect user fairness which benefits from the successive interference cancellation (SIC) decoding in NOMA. Thus, it needs to explore the effect of IRS on a NOMA-based WPCN in terms of throughput and user fairness. Additionally, it needs to compare the impact of the IRS on the system performance in both a NOMA-based WPCN and an OMA-based WPCN.

In this chapter, I consider a WPCN consisting of a H-AP, an IRS, and multiple users each equipped with a single antenna, where users transmit information in NOMA and OMA. The sum-throughput maximization problems subject to minimum throughput constraints are formulated, and are transformed into solvable forms. Numerical results show the IRS enhances throughput performance for both NOMA and OMA. In addition, IRS brings significant change on user fairness in a NOMA-based WPCN, but has a minor impact on user fairness in an OMA-based WPCN.

4.2 System Model

I consider a WPCN consisting of a H-AP with a single antenna, an IRS with N passive elements, and K users each with a single antenna as in Fig. 4.1. The k-th user is denoted by U_k for $k \in \{1, ..., K\}$. For simplicity, I consider a unit transmission time. The time for downlink wireless energy transfer (DL-WET) is denoted by τ_0,

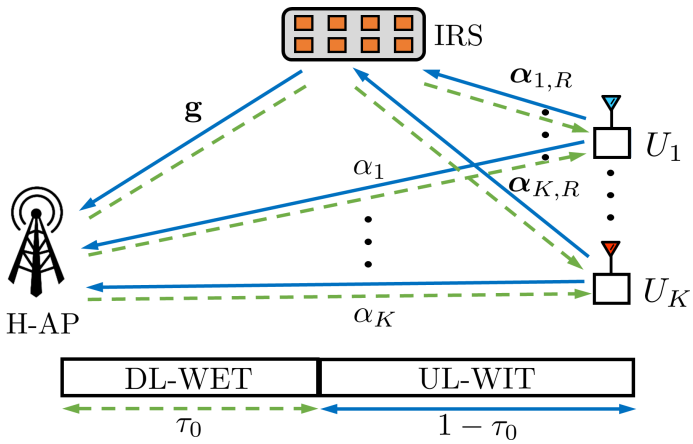

Figure 4.1: An IRS-assisted WPCN with K users

and the time for uplink wireless information transmission (UL-WIT) is then given by $1-\tau_0$. It is assumed that the channel reciprocity holds. The channel coefficients of a H-AP-U_k link, a H-AP-IRS link, an IRS-U_k link are denoted by $\alpha_k \in \mathbb{C}$, $\mathbf{g} \in \mathbb{C}^{1\times N}$, and $\boldsymbol{\alpha}_{k,R} \in \mathbb{C}^{N\times 1}$ where $k = 1, ..., K$, respectively. The H-AP is assumed to have channel state information of all links. The system models for WPCNs based on NOMA and OMA are given in the following.

4.2.1 NOMA-based WPCN

The IRS beamforming matrices for DL and UL are denoted by $\boldsymbol{\Theta}_0$ and $\boldsymbol{\Theta}_1$, respectively, where

$$\boldsymbol{\Theta}_t = \text{diag}(e^{j\theta_{t,1}}, ..., e^{j\theta_{t,N}}), t \in \{0, 1\}, \tag{4.1}$$

and $\theta_{t,i}, i \in \{1, ..., N\}$ denotes the phase shift induced by the ith element of an IRS. During τ_0 of DL-WET, the H-AP transfers an energy signal, x_0 where $x_0 \sim \mathcal{CN}(0, 1)$ with the transmit power of P_0. Then, U_k receives the sum of the signal of direct link between the H-AP and U_k, and the reflected signal at the IRS. Thus, the received

signal at U_k can be written as

$$y_k = (\mathbf{g}\boldsymbol{\Theta}_0\boldsymbol{\alpha}_{k,R} + \alpha_k)\sqrt{P_0}x_0 + n_k, \tag{4.2}$$

where n_k is the receive noise at U_k for all k, and $n_k \sim \mathcal{CN}(0, \sigma_k^2)$ where σ_k^2 is the noise variance. From (4.2), the amount of energy that U_k harvests during τ_0 is given by

$$E_k = \eta_k|\mathbf{g}\boldsymbol{\Theta}_0\boldsymbol{\alpha}_{k,R} + \alpha_k|^2 P_0\tau_0, \tag{4.3}$$

where η_k denotes the energy harvesting conversion efficiency. Since the energy consumed at U_k during $(1-\tau_0)$ cannot be larger than the harvested energy, E_k, the transmit power of U_k during $(1-\tau_0)$, P_k should satisfy $P_k \leq \frac{E_k}{1-\tau_0}$ for all k.

During $(1-\tau_0)$ of UL-WIT, U_k transmits its information, $x_k \sim \mathcal{CN}(0,1)$ with the transmit power of P_k. The received signal at the H-AP is given by

$$y_0 = \sum_{k=1}^{K}(\boldsymbol{\alpha}_{k,R}^H\boldsymbol{\Theta}_1\mathbf{g}^H + \alpha_k^H)\sqrt{P_k}x_k + n_0, \tag{4.4}$$

where n_0 is the receive noise at the H-AP and $n_0 \sim \mathcal{CN}(0, \sigma^2)$ where σ^2 is the noise variance. The messages of U_1, ..., U_k are decoded with the SIC, where the decoding order is in the descending order with respect to the channel status for user fairness (i.e., the message of a user with better channel is decoded before a user with worse channel.) For simplicity, it is assumed that a user with smaller path loss has better channel, and U_i has better channel than U_j where $i < j$. The SINR of U_k after the SIC decoding is given by

$$\text{SINR}_k = \frac{|\boldsymbol{\alpha}_{k,R}^H\boldsymbol{\Theta}_1\mathbf{g}^H + \alpha_k^H|^2 P_k}{\sum_{l=k+1}^{K}|\boldsymbol{\alpha}_{l,R}^H\boldsymbol{\Theta}_1\mathbf{g}^H + \alpha_l^H|^2 P_l + \sigma^2}. \tag{4.5}$$

The throughput of U_k is given by

$$R_k^{(\text{N})} = (1-\tau_0)\log\left(1 + \text{SINR}_k\right), \forall k. \tag{4.6}$$

The sum-throughput is given by

$$R_{\text{sum}}^{(\text{N})} = (1-\tau_0)\log\left(1+\frac{\sum_{k=1}^{K}|\boldsymbol{\alpha}_{k,R}^H\boldsymbol{\Theta}_1\mathbf{g}^H+\alpha_k^H|^2P_k}{\sigma^2}\right). \tag{4.7}$$

4.2.2 OMA-based WPCN

In this subsection, I particularly consider time division multiple access (TDMA) for UL-WIT. The time for UL-WIT, $(1-\tau_0)$ is divided into $\tau_1,...,\tau_K$. As in (4.1) of section 4.2.1, the IRS beamforming matrix for DL is given by $\boldsymbol{\Theta}_0$, and the one during τ_k for UL is given by $\boldsymbol{\Theta}_k$ where $k=1,...,K$. During τ_0 of DL-WET, the received signal and the harvested energy at U_k are the same as (4.2) and (4.3). Then, for all k, during τ_k of UL-WIT, U_k transmits its information, $x_k \sim \mathcal{CN}(0,1)$ with the transmit power of P_k where P_k should satisfy $P_k \leq \frac{E_k}{\tau_k}$. The received signal at the H-AP during τ_k is given by

$$y_{0,k} = (\boldsymbol{\alpha}_{k,R}^H\boldsymbol{\Theta}_k\mathbf{g}^H+\alpha_k^H)\sqrt{P_k}x_k+n_0. \tag{4.8}$$

The throughput of U_k in an OMA-based WPCN is given by

$$R_k^{(\text{O})} = \tau_k\log\left(1+\frac{|\boldsymbol{\alpha}_{k,R}^H\boldsymbol{\Theta}_k\mathbf{g}^H+\alpha_k^H|^2P_k}{\sigma^2}\right). \tag{4.9}$$

4.3 Sum-Throughput Maximization

In this section, I formulate the sum-throughput maximization problems subject to throughput constraints for a NOMA-based WPCN and an OMA-based WPCN. The throughput constraint for U_k is given by ϕ_k. It is assumed ϕ_k is feasible for all k in the following. Due to the non-convexity of the problems, they are transformed into tractable problems by semidefinite relaxation (SDR) and some mathematical manipulations [58], [26]. Let the transmit power vector during UL-WIT be $\mathbf{p}=[P_1,...,P_K]$.

4.3.1 NOMA-based WPCN with throughput constraints

In this subsection, I consider a NOMA-based WPCN which is assisted by an IRS. The sum-throughput maximization problem subject to throughput constraints is given by

$$\text{(P1)}: \max_{\tau_0, \boldsymbol{\Theta}_0, \boldsymbol{\Theta}_1, \mathbf{p}} \quad R_{\text{sum}}^{(\text{N})} \tag{4.10a}$$

$$\text{s.t.} \quad 0 \leq \tau_0 \leq 1, \tag{4.10b}$$

$$0 \leq P_k(1-\tau_0) \leq E_k, \forall k, \tag{4.10c}$$

$$|(\boldsymbol{\Theta}_0)_{nn}| = 1, |(\boldsymbol{\Theta}_1)_{nn}| = 1, n = 1, ..., N, \tag{4.10d}$$

$$R_k^{(\text{N})} \geq \phi_k, \forall k. \tag{4.10e}$$

Due to the non-convexity, I solve (P1) for given τ_0, and τ_0 is optimized via a 1D line-search such as the golden section method. Note that (P1) without throughput constraints (i.e., $\phi_k = 0, \forall k$) has a unique τ_0 that maximizes the objective by the following proposition.

Proposition 1. *(P1) is concave with respect to τ_0 when $\phi_k = 0, \forall k$.*

Proof. The maximum $R_{\text{sum}}^{(\text{N})}$ is achieved when each user consumes all of its harvested energy from (4.7) for $\phi_k = 0, \forall k$. Thus, P_k is given by $\eta_k |\mathbf{g}\boldsymbol{\Theta}_0 \boldsymbol{\alpha}_{k,R} + \alpha_k|^2 P_0 \frac{\tau_0}{1-\tau_0}$ from (4.10c), and $R_{\text{sum}}^{(\text{N})}$ is rewritten as $(1-\tau_0)\log\left(1 + \sum_{k=1}^{K} c_k \frac{P_0}{\sigma^2} \frac{\tau_0}{1-\tau_0}\right)$ where $c_k = |\boldsymbol{\alpha}_{k,R}^H \boldsymbol{\Theta}_1 \mathbf{g}^H + \alpha_k^H|^2 |\mathbf{g}\boldsymbol{\Theta}_0 \boldsymbol{\alpha}_{k,R} + \alpha_k|^2 \eta_k$. Then, $R_{\text{sum}}^{(\text{N})}$ can be maximized by optimizing τ_0 and $(\boldsymbol{\Theta}_1, \boldsymbol{\Theta}_2)$ separately as c_k does not depend on τ_0. Given that $(\boldsymbol{\Theta}_1, \boldsymbol{\Theta}_2)$ is optimized for maximizing $\sum_{k=1}^{K} c_k$ subject to (4.10d), $R_{\text{sum}}^{(\text{N})}$ becomes concave with respect to τ_0 as it is a perspective of a concave function. Hence, (P1) is concave with respect to τ_0. □

Let (P1) for given τ_0 be denoted by $(\text{P1})_{\tau_0}$. Note that $(\text{P1})_{\tau_0}$ is still non-convex. In $(\text{P1})_{\tau_0}$, (4.10e) is equivalent to

$$\text{SINR}_k \geq e^{\frac{\phi_k}{(1-\tau_0)}} - 1 (\triangleq \gamma_k), \tag{4.11}$$

where SINR_k is given in (4.5), and the right-hand side term of (4.11) is denoted by γ_k. To tackle the non-convexity of $(\text{P1})_{\tau_0}$, I optimize $\boldsymbol{\Theta}_1$ and $\{\boldsymbol{\Theta}_0, \mathbf{p}\}$ alternately in an iterative manner. I first solve $(\text{P1})_{\tau_0}$ with respect to $\boldsymbol{\Theta}_1$ for given $\{\boldsymbol{\Theta}_0, \mathbf{p}\}$. $(\text{P1})_{\tau_0}$ for given $\{\boldsymbol{\Theta}_0, \mathbf{p}\}$ is relaxed as the following problem, (P1$'$) by the manipulations given below [58]: for all k,

$$\begin{aligned} \mathbf{v}_{1,k} &= \left[\begin{array}{cc} \boldsymbol{\alpha}_{k,R}^H \text{diag}(\mathbf{g}^H) & \alpha_k^H \end{array} \right], \mathbf{V}_{1,k} = \mathbf{v}_{1,k}^H \mathbf{v}_{1,k}, \\ \mathbf{e}_1 &= \left[\begin{array}{cccc} e^{j\theta_{1,1}} & ... & e^{j\theta_{1,N}} & 1 \end{array} \right]^T, \mathbf{E}_1 = \mathbf{e}_1 \mathbf{e}_1^H, \\ |\boldsymbol{\alpha}_{k,R}^H \boldsymbol{\Theta}_1 \mathbf{g}^H + \alpha_k^H|^2 &= |\mathbf{v}_{1,k} \mathbf{e}_1|^2 = \text{tr}(\mathbf{V}_{1,k} \mathbf{E}_1). \end{aligned} \tag{4.12}$$

Then, I have

$$(\text{P1}'): \max_{\mathbf{E}_1 \succeq 0} \quad \sum_{k=1}^{K} \text{tr}(\mathbf{V}_{1,k} \mathbf{E}_1) P_k \tag{4.13a}$$

$$\text{s.t.} \quad (\mathbf{E}_1)_{nn} = 1, n = 1, ..., N+1, \tag{4.13b}$$

$$\frac{\text{tr}(\mathbf{V}_{1,k} \mathbf{E}_1) P_k}{\sum_{l=k+1}^{K} \text{tr}(\mathbf{V}_{1,l} \mathbf{E}_1) P_l + \sigma^2} \geq \gamma_k, \forall k. \tag{4.13c}$$

Note that maximizing (4.10a) for given τ_0 is equivalent to maximizing (4.13a). It can be easily seen that (P1$'$) is a convex problem, which can be solved by convex tools such as CVX [30]. However, the rank of $\mathbf{E}_1$ should be one from (4.12), but (P1$'$) does not have a rank-1 constraint on $\mathbf{E}_1$ from the SDR. The optimal solution to (P1$'$), $\mathbf{E}_1^*$ is rewritten as $\mathbf{E}_1^* = \mathbf{U} \boldsymbol{\Sigma} \mathbf{U}^H$ from eigenvalue decomposition where $\mathbf{U} \in \mathbb{C}^{(N+1) \times (N+1)}$ is a unitary matrix and $\boldsymbol{\Sigma} \in \mathbb{C}^{(N+1) \times (N+1)}$ is a diagonal matrix consisting of the eigenvalues. As a sub-optimal solution of $\mathbf{e}_1$, I have $\tilde{\mathbf{e}}_1 = \mathbf{U} \boldsymbol{\Sigma}^{1/2} \mathbf{r}$ where $\mathbf{r} \in \mathbb{C}^{(N+1) \times 1}$ is a random vector which follows $\mathbf{r} \sim \mathcal{CN}(0, \mathbf{I}_{N+1})$. The sub-optimal solution of $\boldsymbol{\Theta}_1$ is then given by

$$\tilde{\boldsymbol{\Theta}}_1 = \text{diag} \left(e^{j \text{arg} \left(\frac{\tilde{\mathbf{e}}_1[1]}{\tilde{\mathbf{e}}_1[N+1]} \right)}, ..., e^{j \text{arg} \left(\frac{\tilde{\mathbf{e}}_1[N]}{\tilde{\mathbf{e}}_1[N+1]} \right)} \right). \tag{4.14}$$

Secondly, I optimize $\{\boldsymbol{\Theta}_0, \mathbf{p}\}$ in $(\text{P1})_{\tau_0}$ for given $\boldsymbol{\Theta}_1$, and the problem is trans-

formed into (P1$''$) in the following. As in (4.12), the variables are manipulated as

$$\begin{aligned}
\mathbf{v}_{0,k} &= \left[\begin{array}{cc} \mathbf{g}\text{diag}(\boldsymbol{\alpha}_{k,R}^T) & \alpha_k \end{array} \right], \mathbf{V}_{0,k} = \mathbf{v}_{0,k}^H \mathbf{v}_{0,k}, \\
\mathbf{e}_0 &= \left[\begin{array}{cccc} e^{j\theta_{0,1}} & ... & e^{j\theta_{0,N}} & 1 \end{array} \right]^T, \mathbf{E}_0 = \mathbf{e}_0 \mathbf{e}_0^H, \\
|\mathbf{g}\boldsymbol{\Theta}_0 \boldsymbol{\alpha}_{k,R} + \alpha_k|^2 &= |\mathbf{v}_{0,k}\mathbf{e}_0|^2 = \text{tr}(\mathbf{V}_{0,k}\mathbf{E}_0),
\end{aligned} \tag{4.15}$$

Then, I have

$$\text{(P1}''\text{):} \max_{\mathbf{E}_0 \succeq 0, \mathbf{p}} \quad \text{(4.13a)} \tag{4.16a}$$

$$\text{s.t.} \quad 0 \leq P_k(1-\tau_0) \leq \eta_k \text{tr}(\mathbf{V}_{0,k}\mathbf{E}_0) P_0 \tau_0, \forall k, \tag{4.16b}$$

$$(\mathbf{E}_0)_{nn} = 1, n = 1, ..., N+1, \text{and (4.13c).} \tag{4.16c}$$

(P1$''$) is a convex problem, which can be solved by convex tools. As in (P1$'$), (P1$''$) does not have a rank-1 constraint on $\mathbf{E}_0$. Thus, the approach for determining $\boldsymbol{\Theta}_1$ of (4.14) is applied to finding the sub-optimal $\boldsymbol{\Theta}_0$ with $\mathbf{E}_0^*$ which is the optimal solution to (P1$''$).

(P1)$_{\tau_0}$ is solved through an iterative manner of solving (P1$'$) and (P1$''$) alternately. Particularly, as (P1$''$) is always feasible, it needs to start the iteration by solving (P1$''$). In each iteration except for the first one, the objective function is non-decreasing. In solving (P1$'$), the objective is non-decreasing for $\{\boldsymbol{\Theta}_0, \mathbf{p}\}$ given in the current iteration. Similarly, the objective of (P1$''$) is non-decreasing for given $\boldsymbol{\Theta}_0$ of the previous iteration obtained by solving (P1$'$). Since the objective function is upper bounded by the system limit and non-decreasing, the convergence of the proposed iterative approach is guaranteed.

4.3.2 OMA-based WPCN with throughput constraints

In this subsection, I consider an OMA-based WPCN which is assisted by an IRS. The sum-throughput maximization problem subject to throughput constraints is given by

$$\text{(P2)}: \max_{\{\tau_k\},\{\mathbf{\Theta}_k\},\mathbf{p}} \quad \sum_{k=1}^{K} R_k^{(\mathrm{O})} \tag{4.17a}$$

$$\text{s.t.} \quad 0 \le \tau_k \le 1, k = 0, ..., K, \tag{4.17b}$$

$$\tau_0 + \tau_1 + ... + \tau_K \le 1, \tag{4.17c}$$

$$0 \le P_k \tau_k \le E_k, k = 1, , , , K, \tag{4.17d}$$

$$|(\mathbf{\Theta}_k)_{nn}| = 1, k = 0, ..., K, n = 1, ..., N, \tag{4.17e}$$

$$R_k^{(\mathrm{O})} \ge \phi_k, k = 1, ..., K. \tag{4.17f}$$

As in section 4.3.1, (P2) is solved by optimizing $\{\mathbf{\Theta}_1, ..., \mathbf{\Theta}_K\}$ and $\{\{\tau_k\}, \mathbf{\Theta}_0, \mathbf{p}\}$ alternately in an iterative manner. I first relax (P2) for given $\{\{\tau_k\}, \mathbf{\Theta}_0, \mathbf{p}\}$ and it needs to define

$$\mathbf{e}_k = \left[\begin{array}{cccc} e^{j\theta_{k,1}} & ... & e^{j\theta_{k,N}} & 1 \end{array} \right]^T, \mathbf{E}_k = \mathbf{e}_k \mathbf{e}_k^H,$$

along with $\mathbf{v}_{1,k}$ and $\mathbf{V}_{1,k}$ of (4.12) for $k = 1, ...K$. Then, I have

$$\text{(P2}'\text{)}: \max_{\{\mathbf{E}_k \succeq 0\}} \quad \sum_{k=1}^{K} \tau_k \log\left(1 + \frac{\mathrm{tr}(\mathbf{V}_{1,k}\mathbf{E}_k)P_k}{\sigma^2}\right) \tag{4.18a}$$

$$\text{s.t.} \quad (\mathbf{E}_k)_{nn} = 1, k = 1, ..., K, n = 1, ..., N+1, \tag{4.18b}$$

$$\tau_k \log\left(1 + \frac{\mathrm{tr}(\mathbf{V}_{1,k}\mathbf{E}_k)P_k}{\sigma^2}\right) \ge \phi_k, k = 1, ..., K, \tag{4.18c}$$

which is also a convex problem, and can be solved with convex tools. Since $\mathbf{E}_k$ should have a rank of 1, the sub-optimal solution of $\mathbf{\Theta}_k$ can be obtained as $\mathbf{\Theta}_1$ of (4.14) of (P1$'$) for $k = 1, ..., K$.

Secondly, (P2) for given $\{\mathbf{\Theta}_1, ..., \mathbf{\Theta}_K\}$ is relaxed into (P2$''$) by $z_k = P_k \tau_k$ where

$k = 1, ..., K$, $\mathbf{z} = [z_1, ..., z_K]$, and $\mathbf{W}_0 = \mathbf{E}_0 \tau_0$ along with (4.15). Then, I have

$$\text{(P2}''\text{)}: \max_{\{\tau_k\}, \mathbf{W}_0 \succeq 0, \mathbf{z}} \quad \sum_{k=1}^{K} \tau_k \log\left(1 + \frac{\text{tr}(\mathbf{V}_{1,k}\mathbf{E}_k) z_k}{\sigma^2 \tau_k}\right) \tag{4.19a}$$

$$\text{s.t.} \quad (4.17b), (4.17c) \tag{4.19b}$$

$$0 \leq z_k \leq \eta_k \text{tr}(\mathbf{V}_{0,k}\mathbf{W}_0) P_0, \forall k, \tag{4.19c}$$

$$(\mathbf{W}_0)_{nn} = \tau_0, n = 1, ..., N+1, \tag{4.19d}$$

$$\tau_k \log\left(1 + \frac{\text{tr}(\mathbf{V}_{1,k}\mathbf{E}_k) z_k}{\sigma^2 \tau_k}\right) \geq \phi_k, k = 1, ..., K, \tag{4.19e}$$

which is a convex problem and can be solved by convex tools as well. From the optimal solution of $\{\tau_k^*\}$, $\mathbf{W}_0^*$, and $\mathbf{z}^*$, $\mathbf{E}_0^*$ can be obtained as $\mathbf{E}_0^* = \frac{\mathbf{W}_0^*}{\tau_0^*}$, which should be a rank-1 matrix. Since $\mathbf{W}_0^*$ is not guaranteed to be a rank-1 matrix, the approach for determining $\mathbf{\Theta}_1$ of (4.14) is applied to finding the sub-optimal $\mathbf{\Theta}_0$ with $\mathbf{E}_0^*$. Furthermore, the transmit power is obtained by $P_k = \frac{z_k^*}{\tau_k^*}$ for $k = 1, ..., K$.

4.4 Simulation Results

Numerical results are provided in this section. For (P1) and (P2), the sum-throughputs are evaluated and are compared to the cases when WPCNs are not assisted by an IRS. The problems without an IRS are equivalent to when $\mathbf{\Theta}_k = 0$ where $k = 0, ..., K$. In particular, (P1) without an IRS is solved for given τ_0 and τ_0 is optimized via a 1D line-search. Without an IRS, (P1) for given τ_0 and (P2) can be transformed into equivalent convex problems [9], [23].

Let d_k, $d_{k,R}$, and d_R denote the distances of a H-AP-U_k link, an IRS-U_k link, and a H-AP-IRS link, respectively. For large-scale fading, all channels are assumed to follow a distance-dependent path loss model, $L(d) = 1 + d^\beta$ where d is a given distance and β is the path loss exponent. For simplicity, β is set to 2 for all channels. For small-scale fading, it is assumed that the channel between the H-AP and U_k,

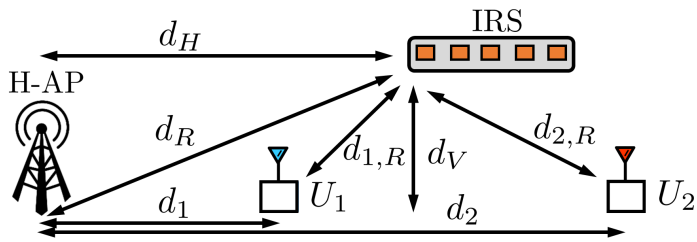

Figure 4.2: Simulation setup

α_k, and the channel between the IRS and U_k, $\boldsymbol{\alpha}_{k,R}$ experience Rayleigh fading, and the channel between the H-AP and the IRS, $\mathbf{g}$ experiences Rician fading. That is, $\mathbf{g} = \frac{1}{\sqrt{L(d_R)}}\left(\sqrt{\frac{\kappa}{1+\kappa}}\mathbf{g}_{\text{LoS}} + \sqrt{\frac{1}{1+\kappa}}\mathbf{g}_{\text{NLoS}}\right)$ where $\mathbf{g}_{\text{LoS}}$ and $\mathbf{g}_{\text{NLoS}}$ are the line-of-sight (LoS) and non-LoS components both modeled by Rayleigh fading. The energy harvesting conversion efficiency, η_k, and the noise power at the H-AP are assumed to be 0.7 and -80 dBm, respectively. In the following, I consider a WPCN of 2 users as in Fig. 4.2 where $[d_1, d_2] = [5, 25]$ m. Particularly, $d_R = \sqrt{d_H^2 + d_V^2}$ where d_H and d_V are horizontal and vertical distances between the IRS and the H-AP, and d_V is set to 5 m. Furthermore, $d_{1,R} = \sqrt{(d_H - d_1)^2 + d_V^2}$, and $d_{2,R} = \sqrt{(d_2 - d_H)^2 + d_V^2}$ where $d_1 \leq d_H \leq d_2$. For simplicity, I let the number of passive elements, N be 5, and the throughput constraint, ϕ_k be ϕ for all k.

In Fig. 4.3, the sum-throughput achieved by solving (P1) for given τ_0 (i.e., $(\text{P1})_{\tau_0}$) is evaluated when $d_H = 5$ m. Particularly, each plot shows the sum-throughput versus τ_0 performance, where ϕ is given by 0 and 3 nats/s/Hz. It is shown that the sum-throughput has no local maximum other than the global maximum with respect to τ_0. Therefore, τ_0 that achieves the maximum sum-throughput can be found by a 1D line-search in solving (P1). It can be observed that when τ_0 exceeds a certain value, the sum-throughput becomes 0 for $\phi = 3$ nats/s/Hz. It is because that $(\text{P1})_{\tau_0}$ becomes infeasible for the given ϕ.

In Fig. 4.4, I consider solving (P1) and (P2) where $d_H = 5$ m or 25 m. Further-

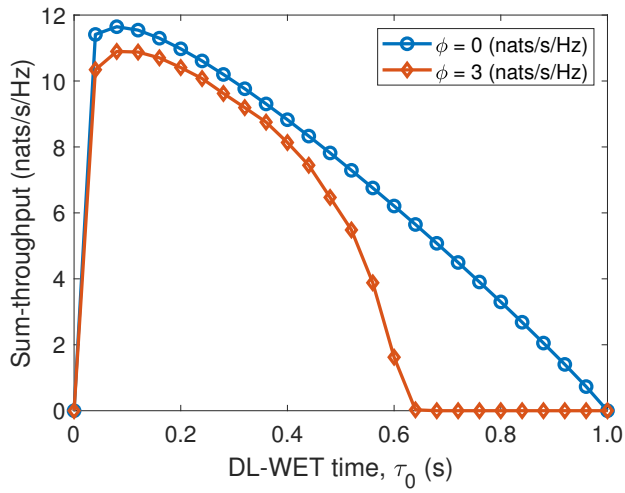

Figure 4.3: Sum-throughput versus τ_0 in a NOMA-based WPCN with an IRS for given throughput constraint, ϕ.

more, the sum-throughput maximization problems of a WPCN without an IRS are solved as well. The number in parentheses of the figure indicates d_H. The plots of Fig. 4.4(a) show the sum-throughput performance of the considered problems along with various throughput constraints, ϕ. It can be seen that NOMA achieves higher sum-throughput than OMA regardless of an IRS for all ϕ except 0 and 6 nats/s/Hz. Furthermore, when $d_H = 5$ m, the system achieves higher throughput than when $d_H = 25$ m for both NOMA and OMA. It is obvious because the channel status of the IRS-U_1 link is better than that of the IRS-U_2 link when $d_H = 5$, and U_1 has better efficiency in both information transmission and energy transfer than U_2. The plots of Fig. 4.4(b) show the throughput ratio of U_2 to U_1 (i.e., $\frac{R_2}{R_1}$) with respect to ϕ for evaluating user fairness. It can be seen that NOMA generally achieves higher user fairness than OMA. However, when $d_H = 5$ m, user fairness is significantly reduced compared to no IRS cases for NOMA. That is, R_1 increases more than R_2 by adopting the IRS. It means that IRS forms an effective channel that is more beneficial

to U_1 than U_2. On the other hand, user fairness degradation of when $d_H = 25$ m is lower than when $d_H = 5$ m for NOMA. Moreover, it shows a higher ratio than no IRS cases when ϕ is low. Note that it is more effective in OMA than in NOMA to impose a throughput threshold for enhancing user fairness.

Additionally, I investigate the throughput performance with various d_H when $\phi = 0$ nats/s/Hz. Fig. 4.5(a) shows that throughput gain from an IRS decreases with growing d_H, which coincides with the result of Fig. 4.4(a). Fig. 4.5(b) shows the throughput ratio with growing d_H. It can be seen that as an IRS becomes close to U_2, user fairness is significantly enhanced in NOMA. On the other hand, the level of improvement in OMA is smaller than that in NOMA. In other words, since users transmit simultaneously in NOMA, the effective channel formed by the IRS can be favorable for U_1 or U_2 depending on d_H. On the other hand, since each user transmits information alone at the time allocated to it in OMA, the IRS beamforming is adjusted to be favorable for each user at each time. Nevertheless, considering that the system suffers from severe user unfairness even with the IRS, an IRS in OMA seems to have a minor impact on user fairness. As a result, in order to guarantee a certain level of user fairness in an IRS-assisted WPCN, it needs to impose different throughput constraints depending on whether the system adopts NOMA or OMA.

4.5 Conclusion

In this chapter, I have formulated the sum-throughput maximization problems of IRS-assisted WPCNs which are based on NOMA and OMA. In particular, the problems are subject to throughput constraints. The maximization problems have been relaxed into convex problems. Numerical results have demonstrated that the IRS enhances the sum-throughput performance for both NOMA and OMA. Moreover, an IRS has a bigger impact on user fairness in NOMA than in OMA. Therefore, to ensure a certain

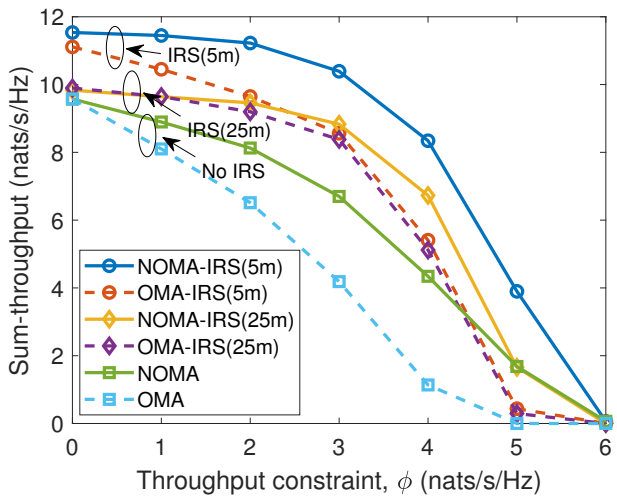

(a) Sum-throughput versus throughput constraint, ϕ.

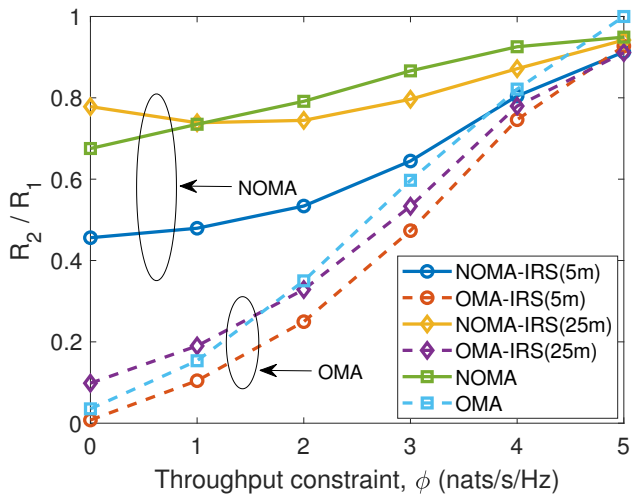

(b) Throughput ratio, $\frac{R_2}{R_1}$ versus throughput constraint, ϕ.

Figure 4.4: Impact of IRS on throughput performance of a NOMA-based WPCN and an OMA-based WPCN along with various throughput constraints, ϕ.

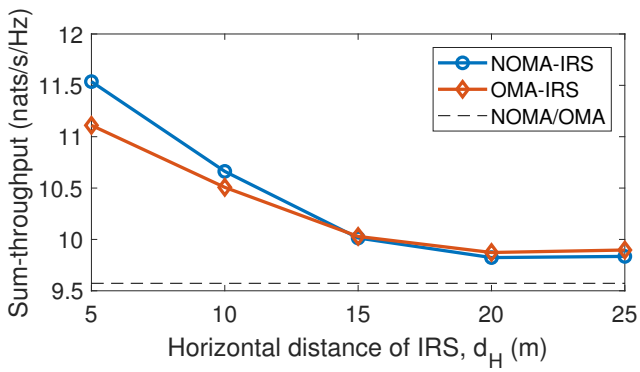

(a) Sum-throughput versus horizontal distance of IRS, d_H.

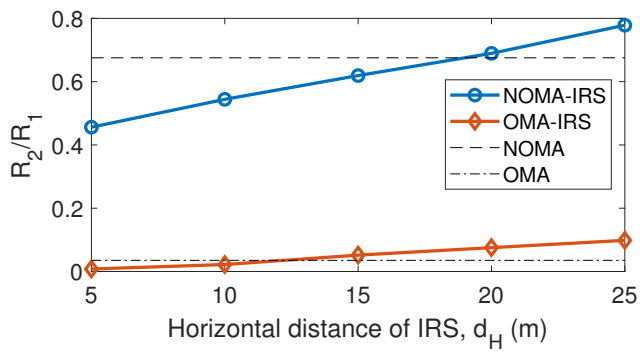

(b) Throughput ratio, $\frac{R_2}{R_1}$ versus horizontal distance of IRS, d_H.

Figure 4.5: Throughput performance of an IRS-assisted WPCN along with various horizontal distances of IRS, d_H.

level of user fairness, it needs to set different throughput constraints depending on NOMA and OMA.

Chapter 5

Conclusion

5.1 Summary

In this dissertation, I have developed several designs for maximizing the sum-throughput with QoS constraints in WPCNs. Due to the various techniques that can be applied to a WPCN, each system encounters different challenge in achieving the maximum sum-throughput. Thus, I have proposed a set of solutions which address the problems for various scenarios. The considered scenarios include a cooperative WPCN, a NOMA-based WPCN with cluster-specific beamforming being adopted, and an IRS-assisted WPCN, and have been shown to bring substantial performance gain. I hope the developed schemes can contribute to the practical use of a WPCN in future wireless systems.

In Chapter 2, I have considered a sum-throughput maximization problem under individual throughput thresholds for a WPCN with user cooperation, and have derived an optimal solution using convex optimization technique. From the analysis of the derived solution, conditions under which user cooperation becomes beneficial have been identified. Based on the new findings, I have then proposed a novel algorithm that classifies the problem into one of the sub-problem and returns the optimal

resource allocation, which has lower computational complexity.

In Chapter 3, I have formulated a sum-throughput maximization problem with SINR thresholds for NOMA-based WPCN with cluster-specific beamforming being utilized. I have designed the beamforming that performs signal alignment for a generalized number of clusters, and signal strength enhancement. In addition, a novel algorithm for maximizing the sum-throughput in the considered network where proposed beamforming is adopted has been presented. Numerical results have demonstrated that the proposed scheme can be effective for avoiding throughput degradation from the SIC error propagation, for enhancing user fairness compared to an OMA-based WPCN, and for increasing the achievable sum-throughput.

In Chapter 4, I have formulated the sum-throughput maximization problems with throughput constraints for IRS-assisted WPCNs which are based on NOMA or OMA. For each considered system model, the maximization problem has been relaxed as solvable forms, which provide the sub-optimal solution. Numerical results have shown that an IRS has a bigger impact on user fairness in NOMA than in OMA, which suggests that it needs to set different throughput constraints depending on whether the system adopts NOMA or OMA to ensure a certain level of user fairness.

5.2 Future directions

In this section, I present some future research directions regarding to the design of a WPCN. I have explored resource allocation for a WPCN to achieve the maximum sum-throughput. The computation for resource allocation is performed at the H-AP side to reduce the processing cost of users due to their scarcity of energy resources. Thus, a H-AP needs to obtain channel state information (CSI) via CSI feedback. Since the part of the coherence time needs to be allocated to the feedback link, the uplink spectral efficiency decreases. Therefore, it is necessary to investigate the

trade-off between achievable sum-throughput versus CSI feedback. Particularly, for WPCNs with multi-antenna system, the uplink overhead from CSI feedback can be high. Furthermore, since an IRS consists of multiple passive elements, further efforts should be made to estimate channel coefficients. Given that the channel estimation of links of an IRS is challenging, one needs to address the design of an IRS beamforming considering ergodicity. Furthermore, channel quantization errors should be taken into account for the practical use of a WPCN.

In addition to the problems related to CSI acquisition, resource allocation for a WPCN needs to be addressed in a time horizon perspective. In an OMA-based WPCN, users can utilize the total amount of harvested energy since there is no inter-user interference. On the other hand, in a NOMA-based WPCN, a part of harvested energy can be used in order not to cause much interference to other users, thereby satisfying QoS constraints. Thus, one can consider how to use the remaining energy efficiently in the next transmission, and develop resource allocation for multiple time sequences. Furthermore, it is worth noting the extension to multi-cell WPCN. Signals from the adjacent cell may occur inter-cell interference in case it is in the same frequency band, but may also provide an opportunity to harvest extra energy.

Bibliography

[1] S. Ulukus et al., "Energy harvesting wireless communications: A review of recent advances," *IEEE J. Sel. Areas Commun.*, vol. 33, no. 3, pp. 360-380, Mar. 2015.

[2] S. Buzzi, C.-L. I, T. E. Klein, H. V. Poor, C. Yang, and A. Zappone, "A survey of energy-efficient techniques for 5G networks and challenges ahead," *IEEE J. Sel. Areas Commun.*, vol. 34, no. 4, pp. 697-709, Apr. 2016.

[3] P. Grover and A. Sahai, "Shannon meets Tesla: Wireless information and power transfer," in *Proc. IEEE Int. Symp. Inf. Theory*, Jun. 2010, pp. 2363-2367.

[4] R. Zhang and C. K. Ho, "MIMO broadcasting for simultaneous wireless information and power transfer," *IEEE Trans. Wireless Commun.*, vol. 12, no. 5, pp. 1989-2001, May 2013.

[5] I. Krikidis, S. Timotheou, S. Nikolaou, G. Zheng, D. W. K. Ng, and R. Schober, "Simultaneous wireless information and power transfer in modern communication systems," *IEEE Commun. Mag.*, vol. 52, no. 11, pp. 104-110, Nov. 2014.

[6] X. Lu, P. Wang, D. Niyato, D. I. Kim, and Z. Han, "Wireless networks with RF energy harvesting: A Contemporary Survey," *IEEE Commun. Surveys Tut.*, vol. 17, no. 2, pp. 757-789, 2nd Quart., 2015.

[7] S. Bi, C. K. Ho, and R. Zhang, "Wireless powered communication: Opportunities and challenges," *IEEE Commun. Mag.*, vol. 53, no. 4, pp. 117-125, Apr. 2015.

[8] S. Bi, Y. Zeng, and R. Zhang, "Wireless powered communication networks: An overview," *IEEE Wireless Commun.*, vol. 23, no. 2, pp. 10-18, Apr. 2016.

[9] H. Ju and R. Zhang, "Throughput maximization in wireless powered communication networks," *IEEE Trans. Wireless Commun.*, vol. 13, no. 1, pp. 418-428, Jan. 2014.

[10] H. Ju and R. Zhang, "Optimal resource allocation in full-duplex wireless powered communication network," *IEEE Trans. Commun.*, vol. 62, no. 10, Oct. 2014, pp. 3528-3540.

[11] M. A. Abd-Elmagid, T. ElBatt, and K. G. Seddik, "Optimization of wireless powered communication networks with heterogeneous nodes," in *Proc. IEEE Global Commun. Conf.*, Dec. 2015, pp. 1-7.

[12] L. Liu, R. Zhang, and K. Chua, "Multi-Antenna wireless powered communication with energy beamforming," *IEEE Trans. Commun.*, vol. 62, no. 12, pp. 4349-4361, Dec. 2014.

[13] W. Huang, H. Chen, Y. Li, and B. Vucetic, "On the performance of multi-antenna wireless-powered communications with energy beamforming," *IEEE Trans. Veh. Technol.*, vol. 65, no. 3, pp. 1801-1808, Mar. 2016.

[14] H. Chen, Y. Li, J. L. Rebelatto, B. F. Uchoa-Filho, and B. Vucetic, "Harvest-then-cooperate: Wireless-powered cooperative communications," *IEEE Trans. Signal Process.*, vol. 63, no. 7, pp. 1700-1711, Apr. 2015.

[15] Y. Gu, H. Chen, Y. Li, and B. Vucetic, "An adaptive transmission protocol for wireless-powered cooperative communications," in *Proc. IEEE Int. Conf. Commun.*, Jun. 2015, pp. 4223-4228.

[16] H. Liang, C. Zhong, H. A. Suraweera, G. Zhang, and Z. Zhang, "Optimization and analysis of wireless powered multi-antenna cooperative systems," *IEEE Trans. Wireless Commun.*, vol. 16, no. 5, pp. 3267-3281, May 2017.

[17] Y. Ma, H. Chen, Z. Lin, Y. Li, and B. Vucetic, "Distributed and optimal resource allocation for power beacon-assisted wireless-powered communications," *IEEE Trans. Commun.*, vol. 63, no. 10, pp. 3569-3583, Oct. 2015.

[18] W. Shin, M. Vaezi, J. Lee, and H. V. Poor, "Cooperative wireless powered communication networks with interference harvesting," *IEEE Trans. Veh. Tech.*, vol. 67, no. 4, pp. 3701-3705, Apr. 2018.

[19] G. Rezgui, E. Belmega, and A. Chorti, "Mitigating jamming attacks using energy harvesting" *IEEE Wireless Commun. Le.*, vol. 8, no. 1, pp. 297-300, Feb. 2019.

[20] D. Mishra, S. De, and D. Krishnaswamy, "Dilemma at RF energy harvesting relay: Downlink energy relaying or uplink information transfer?" *IEEE Trans. Wireless Commun.*, vol. 16, no. 8, pp. 4939-4955, Aug. 2017.

[21] N. Khalfet and S. Perlaza, "Simultaneous information and energy transmission in the two-user Gaussian interference channel" *IEEE J. Sel. Areas Commun.*, vol. 37, no. 1, pp. 156-170, Jan. 2019.

[22] A. Biason and M. Zorzi, "Transmission policies in wireless powered communication networks with energy cooperation," in *Proc. Eur. Signal Process. Conf.*, Budapest, Hungary, Aug. 2016, pp. 592-596.

[23] P. D. Diamantoulakis, K. N. Pappi, Z. Ding, and G. K. Karagiannidis, "Wireless-powered communications with non-orthogonal multiple access," *IEEE Trans. Wireless Commun.*, vol. 15, no. 12, pp. 8422-8436, Dec. 2016.

[24] H. Ju and R. Zhang, "User cooperation in wireless powered communication networks," in *Proc. IEEE Global Commun. Conf.*, Dec. 2014, pp. 1430-1435.

[25] L. Atzori, A. Iera, and G. Morabito, "The internet of things: A survey," *Comput. Netw.*, vol. 54, no. 15, pp. 2787-2805, 2010.

[26] S. Boyd and L. Vandenberghe, *Convex Optimization.* Cambridge, U.K.: Cambridge Univ. Press, 2004.

[27] T. Cormen, C. Leiserson, R. Rivest and C. Stein, *Introduction to Algorithms.* 3rd ed. Cambridge, MA, USA: MIT Press, 2009.

[28] A. Goldsmith, *Wireless Communications.* Cambridge, U.K.: Cambridge Univ. Press, 2005.

[29] Y. Liang and V. V. Veeravalli, "Gaussian orthogonal relay channels: optimal resource allocation and capacity," *IEEE Trans. Inform. Theory*, vol. 51, no. 9, pp. 3284-3289, Sep. 2005.

[30] M. Grant and S. Boyd, "CVX: MATLAB software for disciplined convex programming, version 2.1." http://cvxr.com/cvx, Mar. 2014.

[31] D. Tse and P. Viswanath, *Fundamentals of Wireless Communication.* Cambridge, U.K.: Cambridge Univ. Press, 2005.

[32] P. D. Diamantoulakis and G. K. Karagiannidis, "Maximizing proportional fairness in wireless powered communications," *IEEE Wireless Commun. Let.*, vol. 6, no. 2, pp. 202-205, Apr. 2017.

[33] M. Agiwal, A. Roy, and N. Saxena, "Next generation 5G wireless networks: A comprehensive survey," *IEEE Commun. Surveys Tut.*, vol. 18, no. 3, pp. 1617-1655, 3rd Quart., 2016.

[34] G. A. Akpakwu, B. J. Silva, G. P. Hancke, and A. M. Abu-Mahfouz, "A survey on 5G networks for the Internet of Things: Communication technologies and challenges," *IEEE Access*, vol. 6, pp. 3619-3647, Dec. 2018.

[35] P. Kamalinejad, C. Mahapatra, Z. Sheng, S. Mirabbasi, V. C. M. Leung, and Y. L. Guan, "Wireless energy harvesting for the Internet of Things," *IEEE Commun. Mag.*, vol. 53, no. 6, pp. 102-108, June 2015.

[36] G. Bedi, G. K. Venayagamoorthy, R. Singh, R. R. Brooks, and K. Wang, "Review of Internet of Things (IoT) in electric power and energy systems," *IEEE Internet Things J.*, vol. 5, no. 2, pp. 847-870, Apr. 2018.

[37] L. Dai, B. Wang, Y. Yuan, S. Han, C. I, and Z. Wang, "Non-orthogonal multiple access for 5G: solutions, challenges, opportunities, and future research trends," *IEEE Commun. Mag.*, vol. 53, no. 9, pp. 74-81, Sep. 2015.

[38] Z. Ding, X. Lei, G. K. Karagiannidis, R. Schober, J. Yuan, and V. K. Bhargava, "A Survey on non-orthogonal multiple access for 5G networks: Research challenges and future trends," *IEEE J. Sel. Areas Commun.*, vol. 35, no. 10, pp. 2181-2195, Oct. 2017.

[39] Y. Liu, Z. Qin, M. Elkashlan, Z. Ding, A. Nallanathan, and L. Hanzo, "Nonorthogonal multiple access for 5G and beyond," *Proc. IEEE*, vol. 105, no. 12, pp. 2347-2381, Dec. 2017.

[40] S. M. R. Islam, N. Avazov, O. A. Dobre, and K. S. Kwak, "Power-domain non-orthogonal multiple access (NOMA) in 5G systems: Potentials and challenges," *IEEE Commun. Surveys Tut.*, vol. 19, no. 2, pp. 721-742, 2nd Quart., 2017.

[41] H. Lee, K. Lee, H. Kong, and I. Lee, "Sum-Rate maximization for multiuser MIMO wireless powered communication networks," *IEEE Trans. Veh. Technol.*, vol. 65, no. 11, pp. 9420-9424, Nov. 2016.

[42] Q. Wu, M. Tao, D. W. K. Ng, W. Chen, and R. Schober, "Energy-efficient resource allocation for wireless powered communication networks," *IEEE Trans. Wireless Commun.*, vol. 15, no. 3, pp. 2312-2327, Mar. 2016.

[43] L. Xie, J. Xu, and R. Zhang, "Throughput maximization for UAV-enabled wireless powered communication networks," *IEEE Internet Things J.*, vol. 6, no. 2, pp. 1690-1703, Apr. 2019.

[44] T. A. Zewde and M. C. Gursoy, "NOMA-based energy-efficient wireless powered communications," *IEEE Trans. Green Commun. Netw.*, vol. 2, no. 3, pp. 679-692, Sep. 2018.

[45] Q. Wu, W. Chen, D. W. K. Ng, and R. Schober, "Spectral and energy-efficient wireless powered IoT networks: NOMA or TDMA?" *IEEE Trans. Veh. Technol.*, vol. 67, no. 7, pp. 6663-6667, Jul. 2018.

[46] Y. Yuan and Z. Ding, "The application of non-orthogonal multiple access in wireless powered communication networks," in *Proc. IEEE 17th Int. Workshop Signal Process. Adv. Wireless Commun. (SPAWC)*, Jul. 2016, pp. 1-5.

[47] Z. Ding et al., "Application of non-orthogonal multiple access in LTE and 5G Networks," *IEEE Commun. Mag.*, vol. 55, no. 2, pp. 185-191, Feb. 2017.

[48] A. Benjebbour, Y. Saito, Y. Kishiyama, A. Li, A. Harada, and T. Nakamura, "Concept and practical considerations of non-orthogonal multiple access (NOMA) for future radio access," in *Proc. Int. Symp. Intelligent Signal Process. Commun. Syst. (ISPACS)*, Nov. 2013. pp. 770-774.

[49] H. Tabassum, E. Hossain, and M. J. Hossain, "Modeling and analysis of uplink non-orthogonal multiple access (NOMA) in large-scale cellular networks using poisson cluster processes," *IEEE Trans. Commun.*, vol. 65, no. 8, pp. 3555-3570. Aug. 2017.

[50] Z. Ding, P. Fan, and H. V. Poor, "Impact of user pairing on 5G non-orthogonal multiple access downlink transmissions," *IEEE Trans. Veh. Technol.*, vol. 65, no. 8, pp. 6010-6023. Aug. 2016.

[51] Y. Liu, Z. Ding, M. Elkashlan, and H. V. Poor, "Cooperative non-orthogonal multiple access with simultaneous wireless information and power transfer," *IEEE J. Sel. Areas Commun.*, vol. 34, no. 4, pp. 938-953. Apr. 2016.

[52] Z. Ding, R. Schober, and H. V. Poor, "A General MIMO framework for NOMA downlink and uplink transmission based on signal alignment," *IEEE Trans. Wireless Commun.*, vol. 15, no. 6, pp. 4438-4454, Jun. 2016.

[53] Z. Chen, Z. Ding, and X. Dai, "Beamforming for combating inter-cluster and intra-cluster interference in hybrid NOMA systems," *IEEE Access*, vol. 4, pp. 4452-4463, Aug. 2016.

[54] W. Shin, M. Vaezi, B. Lee, D. J. Love, J. Lee, and H. V. Poor, "Coordinated beamforming for multi-cell MIMO-NOMA," *IEEE Commun. Let.*, vol. 21, no. 1, pp. 84-87, Jan. 2017.

[55] H. Sun, B. Xie, R. Q. Hu, and G. Wu, "Non-Orthogonal multiple access with SIC error propagation in downlink wireless MIMO networks," in *Proc. IEEE Veh. Technol. Conf. (VTC-Fall)*, Dec. 2016, pp. 1-5.

[56] R. Jain, A. Durresi, and G. Babic, "Throughput fairness index: An explanation," *ATM Forum Document Number: ATM Forum/990045*, Feb. 1999.

[57] Q. Wu and R. Zhang, "Towards smart and reconfigurable environment: Intelligent reflecting surface aided wireless network," *IEEE Commun. Mag.*, vol. 58, no. 1, pp. 106-112, Jan. 2020.

[58] Q. Wu and R. Zhang, "Intelligent reflecting surface enhanced wireless network via joint active and passive beamforming" *IEEE Trans. Wireless Commun.*, vol. 18, no. 11, pp. 5394-5409, Nov. 2019.

[59] T. J. Cui, M. Q. Qi, X. Wan, J. Zhao, and Q. Cheng, "Coding metamaterials, digital metamaterials and programmable metamaterials," *Light, Sci. Appl.*, vol. 3, no. 10, p. e218, Oct. 2014.

[60] Q. Wu and R. Zhang, "Weighted sum power maximization for intelligent reflecting surface aided SWIPT," *IEEE Wireless Commun. Lett.*, to be published, doi: 10.1109/LWC.2019.2961656.

[61] Q. Wu and R. Zhang, "Joint active and passive beamforming optimization for intelligent reflecting surface assisted SWIPT under QoS constraints," *arxiv:1910.06220.* [Online]. Available: https://arxiv.org/abs/1910.06220

[62] Y. Tang, G. Ma, H. Xie, J. Xu, and X. Han, "Joint transmit and reflective beamforming design for IRS-assisted multiuser MISO SWIPT systems," *arxiv:1910.07156.* [Online]. Available: https://arxiv.org/pdf/1910.07156

[63] Y. Zheng, S. Bi, Y. J. Zhang, Z. Quan, and H. Wang, "Intelligent reflecting surface enhanced user cooperation in wireless powered communication networks," *IEEE Wireless Commun. Lett.*, to be published, doi: 10.1109/LWC.2020.2974721

초 록

무선 통신이 탑재된 스마트 기기의 폭발적인 성장으로, 사물 인터넷 네트워크와 같은 차세대 통신 네트워크에서 요구하는 성능을 충족하기 위하여 해결해야 할 여러 문제가 발생하였다. 주요 문제 중 하나는 기기의 한정된 배터리 용량으로 네트워크가 제한된 시간 동안에만 동작할 수 있는 것을 극복하는 것이다. 무선 전력 전송은 이와 같이 에너지가 제한된 네트워크에 자기 지속성을 부여할 수 있는 해결 방법으로 고려되고 있다. 사용자들은 무선 전력 전송을 통하여 전용 에너지원에 의해 전송되는 무선 주파수 신호로부터 에너지를 수집하고 배터리를 충전시킬 수 있다. 무선 전력 전송이 가능한 무선 네트워크를 설계하기 위한 체계로서 무선 전력 통신 네트워크(Wireless powered communication network, WPCN)가 제안되었다. WPCN은 기지국과 전용 에너지원의 역할을 같이 하는 hybrid access-point (H-AP)와 여러 사용자로 구성된다. WPCN에서 사용자들은 하향링크를 통하여 무선 전력 전송으로 배터리를 충전시키고, 상향링크를 통하여 해당 에너지로 정보를 전송한다. 이 때, 자원이 부족하므로 WPCN의 시스템을 활용하기 위해서는 효율적인 설계가 필수적이다. 이를 위하여, 본 논문에서는 WPCN을 위한 시스템 설계와 자원 할당에 대하여, 특히 통신량 관점에서 탐구하고자 한다. 또한, WPCN의 특징인 이중 근거리 문제에서 비롯된 높은 사용자간 전송 속도 격차를 완화하고자 한다.

우선, 협력 무선 전력 통신 네트워크에 대해 논의한다. 해당 네트워크에서는 채널 상태가 좋은 사용자가 그렇지 않은 사용자의 정보를 중계하여 사용자 공정성을

향상시킨다. 고려하는 시스템 모델에서 합통신량을 최대화하는 데 각 사용자의 서비스 품질(Quality of service, QoS)을 보장하도록 한다. 위 문제의 최적해를 분석하여, WPCN이 사용자 협력 기법을 통하여 이득을 얻는 조건을 밝히고, 이를 기반으로 사용자 협력 기법을 실용적으로 활용할 수 있는 합통신량 최대화를 위한 새로운 자원 할당 알고리즘을 제안한다. 다음으로, 상향링크에서 비직교 다중 접속(Non-orthogonal multiple access, NOMA)이 적용된 다중 안테나 WPCN에 대하여 논의한다. NOMA를 활용하는 것과 관련된 여러 문제를 해결하기 위하여, 다중 안테나 시스템을 이용한 사용자 클러스터링 기법이 추가로 적용되고, 이에 단일 NOMA 전송의 사용자 수가 감소한다. 합통신량 최대화를 위하여 클러스터별 빔형성과 시간 및 에너지 자원을 공동으로 최적화하는 것이 어렵기 때문에, 먼저 빔형성을 설계한 다음, 해당 빔형성이 적용된 네트워크에 대하여 자원을 최적화한다. 이에, 클러스터별 빔형성 설계와 합통신량 최대화를 위한 새로운 알고리즘을 제안한다. 마지막으로, 무선 통신의 성능을 향상시킬 후보 기술 중 하나인 지능형 반사 표면(Intelligent reflecting surface, IRS)이 도입된 WPCN을 고려한다. IRS를 도입함으로써, 사용자들은 추가로 에너지를 얻을 수 있으며 신호 세기를 높일 수 있다. 고려된 시스템 모델의 합통신량을 최대화하도록 IRS의 빔형성과 자원을 최적화한다. 특히, 상향링크를 위하여 NOMA와 직교 다중 접속이 고려되고, 두 다중 접속 기법간의 성능 비교가 이루어진다.

주요어: 자원 할당, 무선 전력 네트워크, 무선 통신, 에너지 하베스팅, 비직교 다중 접속

학번: 2014-21613

감사의 글

대학원 입학 후 짧지 않은 시간이 흘러 졸업을 앞두고 지난 날을 되돌아보니 여러 감정이 교차합니다. 여전히 부족한 논문을 보며 더 열정적인 자세로 연구에 임했다면 더 잘할 수 있었을 것이라는 아쉬움이 남습니다. 그럼에도 불구하고 학위 과정을 마무리한다는 사실과 작은 결과물을 마주하니 뿌듯하기도 합니다. 아직 연구자로서 부족한 점이 많지만 그간 많은 분들의 도움을 받았기에 이 글을 통하여 감사드리고자 합니다.

우선 지도 교수님이신 이정우 교수님께 감사의 말씀을 드립니다. 학위 논문을 마무리하기까지 학문적 지도뿐만 아니라 끊임없는 격려를 통해 연구자로 성장하는 길을 안내하여 주셨습니다. 앞으로도 교수님께 받은 가르침을 되새기며 더 나은 연구자가 되도록 노력하겠습니다. 또한, 흔쾌히 심사위원장을 맡아주신 노종선 교수님께 감사드리며, 예비 심사부터 논문 지도를 해주신 남상욱 교수님, 소중한 지도 말씀 아끼지 않고 해주신 최완 교수님, 그리고 먼 길 마다하지 않으시고 도와주신 신원재 교수님께 감사드립니다. 부족한 논문을 위해 귀중한 시간을 할애하시어 심사를 맡아주신 교수님들의 지도를 통하여 많은 배움을 얻었습니다.

대학원 생활을 같이 한 통신 및 머신러닝 연구실의 선후배 및 동료들에게도 감사를 전하고자 합니다. 기초적인 공부부터 연구 주제에 대한 접근 방법까지 세세히 알려주시고 같이 고민해주신 선배님들께 감사드립니다. 특히, 학위 논문 심사도 맡아주신 신원재 교수님께 연구실 선배로서 경험과 조언을 아끼지 않고 나누어 주신 점에 대해서 다시 한 번 감사드립니다. 앞이 보이지 않던 연구에 대한 방향을 잡아주시고 앞으로 나아갈 수 있는 동력을 제공해주셨습니다. 그리고, 연구실에 같이 발을 들이며 오랜 시간을 같이 보낸 동기분들께도 감사의 마음을 전합니다. 또한,

열정적으로 연구에 몰두하는 모습으로 자극이 되었던 후배들에게도 감사하며 남은 학위 과정을 후회없이 보내길 바랍니다.

학위 기간 동안 아낌없는 응원과 격려를 보내준 친구들에게 감사드립니다. 학교 안팎에서 보낸 시간들이 스스로를 재충전하여 다시 앞으로 나아갈 수 있는 원동력이었습니다. 또한, 서로의 고민을 나누며 위로하였던 순간들로 더욱 성장하였다고 믿기에 그들에게 감사를 전합니다.

마지막으로 사랑하는 가족에게 감사를 전하고자 합니다. 항상 저를 믿고 기다리며 묵묵히 응원해주신 아버지, 그리고 매일같이 가족을 위해 기도 드리는 어머니께 감사드립니다. 또한, 끊임없이 용기를 불어넣어 준 누나에게 감사하다는 말을 전하며 계속해서 매형과 행복한 가정을 꾸려나가길 바랍니다.

2020년 07월

송동영 올림